

NORTH ATLANTIC TREATY ORGANIZATION
ADVISORY GROUP FOR AERONAUTICAL RESEARCH AND DEVELOPMENT

NASA CC 495

THE EFFECTIVENESS OF THE TRANSONIC WIND TUNNEL
AS A DEVICE FOR MINIMIZING TUNNEL-BOUNDARY INTERFERENCE
FOR MODEL TESTS AT TRANSONIC SPEEDS

By

Ray H. Wright

NASA LANGLEY RESEARCH CENTER

100-475-

FACILITY FORM 502

N 65-83246
(ACCESSION NUMBER)

100
(PAGES)

mx 56231
(NASA CR OR TMX OR AD NUMBER)

(THRU)

Loxe
(CODE)

(CATEGORY)

To be presented at Meeting on Interference Effects in Aerodynamic Test
Facilities to be held at Rhode St. Genese, Belgium, from March 2-5, 1959.

NASA FILE COPY

DIVISION OF RESEARCH
NATIONAL AERONAUTICS
AND SPACE ADMINISTRATION
WASHINGTON, D. C.

Myron C. Nagurny
NASA Evaluation
TMX 56231

①

TABLE OF CONTENTS

	Page
LIST OF TABLES	II
LIST OF ILLUSTRATIONS	II
SUMMARY	V
SYMBOLS	VI
INTRODUCTION	1
THE NATURE OF WIND TUNNEL INTERFERENCE AT SUBSONIC SPEEDS	3
(a) Lift Interference	3
(b) Solid Blockage Interference	5
(c) Wake Blockage Interference	6
(d) Compressibility Effects--Choking	7
(e) Summary and Discussion	10
TRANSONIC WIND TUNNELS AT SUBSONIC SPEEDS	13
(a) Methods of Testing at Transonic Speeds	13
(b) The Slotted Test Section of Circular Cross Section	14
(c) Test Section with Slotted Top and Bottom Walls and Solid Side Walls	23
(d) Test Sections with Porous or Perforated Walls	26
TRANSONIC WIND TUNNELS AT SUPERSONIC SPEEDS	33
EXAMPLES AND COMPARISONS	42
CONCLUSIONS	47
REFERENCES	49
Appendix:	78

7
WO
LNC
CL EV
ARC
REPS

LIST OF TABLES

	Page
I. FIRST-ORDER BOUNDARY INTERFERENCE IN TWO-DIMENSIONAL AND IN CIRCULAR WIND TUNNELS WITH OPEN AND CLOSED BOUNDARIES	53
II. THEORETICAL FIRST-ORDER BOUNDARY INTERFERENCE WITH A SMALL MODEL IN A CIRCULAR WIND TUNNEL WITH UNIFORMLY SPACED STREAMWISE SLOTS DESIGNED FOR ZERO SOLID BLOCKAGE INTERFERENCE	54
III. THEORETICAL FIRST-ORDER BOUNDARY INTERFERENCE WITH A SMALL MODEL IN SQUARE WIND TUNNEL HAVING SLOTTED TOP AND BOTTOM WALLS AND SOLID SIDE WALLS. THE EQUALLY SPACED SLOTS ARE DESIGNED FOR ZERO SOLID BLOCKAGE	55
IV. THEORETICAL FIRST-ORDER BOUNDARY INTERFERENCE WITH SMALL MODELS IN TWO-DIMENSIONAL AND IN CIRCULAR WIND TUNNELS WITH UNIFORMLY POROUS BOUNDARIES. POROSITY DESIGNED FOR ZERO VELOCITY INCREMENT AT MODEL DUE TO SOLID BLOCKAGE	56

LIST OF ILLUSTRATIONS

	Page
Fig. 1.- Lift vortex in two-dimensional tunnel	57
Fig. 2.- Trailing vortices in circular tunnels	58
Fig. 3.- Source-sink doublet in two-dimensional tunnel	59
Fig. 4.- Sources or sinks in two-dimensional tunnel	60
Fig. 5.- Variation of increment of Mach number due to solid blockage interference on fineness-ratio-6 body of revolution in open circular wind tunnel. Body length 1.75 times tunnel diameter	61
Fig. 6.- Blockage interference at center of 3.5-inch-diameter prolate spheroid of fineness ratio 6 in 12-inch-diameter circular tunnels	62
Fig. 7.- Comparison of theoretical with experimental blockage interference at center of 3.5-inch-diameter prolate spheroid of fineness ratio 6 in 12-inch-diameter slotted circular tunnel.	63

LIST OF ILLUSTRATIONS.- Continued:

	Page
Fig. 8.- Comparison of pressure distribution corrected for interference at center of body on 3.5-inch-diameter prolate spheroid of fineness ratio 6 in 12-inch-diameter circular slotted tunnel with pressure distribution on same body in 8-foot circular closed tunnel. Effective Mach number 0.7. Length of body measured from nose	64
Fig. 9.- Shock reflection from slotted boundary of Langley 8-foot transonic tunnel. Stream Mach Number = 1.056	65
Fig. 10.- Comparison of body-surface pressure distributions on a body of revolution tested at supersonic speeds in the slotted test sections of the Langley 8-foot and 16-foot transonic tunnels	66
Fig. 11.- Pressure coefficients at surface of two-dimensional model with several different boundary conditions. $M = 1.400$; blockage 24 percent	67
Fig. 12.- Pressure coefficients at surface of cone-cylinder model with various non-reflecting tunnel boundaries. $M = 1.194$; blockage 1.80 percent	68
Fig. 13.- Pressure coefficients at surface of cone-cylinder model with porous tunnel boundaries. $M = 1.194$; blockage 1.80 percent; constant stream pressure behind walls	69
Fig. 14.- Comparison of drag coefficients on 33.5-inch-long non-lifting body of revolution in Langley 8-foot transonic tunnel with those obtained from free-fall data and from tests in the Langley 16-foot transonic tunnel	70
Fig. 15.- Comparison of lift-curve slopes for a large wall-mounted wing in small slotted, open and closed tunnels with lift on same wing in closed Langley 7- by 10-foot tunnel	71
Fig. 16.- Comparison of pitching-moment characteristics of wall-mounted wing in small slotted tunnels with those of same wing in Langley 7- by 10-foot tunnel	72
Fig. 17.- Comparison of lift coefficients for winged models in Langley 8-foot and 16-foot transonic tunnels. (Single flagged symbols indicate data from small model in the 8-foot tunnel, cross-flagged symbols indicate data from large model in 16-foot tunnel.)	73

LIST OF ILLUSTRATIONS.- Concluded:

Page

- Fig. 18.- Comparison of drag coefficients for winged models in Langley 8-foot and 16-foot transonic tunnels. (Single flagged symbols indicate data from small model in 8-foot tunnel, cross-flagged symbols indicate data from large model in 16-foot tunnel.) 74
- Fig. 19.- Comparison of pitching-moment coefficients for winged models in Langley 8-foot and 16-foot transonic tunnels. (Single flagged symbols indicate data from small model in 8-foot tunnel, cross-flagged symbols indicate data from large model in 16-foot tunnel.) 75
- Fig. 20.- Comparison of lift coefficients for a large complete model tested in the Langley 8-foot transonic pressure tunnel and in the Langley 16-foot transonic tunnel 76
- Fig. 21.- Comparison of moment coefficients for a large complete model tested in the Langley 8-foot transonic pressure tunnel and in the Langley 16-foot transonic tunnel 77

SUMMARY

The nature of the tunnel-boundary interference at transonic speeds is discussed and the theory of the use of the transonic tunnel in minimizing this interference is presented. The requirements for eliminating the lift interference at subsonic speeds are different from those necessary for eliminating the blockage interference and some interference in model testing must therefore be tolerated. For this reason and also because of certain distortions of the flow field, the model size must be restricted. The model size is more seriously restricted by the interference at low supersonic speeds. The prevention of bow-shock reflection is not sufficient to assure freedom from boundary interference and it is, in general, impractical to remove the remaining part of the supersonic interference. In spite of these restrictions, careful use of the transonic tunnel significantly extends the range and usefulness of wind-tunnel testing.

SYMBOLS

b	source strength with incompressible flow
C _d	drag coefficient
C _L	lift coefficient
C _m	pitching-moment coefficient referred to quarter-chord line of the mean-aerodynamic chord
C _p	pressure coefficient
h	half tunnel height
k	quality factor relative to closed tunnel
k'	quality factor relative to open tunnel (Quality factor is quantity by which closed or open tunnel interference must be multiplied to obtain slotted or porous tunnel interference)
m	doublet strength for incompressible flow
M	reference (free-stream) Mach number
M	interference Mach number increment; the increment to be added to the reference Mach number to obtain the effective test Mach number at the model
p	static pressure
p _t	total pressure
q	dynamic pressure, $\frac{1}{2}\rho v^2$
r	radial coordinate or distance
r ₀	radius of circular tunnel
R	permeability factor defined in references 25 and 26
s	semispan of vortex pair, approximately semispan of wing
S	wing area
u	induced velocity in direction of x-axis
v	velocity in direction of y-axis
V	reference (free-stream) velocity in tunnel, velocity far upstream
w	velocity in direction of z-axis

SYMBOLS.- Concluded:

x, y, z	rectangular cartesian coordinates, x in direction of reference velocity along tunnel axis or center line
α	angle of attack, degrees
β	$\sqrt{1 - M^2}$ for $M < 1$; $\sqrt{M^2 - 1}$ for $M > 1$
γ	ratio of specific heats of tunnel test gas
Γ	vortex strength, positive in direction of y -axis
ρ	density of tunnel test gas
*	superscript emphasizing an interference value

INTRODUCTION

Transonic wind tunnels of the slotted-wall type have been in operation by the NACA (now NASA) since 1950. It is therefore appropriate at this time to attempt some evaluation of such wind tunnels and of other partly open-wall tunnels of the porous and perforated types. The transonic test section was originally developed as a device for obviating certain boundary interference corrections, and its effectiveness in accomplishing this purpose is the criterion for this evaluation.

The application of tunnel-boundary interference corrections can be quite complex and tedious. In order to avoid such complexity and tedium, and, even more important, to provide that simplicity of approach necessary for a clear appreciation of the over-all status, attention is directed to the physical phenomena rather than to correction procedures; which, once the interference velocities, pressures, Mach numbers, and flow angles have been determined, can be made by methods already presented in the rather extensive literature applying to open and closed tunnels.

At the expense of some care and labor in application of corrections, the usefulness of the transonic wind tunnel could be extended to permit the testing of larger-than-normal models and to unusual model-tunnel configurations, but except for a few cases (See, for instance, ref. 1), the theoretical and experimental investigations needed to permit such extension have not been performed. Partly for this reason, and partly also in the interest of simplicity, this treatment is limited to the consideration of first-order interference effects. The evaluation is based on a combination of theoretical indications, physical reasoning, and experimental results. Some simple derivations have been included in the Appendix for ready reference. The

extensive reliance upon theoretical considerations is necessary in the treatment of wind-tunnel interference problems because the interference is essentially second-order relative to most test measurements that can be made and is at best difficult to determine with adequate accuracy from experimental investigations.

In order to gain an appreciation of the problem that first led to the investigation of wind-tunnel test sections of the mixed-boundary type, it is instructive briefly to review some simple examples of the subsonic first-order interference theory for open and closed test sections. According to this theory, the interference is due to the reaction of the boundaries of the test stream to only three characteristics of the test model, namely its lift, its displacement, and the displacement of the wake due to its profile drag. Other characteristics such as the distribution of lift and displacement give rise to second-order interference effects. But, if the size of the model is properly small relative to the size of the tunnel, the interference reaction of the boundaries can be adequately estimated by representing the lift with a single horseshoe vortex, the displacement of the model with a single doublet, and the displacement of the wake with a single source. In the simplest case, the model is supposed to be placed at the center of the tunnel symmetrical with respect to a plane containing the tunnel axis or center line and with the tunnel boundaries extending parallel up and downstream without limit. In this simplest case, the interference phenomena are easy to comprehend.

Lift interference.— Consider first the boundary interference in the presence of the lift. For convenience in analysis, the bound part of the horseshoe vortex is separately treated and is placed in a two-dimensional tunnel. The case of a two-dimensional vortex of strength Γ in a closed tunnel is illustrated in figure 1(a). The required boundary condition, that the velocity at the boundary normal to the wall be zero, is exactly satisfied by an infinite system of alternately negative and positive vortex images. Because of the alternate signs of the image vortices, the effect of the bound vortex system is sensibly zero only a short distance upstream or downstream. The interference is therefore due entirely to the induced velocities near the

model location.

Examination of figure 1(a) shows that since the images are equal in absolute strength, those equidistant from $y = 0$ can be paired to yield zero induced velocity at the model. Further examination suggests, since the effects of the nearer images predominate, that a downwash exists upstream from the model and an upwash downstream from the model; and this is the effect indicated by theory. This is the only effect produced by the boundary interference of solid walls on a two-dimensional vortex across the center of the tunnel. In the closed tunnel, the positive induced curvature of the flow (increasing slope of the streamline) has an effect like the opposite curvature of the airfoil chord, that is like positive camber, and the lift of the model is therefore increased. A horizontal tail-plane a short distance behind the wing receives an increased angle-of-attack, therefore, an increased lift and corresponding negative increment of model moment, otherwise a decrement in tail angle for trim.

In the open tunnel with a two-dimensional vortex at $(0, 0)$ the required boundary condition, zero induced velocity in the stream direction at the boundary, is again satisfied by an infinite set of vortices equally spaced along the y axis. In this case, however, the original vortex and the images are all of the same sign. Since this sign is opposite to that of the nearest two of the images representing the interference in the closed tunnel, it is reasonable to suppose that the sign of the induced interference velocities in the open tunnel is opposite to that of those in the closed tunnel; and, since the vortices are all of the same sign, rather than of alternate signs, the magnitude of these induced velocities should be greater than that of those in the closed tunnel. This supposition is borne out by the theory, and in fact it is found that the flow-curvature interference in the open tunnel is of opposite sign and just double the magnitude of that in

the closed tunnel.

The interference in the open tunnel with two-dimensional vortex differs from that in the closed tunnel in another respect, that has sometimes been overlooked. The infinite set of vortex images all of the same sign now yields upstream from the model an upwash which in only a short distance becomes sensibly equal to its final value attained as the upstream distance approaches infinity. Relative to the reference velocity V therefore a downwash $-v$ occurs at the model.

Consider now the interference in the presence of that part of the horse-shoe vortex trailing downstream in the tunnel. For the open and closed tunnels and also for the slotted tunnel (but not for the porous-wall tunnel) the problem can be simplified by treating the flow in a plane, the Trefftz plane, normal to the tunnel axis at some position far downstream from the model. The essentially three-dimensional problem is thus reduced to one in two dimensions, and theory gives the downwash interference at the model as exactly half that calculated in the Trefftz plane. The theory is especially simple for closed or open circular boundaries. Thus, in figure 2, the boundary conditions are satisfied with only two image vortices, one for each of the two trailing vortices, placed at the inverse points, i.e. $\frac{r'}{r_0} = \frac{r_0}{r}$. For each of the image vortices, another vortex at the center of the tunnel is also required, but since these two vortices are of equal magnitude but of opposite sign, their effects compensate and therefore need not be considered. In the closed tunnel (fig. 2(a)), the image vortices are of the same strength as but of opposite sign to that of their originals, and, as is easily seen, an upwash results near the center of the tunnel. In the open tunnel (fig. 2(b)) the interference is of the same magnitude as that in the closed tunnel, but opposite in sign; a downwash occurs.

Solid blockage interference.— Because of the thickness of the model, the streamlines of the flow are displaced laterally; and, the reaction of the

tunnel boundaries to this displacement constitutes an interference relative to conditions with the model in an unrestrained flow field. For a first-order calculation of this interference, the model can be replaced with a single source-sink doublet.

The two-dimensional case with open and with closed boundaries is illustrated in figure 3. In the closed tunnel (fig. 3(a)) the zero-normal-velocity boundary condition at the walls is exactly satisfied with an infinite set of mirror images of the original source-sink doublet spaced one tunnel-height apart along the y-axis. The resulting crowding of the streamlines produces an increase in velocity in the x-direction for the interference at the position of the model. In the open tunnel (fig. 3(b)) the two images nearest the model must be of the same strength as the original but opposite in sign, and the farther images must be alternately positive and negative. As a result, the solid blockage interference in the open tunnel is of opposite sign and of half the magnitude of that in the closed tunnel.

The three-dimensional solid blockage phenomena are fundamentally the same as those in two dimensions, but in this case, the magnitude of the interference in the open tunnel of circular or square cross-section (but not for shapes much different from these) is only about a fourth of that in the closed tunnel.

Wake blockage interference.— The profile drag of the model results in a wake of reduced velocity downstream from the model, and the effect of this wake on the outside flow can be represented, for the purpose of first-order boundary-interference calculation, by a single source located at the position of the model. The systems of images satisfying the boundary conditions for closed and for open two-dimensional tunnels are indicated in figure 4. For the closed tunnel, the infinite set of sources along the y-axis, corresponding to the original source, evidently produces a decrease in velocity on the

forward part of the model and an increase over the rearward part, that is, a positive velocity gradient or, otherwise, negative pressure gradient. An increase in drag is therefore measured on a force balance, or what amounts to the same thing; an increase in surface pressure is measured near the nose of the model and a decrease near the tail.

As for the case of the bound vortex, the infinite set of source images all of the same kind produces a disturbance far upstream. For the source images, this disturbance is a reduction in velocity in the x-direction. Relative to the reference velocity V therefore an increase of tunnel velocity occurs at the model.

For the open tunnel, the images must alternate in sign with the original as indicated in figure 4(b). The velocity gradient is therefore opposite in sign and, as shown by the theory, is of half the magnitude of that in the closed tunnel. The velocity interference is zero, because the alternately positive and negative infinite set of images produces zero velocity increment for $x \rightarrow -\infty$.

The interference effects of open and closed three-dimensional boundaries in the presence of a source are in every way comparable to those of two-dimensional boundaries. The phenomena are fundamentally the same, but again, as for the velocity interference due to wake blockage in the presence of a source-sink doublet, the velocity gradient due to three-dimensional wake blockage is, for circular or square cross-section, only a fourth as large (and opposite in sign) in the open tunnel as in the closed tunnel.

In the presence of a sink, both the velocity- and velocity-gradient-interference effects are the negative of those experienced with a source. The sink is useful in estimating the first-order interference effects on a propeller.

Compressibility effects--choking. - To the first-order accuracy herein considered, the effects of increasing Mach number can be estimated by means

of the well-known Prandtl-Glauert rule. The rule is simple enough, but its application to wind-tunnel interference is of such subtlety that several of the early attempts to estimate the compressibility effects contained incorrect results. The various first-order interference effects generally increase with Mach number, but the upwash or downwash due to lift is an exception to this rule, provided the actual measured lift is used in estimating the interference velocities. However, in applying corrections, the vertical velocities (upwash or downwash) must be read off at $x/\sqrt{1-M^2}$ rather than at x , where x is the distance in the free-stream direction and M is the reference Mach number. At the position of the model, $x = 0$, the vertical interference velocity remains unaffected by increase in Mach number. The flow curvature, on the other hand, receives a compressibility factor $1/\sqrt{1-M^2}$.

A much more severe compressibility effect according to the linearized interference theory applies to the solid blockage. The increment of velocity in the x -direction receives a factor $1/(1-M^2)^{\frac{3}{2}}$; but this is not all. Within a range of Mach number for which the compressibility effect on the interference (but not on the flow about the model) might otherwise be adequately represented by means of the Prandtl-Glauert rule, a fundamental flow change occurs. With the attainment of sonic velocity in a region of the flow field near the model, the mass rate of flow is restricted in that region and the streamlines are crowded in the vicinity of the tunnel walls. The effect is similar to that of an increase in model thickness, and an increase of the strength of the doublet representing the model is therefore required.

A further similar effect arises from the boundary layer and wake. The wake is never represented with complete accuracy by means of sources; and as shock waves terminating the supersonic flow region lead to flow separation with increasing boundary-layer and wake thickness, the additional doublet strength required in an adequate representation of the boundary layer and

wake may become appreciable. Because of these effects, the solid blockage interference may increase with Mach number over part of the subsonic Mach number range more strongly than is indicated by the factor $1/\beta^3$ where

$$\beta = \sqrt{1 - M^2}.$$

In applying the solid blockage compressibility factors, no distinction is required between two-dimensional and three-dimensional configurations. The compressibility effects are essentially the same, though in two dimensions part of the linearized compressibility factor is sometimes applied directly to the representing doublet strength.

The wake blockage interference velocity receives a compressibility factor $1/\beta^2$ and the velocity gradient due to wake blockage a factor $1/\beta^3$; but if the interference is based on drag, a further factor, $[1 + (\gamma - 1)M^2]$, where γ is the ratio of specific heats, is required to account for the increase of the representing source strength with increase of Mach number. In the range of Mach numbers greater than that for which sonic velocity first occurs in the flow field about the model, the wake blockage interference may increase with Mach number more strongly than is indicated by these factors because of the great increase in drag.

As the tunnel Mach number approaches unity, the linearized theory becomes increasingly unreliable and the compressibility factors inapplicable. (This inapplicability is apparent from the fact that $1/\beta$ approaches ∞ as M approaches unity). Moreover, in the closed tunnel, the indicated reference Mach number can be increased little beyond that corresponding to the first attainment of sonic velocity at the wall near the model. Because of the solid and wake blockage (and perhaps affected also by the lift and by the attitude of the model) this maximum Mach number may be considerably less than unity, and the tunnel is said to be choked. In this condition the flow over the forward part of the model is insensitive to that over the rear, and adequate tunnel-boundary interference corrections are difficult or impossible to make.

In the open tunnel, the interference is somewhat less severe, but the large power requirement and the instability often found at high subsonic Mach numbers has discouraged the use of this kind of tunnel.

Summary and discussion.- First-order interference effects with the model placed on the center-line at $x = 0$ in two-dimensional and in circular wind tunnels with open and with closed boundaries are summarized in Table I, wherein also appropriate references are given. Reference 2 is an excellent summary of the interference effects and corresponding corrections with incompressible flow. Interference effects with compressible flow are treated in references 3 through 8 and in the Appendix. References 3 and 7, in particular, are recommended as reliable and rather complete summaries of lift and solid and wake blockage interference in two-dimensional closed tunnels and of solid and wake blockage interference in closed three-dimensional tunnels, respectively. The references relate the vortex strength to the lift (which relation is the same for compressible as for incompressible flow, i.e., lift per unit span $= \rho V \Gamma$); the doublet strength to the volume of the model, and the source strength to the drag, and also show how to derive the various corrections from the known interference. All these relations are the same for slotted or porous as for open or closed boundaries, and will not be further discussed.

Consider now the relative magnitudes of the various kinds of interference. Because of the importance of three-dimensional effects in high-speed aerodynamics, two-dimensional testing has become of relatively lesser importance than testing in three dimensions. For this reason, since for a three-dimensional model the chord and span of the wing and therefore also the lift and corresponding total vortex strength are normally smaller, the interference on the bound vortex also becomes of lesser importance. In fact, the effect of streamline curvature is commonly ignored in complete-model testing. Moreover, as seen from Table I, as the Mach number increases, the downwash interference remains

unchanged (for constant lift), so that the lift interference becomes still less significant relative to the strongly increasing solid and wake blockage. For models with properly small drag coefficient, the wake blockage becomes large only at Mach numbers greater than about 0.8, whereas the solid blockage may be significant throughout the Mach number range and increases very strongly in the range above about 0.7. In most cases therefore involving the consideration of transonic wind tunnels for subsonic testing, attention should be directed first of all to the solid blockage.

The solid blockage interference and other types of interference as well are further affected by compressibility in a way not apparent in Table I. Even with incompressible flow, the solid blockage interference, for instance, cannot be accurately represented by a single velocity or Mach number increment unless the model is properly small relative to the tunnel size. With increase in Mach number, this distortion of the flow field is accentuated. Not only does the maximum interference increase, but the x-region within which a given percentage of variation occurs becomes narrower as the Mach number increases (See for instance ref. 5).

This effect was illustrated in an unpublished theoretical investigation of the solid blockage interference on a fineness-ratio-6 body-of-revolution of length 1.75 times the diameter of the open tunnel in which it was placed. For incompressible flow, the interference near the ends of the body as contrasted to that at the center had already fallen to practically zero, but for a Mach number of 0.7, because of the flow distortion due to increase of Mach number, the interference in the same region had attained an appreciable value opposite in sign to that at the center (fig. 5). It is this same distortion of the flow field with increase in Mach number that introduces the extra factor $1/\beta$ into the compressibility factor for the flow curvature and for the pressure gradient.

Besides these obvious distortions of the flow field, others more difficult to estimate are to be expected. With increasing Mach number, various second-order effects almost certainly become of increasing importance, and, as already pointed out, the attainment of choking in closed tunnels not only limits the test range, but also may correspond to flow conditions at the model that cannot be related to any free-field condition. Model sizes must therefore be progressively decreased as the test Mach number approaches unity or else some way must be found to circumvent the problem.

TRANSONIC WIND TUNNELS AT SUBSONIC SPEEDS

Methods of testing at transonic speeds.— The problem of wind-tunnel testing at transonic speeds can, of course, be avoided by means of flight testing of piloted aircraft or of pilotless models (see, for instance, ref. 9) or even by allowing a model to fall freely (refs. 10 and 11). However, these free-flight methods are usually more expensive and less convenient than wind-tunnel testing, and with these methods accuracy comparable to that normally attained with a fixed installation is difficult to achieve. By another method, the transonic bump method, a model is tested in the flow field surrounding another body, but the model is almost necessarily small, the interference due to the presence of the body may be difficult or impossible to determine and nonuniformity exists in the flow field into which the model is inserted, so that again satisfactory accuracy is difficult to attain (ref. 12).

The free-field conditions could evidently be represented in the wind tunnel if the (solid) walls were shaped to conform to stream surfaces in the free-field flow about the model. This method has actually been used (ref. 13), but it is evidently awkward and inconvenient and becomes increasingly difficult to apply as the Mach number increases in the upper subsonic range.

Another method of circumventing at least part of the wind-tunnel interference problem is suggested by reference to Table I, where for the critical solid blockage the interference in the open tunnel is seen to be of opposite sign to that in the closed tunnel. It therefore seems reasonable to suppose that a mixed boundary containing some particular arrangement of open and closed portions might reduce the solid-blockage interference to zero. This is the idea that led to the NACA transonic test sections. The same idea had been previously used to remove the low-speed lift interference (see, for instance, ref. 14).

The slotted test section of circular cross section.- The solid blockage interference in a rectangular tunnel with two opposite open sides and two opposite closed sides had been treated in reference 15, wherein it was found that the interference at the position of the model would be zero if the length of each closed side were 1.17 times the length of each open side. This arrangement of two open and two closed sides appears to involve an unnecessary risk of flow-field distortion. Uniformity of flow in the test region is evidently favored by using many open and many closed segments of the boundary symmetrically arranged. A ten-slotted circular tunnel with the slots running in the streamwise direction was therefore theoretically investigated and tested (ref. 16). Some of the results follow.

The attempt to satisfy exactly the boundary conditions at the open and closed portions of the boundary in the presence of a source-sink doublet led to an infinite set of linear simultaneous equations for the determination of the functions required in calculating the interference. Nevertheless, the behavior of the slotted tunnel at subsonic speeds became immediately apparent, and on the basis of some approximate solutions with various slot widths, it was estimated that the blockage interference in the ten-slotted circular tunnel would be approximately zero if about one-eighth of the total boundary were open. This estimate has been shown by later investigations to be too large, but it is conservative, because for open ratios greater than that required for zero blockage, the interference is relatively insensitive to variation of slot width. The excess width also provides some allowance for viscous effects near the slot edges.

The theory shows that with increase in the number of the (symmetrically spaced) slots, the ratio of open to total boundary corresponding to zero blockage decreases. An analogous effect is found in electrical shielding, for which the required amount of constant-potential material decreases as the screen becomes finer.

The compressibility factor for the blockage interference in the slotted tunnel was shown to be the same as that for blockage interference in open or closed tunnels. It follows that within the range of applicability of the Prandtl-Glauert rule, a slotted wind tunnel giving zero blockage interference with incompressible flow will also give zero blockage interference with compressible flow at all subsonic Mach numbers.

The elimination of the solid blockage interference with Mach numbers approaching unity suggests that the associated tunnel choking should also be eliminated. The same result was derived by arguing that because the streamlines were now free to expand outward through the slots, choking could not occur.

On the basis of this theoretical investigation, a ten-slotted, $1/8$ -open circular tunnel one foot in diameter was designed to check the theory. Care was taken to represent the theoretical assumptions as well as practically could be done. Thus, the slotted test section was made relatively long, 3 diameters; and in order to assure constant pressure at the slots the material of the test section was cut away outside the slots and the diameter of the surrounding constant-pressure tank was made twice that of the test section.

To assure a large enough interference effect for reasonably accurate determination, the body-of-revolution test model was much larger relative to the tunnel than would normally be employed. The length of the body was 1.75 times the diameter of the tunnel and its maximum cross section occupied 8.5 percent of the tunnel cross section.

The interference at the center of this large body in the slotted tunnel is compared with that in the open and in the closed tunnels in figure 6. The interference Mach number increments are based on the assumption of zero interference in the eight-foot closed circular tunnel, where the interference

is theoretically $1/128$ of that in the twelve-inch open tunnel. The presence of a small negative interference Mach number increment for the slotted tunnel must be considered a consequence of the too-large ratio of open to total boundary. The interference for the open tunnel at the highest Mach number for which the interference is shown is based on a single datum point and is perhaps unreliable.

The equations of reference 16 are inconvenient for use in calculating the interference in a slotted tunnel. A convenient method based on average rather than exact boundary conditions is given in reference 17. From figure 7 of that reference with values of the abscissa $\sqrt{\frac{1}{C+1}}$ zero for the closed tunnel and 0.86 for the $1/8$ -open 10-slotted tunnel, the interference in the slotted tunnel was estimated to be about (-0.063) times that in the closed tunnel. This factor was applied to the closed tunnel interference calculated for the prolate spheroid in the circular tunnel by means of equations (44) and (50) of reference 7. The resulting estimated interference is shown for comparison with the measured slotted-tunnel interference in figure 7. Most apparent is the, not unexpected, failure of the compressibility factor to agree with the experimental results in the Mach number range near unity. It seems reasonable to conclude that the performance of the slotted tunnel is more reliable than the theory of wind-tunnel interference. This behavior is indeed fortunate and is in considerable measure responsible for the improvement that the NACA transonic test section has brought to the technique of transonic testing.

The variation of the interference near the model position must also be considered. The radial variation with many slots is theoretically small, and there is no reason to suppose that this characteristic will not be achieved in practice. The variation in the streamwise direction on the other hand is theoretically zero at the center of the model and symmetrical upstream and downstream from the center; and this theoretical prediction is not achieved

in practice. Thus, figure 8 shows a significant negative pressure gradient in slotted tunnel. An explanation of this pressure gradient based on departure from the assumed potential flow will appear in the sequel. The pressure gradient interference in the slotted tunnel is less important than might be supposed because with decrease in model size both the pressure gradient interference and the effect of a given pressure gradient on the model coefficients decreases.

Some further characteristics of the slotted tunnel may be pointed out. First, the residual tunnel pressure gradient often present in closed tunnels is absent from a slotted tunnel. A gradient can be introduced, however, if the cross section of the entrance to the diffuser is appreciably different from the effective cross section of the jet in the test region and if the diffuser entrance is too near to the model test position. Second, the slotted tunnel provides a particularly simple and reliable method of determining the reference Mach number. It is necessary only to measure the static pressure in the tank surrounding the slots and to determine the Mach number by applying a pre-determined tunnel-empty calibration factor (near unity) to the Mach number corresponding to the ratio of this static pressure to the total pressure in the tunnel. This method is reliable provided the tank is sufficiently large as not to interfere with the flow through the slots and provided the model is located sufficiently far downstream from the upstream end of the slots as not to influence perceptibly the flow in that region. The reliability of this calibration method is a direct result of the fact that flow conditions upstream from the model are determined by transmission of pressure through the slots in that region. Some indication of the required distance of the model downstream from the slot beginning may be obtained from reference 18, wherein it is found that a lifting model should be no closer than about one-half the tunnel height from the upstream or downstream end of an open jet. Examination of the calculated wall velocities shown in reference 19

suggests that a somewhat longer test section would be desirable in the case of the slotted tunnel. This result applies with incompressible flow. With compressible subsonic flow, the upstream or downstream distance should perhaps receive a factor $1/\beta$. With supersonic flow, the model location is determined by the distance required for development of a uniform test region.

The inadequacies of the linearized potential-flow theory of references 16 and 17 have already become apparent. It is quite evident however, since the interference is theoretically proportional to the cube of the ratio of body diameter to tunnel diameter, that if the ratio of model size to tunnel size had been reduced to a more usual value, halved say, the blockage interference in the slotted tunnel of figure 6 would have been hardly measurable. Simultaneously, an even greater proportional reduction of the pressure gradient effect should have occurred. Even with the somewhat too large open ratio therefore the solid blockage with the smaller model should be approximately zero even near a Mach number of unity. The linearized theory is, of course, inapplicable in the vicinity of Mach number one, but by virtue of the well-known stationarity of flow conditions near a Mach number of unity one can reason that if the interference is sensibly zero at a Mach number slightly less than one it is small also at Mach number one and at a Mach number slightly greater than one. These surmises were partially checked by testing a winged model of equivalent size 0.38 times that of the 3.5-inch-diameter prolate spheroid. The results are reported in reference 16, where it is shown also that the choking phenomenon does not appear and that the slotted tunnel is operable through Mach number one. Corroborating data of a similar nature will be shown in a subsequent section. Such data showing absence of measurable interference indicate little about the nature of the interference but do serve to certify the tunnel as suitable for model testing without the application of corrections. A sonic boundary interference theory reported in reference 20 tends to support the arguments of this paragraph.

The effect of the model wake blockage interference on the tunnel effective Mach number and on the pressure gradient in the slotted tunnel has so far tacitly been assumed to be negligible. For the models tested, this is a reasonable assumption. It is, moreover, susceptible to some analytical investigation. As for the open and closed tunnels, the wake is approximately represented by a source, and in analogy with these cases, the interference velocity at the model due to the wake blockage is almost certainly zero. For in the slotted tunnel, as in the open tunnel, the continuity condition which in the closed tunnel requires an increased velocity outside the wake no longer applies. This result is formally derived in the appendix; the velocity (or Mach number) interference due to wake blockage in a circular slotted tunnel is zero with any slot width that is effective in reducing the solid blockage. Moreover, the same formal derivation shows that if the solid blockage is zero, the velocity (or pressure) gradient due to wake blockage is also zero. Since, in addition, the wake blockage interference on wings and bodies suitable for aircraft is normally much smaller than the solid blockage interference, its neglect in the case considered is believed to be fully justified; though no experimental basis for this conclusion is known to the author.

The source is also useful to investigate the interference on a model producing thrust. Inasmuch as the tunnel boundary interference on a thrusting propeller, for instance, is approximately the same as that on a negative source (sink) the slotted circular tunnel appears to be particularly well suited for propeller testing. A similar conclusion applies for any device producing thrust in the direction of the tunnel axis.

The downwash due to lift interference in a circular slotted tunnel was treated as early as 1940 in reference 21. Essentially, the same results were independently derived and subsequently extended to various model-tunnel configurations in reference 22. Both references 21 and 22 consider exact

boundary conditions, but again the results of reference 17, which are derived from average boundary conditions, are more convenient where applicable. For circular tunnels containing equally spaced streamwise slots all of the same width, the ratio of open to total boundary necessary for zero downwash due to lift interference is less than that required for zero solid blockage interference. In such a tunnel designed for zero solid blockage, the downwash due to lift interference is of the same sign as that in an open tunnel. A circular slotted tunnel having both zero solid blockage interference and zero downwash interference due to lift could perhaps be designed by concentrating the slots in the part of the tunnel boundary near its intersection with the horizontal plane through the axis, that is opposite the wing tips, but the interference would then be substantially non-uniform over the tunnel cross section. The theory indicates no compressibility effect on the downwash at the model; only the stretching factor $1/\beta$ is to be applied to axial distances, as already noted for the open and closed tunnels, in reading charts and figures prepared for incompressible flow.

The streamline curvature, of camber correction, due to lift interference in such a slotted circular tunnel designed for zero solid blockage is found in reference 19 to be of the same sign as that in the open tunnel, but so small as to be practically negligible. Because the effect of streamline curvature on the lift is proportional to the ratio of the wing chord to the tunnel radius, it becomes of even lesser relative importance as the model size is made smaller. No adequate experimental data are available for checking either the streamline curvature or downwash due to lift interference.

The theoretical first-order boundary interference with a small model in a circular wind tunnel with uniformly spaced streamwise slots of such width as to reduce the blockage interference to zero is summarized in Table II. The interference is presented as the ratio K of the slotted tunnel interference to the corresponding closed tunnel interference. The streamline

curvature at the model in the closed tunnel, which has not hereinbefore been tabulated, is found from reference 19 and with the application of the proper compressibility factor to be $\frac{1}{V} \frac{\partial w^*}{\partial x} = \frac{SC_L}{8\pi\beta r_0^3}$, where S is the wing area and C_L the model lift coefficient. The curvature in the open circular tunnel is about 0.80 as large and opposite in sign to that in the closed tunnel. Because the compressibility factors are the same for the closed as for the slotted tunnel, Table II is applicable to compressible flow within the validity of Prandtl-Glauert rule.

In consideration of the experimental evidence that has been presented, the theoretical prediction of zero solid blockage interference in a properly designed slotted tunnel is believed to be correct. The theory should be reliable in monitoring the design, provided the slot edges are relatively thin, provided the test section is sufficiently long (two diameters should be long enough), and provided the number of slots is sufficiently small to permit a slot width large relative to the boundary-layer thickness.

With regard to the source representing the wake, the theory leading to the prediction of zero velocity increment interference due to wake blockage in any slotted tunnel is so solidly based as to permit practically no doubt of its validity. The velocity gradient, on the other hand, in the presence of the source arises from slot reactions very similar to those existing in the presence of solid blockage, so that it seems almost necessary that in a tunnel designed for zero solid blockage interference, the velocity gradient due to wake blockage should be at least small. The velocity gradient noted in the experimental results is believed to be due largely to non-potential flow effects in the solid blockage interference.

An effect similar to that of the wake may be expected to exist for model support systems extending far downstream from the model. Such a support system exerts a direct influence on the model test results, but its secondary influence arising from the boundary interference should be greatly relieved

in the slotted tunnel.

Aside from the experimentally discovered velocity gradient, it is evident that the zero-blockage-interference wind tunnel also suffers from some lift interference. Because the streamline curvature is so small and the downwash is theoretically unaffected by compressibility, this lift interference need not be large and could be compensated by the application of corrections. However, the boundary conditions for the lift interference in a slotted tunnel are less certain than in a closed tunnel and there is some experimental evidence to suggest that the interference is greater than predicted by the theory. Such an effect appears reasonable because with any appreciable downward displacement of the jet due to the lift reaction, the inflow above the wing must increase the boundary layer thickness over the slotted surface on that side of the tunnel, so that the actual boundary conditions in such a region approach those for an open tunnel.

Several reasons for limiting the size of the test model in a slotted tunnel can now be suggested:

- a. Even though the first-order theory may predict zero interference of a particular kind, a distortion of the flow field corresponding to second-order or non-linear effects may still exist. Such distortion may be expected to decrease strongly with decrease in model size.
- b. The magnitude and effect of the experimentally discovered pressure gradient cannot be theoretically determined but may also be expected to decrease strongly with decrease in model size. This type of interference could perhaps be roughly determined by a careful experimental investigation.
- c. The lift interference is not well determined and should therefore be kept small.

d. As the Mach number approaches unity, the theory becomes less reliable and the determination of satisfactory tunnel performance rests largely on comparison tests. The fact that the interference decreases with decrease in model size relative to tunnel size is still solidly based, however, for any subsonic Mach number.

Even stronger reasons for limiting the size of the model will appear in the discussion of supersonic interference.

By analogy with the case of open or closed tunnels, slotted tunnels with cross-sectional shapes near circular are expected to exhibit interference characteristics similar to those of circular tunnels. In particular, reference 17 shows that the lift interference in a square slotted tunnel is practically the same as that in a circular slotted tunnel having the same cross-sectional area and the same ratio of open to total boundary.

Before taking up the supersonic interference, the subsonic interference in tunnels with slotted top and bottom walls and solid side walls and in porous or perforated tunnels will be briefly considered.

Test section with slotted top and bottom walls and solid side walls.- A type of slotted tunnel that is relatively easy to construct and convenient for the generation of supersonic flow and for the use of optical methods of observation has the slots only in the top and bottom walls. The solid side walls are then free for observation windows and for any model-support equipment that might be needed. With cylindrical models extending between the side walls the flow is essentially two-dimensional, but the tunnel is also suitable for three-dimensional tests of winged models with span perpendicular to the side walls. Unfortunately, with this latter arrangement, the open-ratio required for zero solid blockage interference is so large that substantial lift interference exists. The lift interference could be reduced with small

effect on the blockage interference by rotating the model through a right angle, so that some plane containing the span would be parallel to the side walls, but this artifice would remove the advantage of the solid side walls for optical observation and would besides accentuate the distortion of the flow field. For three-dimensional testing such a wind tunnel must be regarded as a compromise in the interest of convenience, particularly of supersonic operation. If, because of supersonic interference, the three-dimensional models must be kept quite small relative to the tunnel, the subsonic interference may be negligible.

The theoretical first-order interference for two-dimensional models and for small three-dimensional models in tunnels with only top and bottom walls slotted is summarized in Table III. In each case, the number and width of slots are assumed to be such as theoretically to reduce the solid-blockage interference to zero. In the two-dimensional case, the lift interference is computed as that corresponding to a two-dimensional vortex extending perpendicularly from one solid side wall to the other across the center of the tunnel. The same arrangement of the two-dimensional source-sink doublet and of the two-dimensional source yields the solid blockage interference and the wake blockage interference, respectively.

The lift interference in the three-dimensional case is treated in references 22 and 23 by a method of synthesis, by which the interference is computed as the sum of that due to the trailing vortex images in the solid side walls plus that due to the effect of the slotted top and bottom walls in the presence of the trailing vortices. It is found that the lift interference due to the slotted walls is almost the same as that on a two-dimensional model spanning the tunnel and having the same total lift. A similar treatment is given in reference 1; but the slotted-wall effect is there ascribed mostly to the interference on the bound vortex, and the slotted-

wall effect on the trailing vortices is used only to derive a small correction. A cursory consideration of the problem would suggest that the slotted-boundary interference on both bound and trailing vortices should be included. However, the major effect of the slotted walls in the presence of the trailing vortices changes so slowly with upstream and downstream distance that over any finite length it is essentially constant. Since the test section is necessarily of finite length, the reference velocity is affected no differently than is the velocity at the model and this particular type of interference is therefore inapplicable.¹ For this reason, the analysis of reference 1 is preferred, though the two methods arrive at essentially the same results. Reference 23 considers the streamline curvature in addition to the downwash. The curvature is not specifically treated in reference 1, but may become significant for large models. As for the circular slotted tunnel, the lift interference is expected to be larger than predicted. However, the experimental results of reference 23 show lift interference larger in some cases than would be theoretically predicted even if the top and bottom walls were completely open. Tentatively, at least, these experimental results are regarded as less reliable than the theory.

The interference in the presence of a three-dimensional source is easily derived from the theory for the solid blockage interference. The total potential for the source at the center of a tunnel with only top and bottom walls slotted is given by integrating from $-\infty$ to x the sum of equations (45) and (57) of reference 17. The x -derivative of this potential yields the total axial induced velocity for the source, which is evidently the same as the total potential for the doublet. If the potential of the original

¹For this explanation, the author is indebted to Dr. S. Katzoff of the NASA Langley Research Center.

doublet (summation parameter $k = 0$ in equation 45) is subtracted out, the remainder yields the interference velocity for the source. This interference velocity is evidently zero at the position of the model, $x = y = z = 0$. It also approaches zero far upstream, so that the interference velocity in the presence of the source is zero whatever the slot configuration. Similarly, the velocity gradient in the presence of the source is given by the same equation as the interference velocity for the doublet and is therefore zero for the case considered in Table III.

Test sections with porous or perforated walls. - Porous or perforated boundaries have some advantage for supersonic testing not only with respect to supersonic interference but also, because of their strong tendency to damp out flow disturbances, with respect to the establishment of a uniform test region. In addition, there is some experimental evidence to suggest that a tunnel with such boundaries may require less power than the slotted tunnel (see, for instance, reference 24). On the other hand, the problems involved in constructing and operating porous or perforated tunnels are much more severe than those characteristic of slotted tunnels. The disadvantages with respect to optical methods of flow observation are obvious. Some not-so-obvious disadvantages will appear in the discussion of the interference.

Because of the severe constructional difficulties and of the practical impossibility of obtaining and maintaining porosity control, true porous materials have been little used in wind-tunnel construction. As a compromise, perforated materials have been employed and, again to facilitate construction, the perforations (usually round holes) have been made larger than would otherwise appear desirable. Variations in shape and arrangement of the perforations have also been tried (see, for instance, references 24 and 25). One of the most successful of these has the holes so slanted that the outside

end of a hole lies farther downstream than the end at the inside surface of the tunnel wall. Another is a compromise with the slotted tunnel by which the place of a slot is taken by a strip of perforated material.

With such wide variation in shape and arrangement of perforations, it is not surprising that wide variations also exist in the ratio of open to total boundary, the open-ratio, required for the best attainable interference characteristics. The performance of a wind tunnel of this type cannot be theoretically predicted but must be determined by experiment. Moreover, in this experimental determination, the conditions to be encountered in model testing must be adequately represented. One of these conditions has to do with the boundary layer. Since the dimensions of the perforations are usually of the same order as the thickness of the tunnel boundary layer, its influence may be expected to be quite large. It is easy to see that the presence of a boundary layer on a perforated wall of given open-ratio will cause that wall to react as if the open-ratio were larger. Such a result is found experimentally in reference 25. As a result of this behavior, the effective porosity in a region of inflow may be much greater than that in a region of outflow through the wall. The actual boundary conditions at a perforated wall are therefore far from certain even with the most reliable experimental determination of the wall characteristics.

For this discussion, the tunnel will be assumed to be uniformly porous. (The tunnel with the porosity concentrated in streamwise strips could perhaps be treated as a combination slotted and porous tunnel after the manner of reference 6). The distinguishing characteristic of the porous wall is the linear variation of velocity normal to the wall with pressure difference across the wall. A permeability factor for the wall is then conveniently defined as

$$R = \frac{2 v/V}{p/q}$$

where v is the velocity normal to the wall and p is the pressure difference across the wall (see refs. 25 and 26). With truly porous material, the permeability factor R should vary directly with the stream velocity and with the density. An increase of porosity with density was found in reference 27, even though the perforations tested were considerably larger than would correspond to a true porous material.

In any practical perforated wind tunnel, the perforations are likely to be much too large to permit the justification of the linear pressure-velocity relation on the basis of porous-wall theory. For flow normal to the wall, the pressure difference across a wall with holes normal to the surface would be expected to vary with approximately the square of the velocity. However, since the hole size is of the same order as the boundary-layer thickness, the velocity parallel to the surface at the entrance to the hole should not be assumed zero.

A simplified treatment of the flow into a hole in the presence of the streamwise velocity is given in reference 28. For this investigation, the hole is supposed to be a two-dimensional slot with thin edges transverse to the stream. In spite of the simplifications, this theory is believed to give a valid indication of the phenomena attendant upon the flow into a hole. It is indicated that with many transverse slots, the velocity normal to the surface is approximately a linear function of the pressure difference across the slots. The value of R is found to require the compressibility factor β . The corresponding supersonic factor β is stated in reference 24 to be applicable also with supersonic flow over the perforated material. The approximately linear pressure-velocity relation is shown experimentally for circular perforations both in the experimental results of reference 28 and in figure 10 of reference 27. However, in reference 27, the pressure-velocity curves are approximately straight also for the case of zero velocity parallel to

the perforated surface. Evidently, the porous-wall condition persists for larger perforations than would be indicated by the theory. The curvature shown in the pressure-velocity curves of figures 28 and 29 of reference 24 is perhaps at least partly due to the boundary-layer effects.

The predicted variation of the permeability factor R with Mach number is not supported by the available data. Neither the data of reference 27, when analyzed in terms of the permeability factor, nor those given in reference 24 show any certain consistent variation of the non-dimensional pressure-velocity ratio with Mach number, certainly no tendency for the effective permeability factor to approach zero at Mach number one. The same conclusion can be inferred for supersonic velocity from figure 13 of reference 25.

The absence of any appreciable compressibility effect on the effective permeability factor is believed to be partly due to the small aspect ratio of the perforations as suggested in reference 28 (Sweptback edges would have a similar effect), but it could also be due partly to the boundary layer, since particularly with small holes the effective velocity at the surface of the perforated material must always be considerably less than that in the center of the tunnel. Moreover, it will be remembered that the porous-wall theory predicts that the permeability factor R will increase with velocity over the porous material, so that insofar as the perforated material behaves like the porous wall any compressibility effect with subsonic velocity at and parallel to the surface tends to be counteracted. This is perhaps the reason that the slopes of the curves of pressure difference against stream velocity with constant normal velocity given in figure 11 of reference 27 first decrease with increase of stream velocity before increasing at the larger velocities. It appears that the linear pressure-velocity relation, with permeability factor R dependent only on the geometry of the wall, describes the behavior of the perforated material as well as can be

determined from the available data. However, a more sophisticated treatment is given in reference 31.

The theoretical first-order interference in two-dimensional and in circular porous-wall wind tunnels is summarized in Table IV. The porosity is assumed to be of such a value that the velocity interference due to solid blockage is zero at the position of the model. However, for every case shown, including the solid blockage case, the interference is a function of β/R and not of R alone, so that for constant interference R must be varied with Mach number. This is a serious disadvantage, theoretically at least, of the porous-wall wind tunnel.

With values of $\beta/R = 1.28$ for the two-dimensional tunnel and 1.22 for the circular tunnel which are suitable for reducing to zero the velocity interference due to solid blockage the velocity gradient interference due to wake blockage is also zero, as is shown in the Appendix.

The lift interference for the two-dimensional case is derived in the Appendix. With $\beta/R = 1.28$ both downwash and curvature are rather large and have the sign of the interferences in open and closed tunnels, respectively.

The lift interference for the circular tunnel was obtained from equations of reference 6, the downwash from equation (49), and the curvature from the x-derivative of equation (47) of that reference. The downwash is negligible but the curvature, of the same sign as that in the closed tunnel, is relatively large. It is not the lift interference, however, that imposes the most severe limitation on the size of the model.

The porous boundary condition imposes a velocity gradient interference due to solid blockage, a phenomenon that is not theoretically found for open, closed, or slotted tunnels. The expressions for the gradient given in Table II were obtained by taking the second x-derivatives of the applicable

potentials of reference 6 and substituting the appropriate values of β/R . The gradients are seen to increase very strongly, as $1/\beta^4$, with Mach number. An indication of the significance of these gradients with $\beta = 1$ is given by noting that for both the two-dimensional and the circular tunnels, the interference velocities, zero at the center of the model, are predicted to increase to the closed-tunnel value (at the center) in about 0.8 of the tunnel height or diameter. This distance receives in compressible flow the factor β , so that if the Prandtl-Glauert rule should be valid to high Mach numbers the gradient would be very large indeed. As may be seen from reference 30 for the two-dimensional case, the velocity gradient is large over a wide range of permeability factors, so that little possibility exists of any compromise to reduce the gradient.

As seen from Table IV, the porous tunnel designed for zero solid blockage velocity interference at the center of the model also suffers from a velocity interference due to wake blockage. The values, calculated from formulae derived in the Appendix, approximate half the magnitude of the wake-blockage velocity interference in the closed tunnel, but are opposite in sign. With somewhat greater values of β/R than those used in this investigation, the interference velocities due to wake blockage would tend to compensate those due to solid blockage. However, with models small enough to reduce the solid blockage velocity gradients to permissible values, the wake blockage is likely to be negligible.

In spite of the uncertainty of the boundary conditions in porous wind tunnels the theory is believed to give a valid indication of their behavior. In particular, the velocity gradient noted in the discussion of the very large model in the slotted tunnel is believed to be an example of that predicted for the porous tunnel. The gradient is believed to arise from the viscous effects associated with the flow through the slots. These effects would be expected to increase with increase in number and decrease in width of the slots.

The porous-wall tunnel is evidently not well suited for minimizing the boundary interference at subsonic speeds, for

- a. With given geometry of the wall the interference characteristics of the tunnel change with Mach number.
- b. The influence of the boundary layer on the performance of such a tunnel may be expected to be large.
- c. For such a wind tunnel, no matter what the porosity, theory indicates serious interference effects.
- d. Because of the uncertainty of the boundary conditions theoretical corrections cannot be applied.

To these theoretical disadvantages must be added the previously-mentioned difficulties of construction and operation of this type of tunnel. For purely subsonic testing, the slotted tunnel is much to be preferred.

On the other hand, the linearized subsonic theory is not applicable very near Mach number one and the porous-wall tunnel has the same advantage as the slotted tunnel with respect to the prevention of choking and with respect to operation through the speed of sound. The interference near sonic speeds must be determined by experiment. As will be seen in the next section, the porous wall has some advantage with respect to the supersonic interference, and if this advantage should prove decisive, the model could perhaps be made sufficiently small to render the subsonic interference tolerable.

TRANSONIC WIND TUNNELS AT SUPERSONIC SPEEDS

No such tunnel boundary interference theory exists for the supersonic operation of transonic wind tunnels as has been described for the subsonic operation. What few attempts have been made to calculate the supersonic interference, reference 32 for instance, involve such simplifications that the results are of doubtful reliability for actually computing the interference in specific cases. However, the general result of reference 32 that in a circular slotted tunnel the overall lift interference may not be excessively large is believed to be correct.

The supersonic interference possesses several characteristics not found in the subsonic interference:

(a) Positive velocity gradients tend to become localized along surfaces (shock waves).

(b) The boundary interference reflects the detailed flow disturbances due to the detailed shape of the model.

(c) An upstream part of the model, depending in extent on the stream Mach number, is completely free of any boundary interference.

The first boundary disturbance to reach the model is the reflection of the model bow wave. The extent of the interference-free region may be considerably less than would be computed by assuming a shock wave of vanishingly small intensity (Mach wave) making the angle $\sin^{-1} \frac{1}{M}$ with the tunnel velocity. Some experimental data showing the magnitude of this effect are given in reference 33. In addition, the interference-free region is further reduced by the upstream transmission of pressures through the boundary layer near the intersection of the reflected shock wave with the model. This effect may be appreciable, especially if the reflected shock intersects the rear of the model or a sting support, where the boundary-layer thickness may

be relatively large (see, for instance, refs. 34 and 35). The distance of the bow wave upstream from the nose must also be considered as is done in reference 33.

Inasmuch as disturbances in the supersonic flow are reflected from solid walls without change in kind (shock waves as shock waves, expansion waves as expansion waves) whereas the disturbances incident on open boundaries are changed in reflection to waves of the opposite kind, it seems reasonable to suppose that slotted walls might reduce supersonic as well as subsonic interference. In practice, the slotted walls are found to be beneficial, but their effectiveness is much reduced because of the localization of disturbance effects previously mentioned. The assumption of average boundary conditions is contrary in the supersonic case to physical reality. Thus, the shock wave arising from the reflection of the bow shock from a solid part of the boundary is inclined to the flow direction at a greater angle than is the expansion wave arising from the reflection of the same disturbance from a slot. Even if some average of the reflections could be made zero; therefore, a ripple characterized by an increase in pressure followed by a decrease would appear at the model.

An investigation of the nature of the supersonic interference in a slotted tunnel is reported in reference 33. Figure 9, which is reproduced from that reference, shows by means of schlieren photography and of the body surface pressure distribution the interference effect of the bow wave reflection. The pressure disturbances at the wall are also shown. The pressure increases at the shocks are evident.

Schlieren photography does not show clearly the part of the interference manifest as expansion waves, because these are spread out rather than concentrated. The expansions become evident, however, in figure 10, where the body pressure distributions obtained in the eight-foot slotted tunnel are

compared with those obtained in the sixteen-foot slotted tunnel. The sixteen-foot tunnel data are interference-free at Mach numbers greater than about 1.05, and the interference is believed to be small at lower Mach numbers.

As can be seen from figure 9, the model tested was properly small relative to the eight-foot tunnel. With larger models, the interference would be larger, but in an approximately circular tunnel, because of the tendency to focus disturbances toward the center, the effect of reduction in model size is not as large as might be expected. The principal benefit of decrease in model size arises from the decrease in the Mach number for which the model becomes completely interference-free. With respect to shock wave reflection, this effect is doubly important, however, because of the decrease of shock wave intensity with decrease in Mach number.

The interference could be spread out to achieve some of the effects of average boundary conditions and of the average interference characteristic of subsonic flow by testing in square rather than circular tunnels. However, because of the solid side walls, the tunnel with only top and bottom walls slotted does not appear to be well suited interference-wise for testing three-dimensional models at low supersonic speeds. Also, in this case, the schlieren system will normally be improperly oriented for detecting reflections from the side walls.

Interference disturbances such as those seen in figures 9 and 10 evidently need not in themselves cause any substantial effect on the model force coefficients. Thus, a wave having no net change in velocity would be expected to have an entirely negligible effect on drag if it should intersect the mid-section of the body, where the streamwise slopes of the surface are small. The smallness of the effects of some such disturbances are shown in reference 36. On the other hand, it is clear that if a reflected disturbance should strike

a tail surface, the moment might be appreciably falsified. Similarly, the drag might be falsified if a reflected disturbance should strike near the tail or trailing edge of a model. The supersonic interference effects may therefore be expected to be quite irregular with respect to both model configuration and Mach number. These effects should be considered in any tests planned to detect or to investigate the supersonic interference. The smallness or absence of supersonic interference found in certain test results may in some cases be the result of crudeness of the tests or of insensitivity of measurement.

In order to achieve at least approximately the average uniform boundary condition and to cancel the disturbances in the vicinity of the wall, porous walls, walls with many small slots, and perforated walls have been considered. As might be expected, the operation of such walls is strongly affected by the boundary layer. In addition, as pointed out in reference 37, the slotted tunnel is affected by transmission of pressure upstream in the slots.

These boundary-layer and slot effects complicate the reflection and again lead to compressions followed by expansions. The expansions may be quite large if the boundary layer is of considerable thickness, and are then followed by further compression after the boundary-layer thickness has been reduced by flow through the wall. (See, for instance, ref. 24). As has already been pointed out, the increasing thickness of the boundary layer in regions of inflow, as would exist behind a single expansion wave for instance, greatly increases the effective porosity of the wall, so that in such regions the porous wall may perform as an almost open wall. These effects can be reduced by converging the walls and drawing off the greater part of the boundary layer; but this procedure is rather inconvenient and introduces the danger of producing a pressure gradient in the tunnel by improper adjustment of convergence and suction.

On the assumption that the average velocity normal to the wall is a linear function of the pressure difference across it and that the behavior of the wall can be characterized by a permeability factor R , the value of R required for shock cancellation is easily derived. Such a derivation is given in reference 38, where the required value of R is found to be equal to the cotangent of the shock angle. It is thus a function both of the Mach number and of the shock strength. However, with small three-dimensional models, the shocks and expansion waves reaching the walls are expected to be relatively weak, and as the shock strength approaches zero, the required value of R is shown to approach the compressibility factor β . (The experimental results of reference 25 tend to confirm this theory.) Since, as concluded hereinbefore, the permeability factor depends almost solely on the geometry of the wall, it seems that a given wall is suitable for only one Mach number. On the other hand, the Mach number range over which small models (relative to tunnel size) are subject to supersonic interference is small. Moreover, near Mach number one, the interference is small, so that if the porosity is adjusted for zero reflection of the bow wave at a Mach number near the upper end of the range, the interference may be negligible at all supersonic Mach numbers. With properly small models, the minimization of the interference due to bow wave reflection therefore appears possible.

The cancellation of the bow wave is evidently insufficient of itself to assure freedom from boundary interference. Other disturbances produced by the model, both shock and expansion waves, must be considered. The cancellation of each disturbance as it intersects the wall is no simple matter, even for a single stream Mach number and without any consideration of boundary-layer effects, because the permeability factor is required to vary along the wall opposite the model. In two dimensions, because of the unique relation between velocity and flow angle, this variation is not large, but in three

dimensions, for which no such relation exists, the variation is great and even a negative value of R may be required, as can be seen from figure 4 of reference 25.

Even if cancellation of disturbances is assumed, the boundary interference does not thereby become zero; because in the unrestricted flow part of the field outside the position of the walls influences the model in other ways than simply permitting free transmission of the disturbances, and this influence must be adequately represented.

These effects have been investigated by Mr. Clarence Matthews of the NASA Langley Research Center. In this investigation, the restricted and unrestricted flow fields about two- and three-dimensional models were calculated numerically by characteristics methods. The two-dimensional model assumed was a symmetrical 10-percent-thick almost parabolic airfoil blocking approximately 24 percent of the two-dimensional tunnel in which it was placed. The three-dimensional model consisted of a 17.5° (half-angle) nose cone followed by an infinite circular cylinder. This model blocked approximately 1.8 percent of the cross section of the circular tunnel in which it was placed.

For the two-dimensional model, the calculated distributions of pressure coefficient with various tunnel boundary conditions are shown in figure 11. The non-reflecting wall with Prandtl-Meyer expansion outside the walls yields pressure coefficients practically the same as obtained with the free-field boundary condition. The effect of the cut-off part of the flow field is therefore adequately represented by neglecting any disturbances returned from that part of the field to the model and simply cancelling each disturbance wave at its intersection with the wall. This result is to be expected from the fact that the flow about an airfoil in supersonic flow is approximately given by assuming a Prandtl-Meyer expansion downstream from the attached

bow wave. To achieve the cancellation of disturbances with free-stream pressure behind the walls, the permeability factor R is required to be a function of the local Mach number at the wall and must therefore vary both with free-stream Mach number and with position along the wall. However, even with a constant porosity designed to cancel the bow shock, the interference is seen to be quite small in contrast to the very large interference shown for the open boundary case.

In two dimensions, the major difficulties appear to be connected with the required variation of permeability and with the previously-discussed boundary-layer effects. Since over the part of the boundary downstream from the position of bow-wave intersection the permeability for non-reflectivity is required to increase, some downstream increase in boundary-layer thickness may be beneficial. Moreover, since the expansion waves, which are characteristic of this region, are spread out rather than concentrated, any such benefit can be realized without the complications previously noted in connection with the intersection of the bow wave with a wall containing a boundary layer. If the ripple caused by the shock wave-boundary layer interaction can be tolerated, some of the variation with stream Mach number of the permeability required to cancel the bow wave can be achieved by controlling the boundary-layer thickness as suggested in reference 25.

For the three-dimensional model, the pressure distributions at the surface of the model in the presence of various non-reflecting walls are shown in figure 12. Although the results for the three-dimensional model are rather crude, because of practical limitations on the fineness of the computational characteristic net, they show clearly the influence (in addition to allowing free transmission of the disturbances) of the part of the flow field outside the wall position. The assumption of non-reflectivity is seen to be entirely insufficient to assure non-interference. The assumption of constant velocity

and flow angle across the wall is equivalent to cutting off all disturbances from the outside flow. In the absence of the compressing effect of this part of the flow field, the pressures over the part of the model subject to interference are too low. The conical-shock case, on the other hand, allows some influence of the outside field, but does not include the effect of decrease of intensity of the bow shock with distance outward from the position of the wall. In this case, the correct pressures are much more closely approximated. The third assumption, that the change of velocities and angles with distance along characteristic lines is constant across the boundary, leads to decreasing velocity in the outside field and a corresponding positive pressure gradient on the model.

In practical model testing, the outside flow field is unknown, and in any case, an accurate representation of its effect on model characteristics does not seem likely. Nevertheless, if the model is kept small relative to the tunnel size, the maintenance of stream static pressure outside of perforated tunnel walls may provide a reasonably good approximation to the average influence of the part of the free field outside the position of the tunnel boundary.

The effects of two different porous walls are shown in figure 13. In both cases constant, free-stream pressure is assumed outside the porous walls. As could be expected because of the large variation along the wall of the permeability required for interference-free flow in the three-dimensional case, the disturbances with the constant-porosity wall are large. However, these disturbances are soon damped out and the pressure at the model returns to the free-stream value maintained outside the walls.

For the slant-hole wall, in simulation of the possible physical behavior, the shock-cancellation value of permeability was assumed for the region of the wall opposite the forward part of the body, where outflow through the wall


is required, whereas over the part requiring inflow an average of the values required for zero interference was assumed. In this case, the disturbance to the flow is even larger and does not damp out so rapidly downstream. The large disturbance is due to the mis-match of the assumed permeability with that required in the region of intersection with the wall of the strong expansion wave arising from the corner at the juncture of the cone with the cylinder of the body. Perhaps the principal advantage to be obtained from the slant holes lies in their use to prevent too large increase of effective permeability in regions of inflow. In this connection, it should be noted that in the three-dimensional case, even if the permeability distribution were correct for non-interference, it would in most places not be correct for the cancellation of superposed disturbances. Moreover, the distribution of permeability required for non-interference would be different for every different model and for every different Mach number. Even without consideration of the additional practical problems, it is evident that interference-free wind-tunnel testing of three-dimensional models is quite unlikely.

Nevertheless, the interference due to reflection of the bow wave can be greatly reduced and with sufficiently small models, the total interference may be reduced to tolerable values. In a square tunnel, the disturbances would be less concentrated than in the circular tunnel, for which figure 13 applies. Moreover, a model with smaller streamwise curvature of the surface than that at the cone-cylinder juncture would cause less concentrated expansion disturbances, and the required variation of permeability factor would be less.

For practical testing, a compromise between slotted and perforated tunnels such as used in reference 39 may be acceptable. In any case, the tendency of the interference disturbances to accumulate locally and the consequent possibility of large and irregular effects on the model coefficients, especially moment coefficients, should be remembered.

EXAMPLES AND COMPARISONS

Comparisons of the results of testing different models in the same transonic wind tunnel and of testing the same or similar models in transonic tunnels of different size or in free flight will give some appreciation of the interference effects to be expected in practical model testing and of the limitations on model size required to keep such interference small. Such a comparison for the surface pressures on a body of revolution have already been shown in figure 10. From the same source, reference 33, the drag coefficients for the body of revolution are shown in figure 14. The drag coefficients in the Langley 8-foot transonic tunnel were obtained from both force tests and pressure distributions. These data are compared with data obtained on approximately the same body shape in free-fall tests and on the same body in the Langley 16-foot transonic tunnel. Both the 8-foot and 16-foot tunnels were approximately circular and slotted to give open-ratios slightly too great for zero solid blockage interference. In spite of the relatively small size of the model with respect to the 8-foot tunnel, about 0.14 percent area blockage and length about 0.8 of the tunnel radius, some supersonic interference is seen to be present. This interference can be explained, except for the uncertain region just above Mach number one, as due to the passage of the bow-wave reflection over first the forward and then the rearward part of the model. With an off-center location of the model, the interference is seen to be reduced. This reduction is taken to indicate that a square tunnel cross section would be preferable to the circular cross section for supersonic testing. The model size is considered to be sufficiently small for most testing in the 8-foot tunnel.

Some comparison tests for a wing alone are reported in reference ⁴¹ . Examples of the results of these tests are shown in figures 15 and 16, where

lift and pitching-moment characteristics in a 4.5 x 6.25-inch tunnel are compared with similar data obtained from tests of the same side-wall-mounted wing in a 7- by 10-foot closed tunnel. The wing was mounted next to the solid wall with the semispan in the direction of the greater dimension of the tunnel. The walls above and below the wing surface in the small tunnel were then slotted with two different open ratios, $1/5$ or $1/8$, or were open or closed as indicated in figures 15 and 16. The wing semispan was 4.24 inches, its mean-aerodynamic chord 2.17 inches, and its half-area 9 square inches. In spite of the large size of the wing relative to that of the small tunnel, the lift in the slotted tunnel with open-ratio $1/8$ is seen to be not much different from that in the 7- by 10-foot tunnel, whereas with open or with closed boundaries the difference is great. Figure 16 shows that, as might have been expected, the differences in pitching moment are greater than those in lift. Because of the large number of slots used, the theoretical characteristics of the slotted walls used in these tests are almost the same as those of open boundaries. However, partly because of the large number of slots and partly because of the large depth of the slots, slot-width-to-depth ratios 0.074 and 0.132, the slotted-wall theory is not applicable, and the walls are believed to partake more of porous-wall than of slotted-wall characteristics. All that figure 15 shows, therefore, is that with such boundaries the lift interference can be greatly reduced.

Some comparisons of 8-foot and 16-foot slotted tunnel tests of a body with sweptback wings are given in reference ⁴² ~~41~~. Both tunnels, of approximately circular cross-section, were slotted to give an open-ratio slightly too great for zero solid-blockage interference. The body fuselage for these tests was approximately 32.6 inches in length and 3.33 inches in maximum diameter. The wing was of semispan 12 inches, its mean-aerodynamic chord 6.25 inches, area 1 square foot, sweepback 45° , and taper ratio 0.6. The

size of this model is representative of the sizes of models ordinarily tested in the Langley 8-foot transonic tunnel. The results of the tests of this model are also compared with data from tests of a geometrically similar model three times its size in the Langley 16-foot transonic tunnel. Comparisons for lift, drag, and pitching-moment coefficients are given in figures 17, 18, and 19, respectively. Except at the largest angles of attack, the interferences on the small model appear to be small. In these cases, differences that can certainly be assigned to boundary interference rather than to measurement errors appear only at near-sonic or supersonic speeds. The sweepback of the wings is perhaps favorable in lessening and in spreading out the effects of the supersonic interference. Even with the larger model in the 16-foot tunnel the interferences are not large, but this model is perhaps larger than should ordinarily be tested at Mach numbers near one in a tunnel of this size.

Some unpublished lift and moment data obtained for a large complete model tested in the Langley 16-foot transonic tunnel and in the Langley 8-foot transonic pressure tunnel are compared in figures 20 and 21. The approximately circular tunnel, 16-foot, was slotted as described in the next preceding paragraph. The square 8-foot pressure tunnel had four shaped slots in each of the top and bottom walls with average open ratio opposite the model approximately 7.9 percent for each wall. The model, mounted at the center with wing span perpendicular to the solid side walls of the tunnel, was very large relative to the size of the 8-foot tunnel. Its length was about 86-percent and its span almost 64-percent of the width of the tunnel. Its frontal area was 0.96 percent and its wing area 7.6 percent of the tunnel cross-sectional area. Because of the large power requirement, the model was tested at 0.4 atmosphere total pressure in the 8-foot pressure tunnel rather than at 1 atmosphere as in the 16-foot tunnel. In spite of the large size of

the model, the differences between 8-foot and 16-foot tunnel results are not large. As expected, the moments show larger differences than the lift. The theoretical streamline curvature in the 8-foot tunnel is practically negligible, but the downwash due to lift interference at subsonic speeds requires a theoretical angle-of-attack correction of about $-0.2C_L$ degrees. The application of this correction would evidently improve the 8-foot tunnel results. At supersonic speeds, the lift interference seems to be less than at subsonic speeds.

It is remarkable that in all the applicable test results examined, the interference in transonic wind tunnels does not increase with approach to Mach number 1 as suggested by the (inapplicable) linearized subsonic theory. This behavior is of great importance for the usefulness of transonic tunnels and also suggests the possibility of small interference near Mach number one for small models tested in tunnels designed primarily to reduce the supersonic interference. Tests of winged models in such a tunnel are described in reference 39.

In these tests, models of three different sizes were placed in a 2- by 2-foot tunnel having walls containing many narrow streamwise strips of swept perforated material to give an open-ratio of 6 percent. Such a tunnel may be regarded as a compromise between the slotted tunnel and the porous-wall tunnel. The reader is referred to reference 39 for details of models, tunnels, and tests. For this tunnel, a large reduction was obtained in boundary interference compared to that in a closed tunnel. With a model blocking 0.51 percent of the tunnel cross-sectional area, the interference was found tolerable at all test Mach numbers (0.6 to 1.3). It is not clear, however, except perhaps in the matter of lower power requirements, that a tunnel of this type is superior to a slotted tunnel of the same cross-sectional shape, even for supersonic testing. The performance of the walls used is

not theoretically predictable; and the open-ratio required was determined from experiment.

In comparing boundary-interference data from different wind tunnels, it should be remembered that the detection of interference is dependent on the accuracy of measurement and that the measurement accuracy is likely to be less for small than for large models. For these reasons, tunnel boundary interference from the larger facilities is in general considered more reliable.

CONCLUSIONS

1. For Mach numbers well below one, coarsely slotted tunnels, which are relatively easy to build and operate, are extremely effective in reducing the boundary interference even with very large models. The permissible model size is somewhat limited, however, by the fact that the lift interference is not reduced to zero for the same wall geometry as is required for zero blockage and that because of viscous effects, a residual pressure gradient exists.
2. Perforated tunnels, which involve difficulties in construction and operation, operate much like porous-wall tunnels, and the interference characteristics with given geometry therefore change with Mach number. The interference in such tunnels is further characterized by relatively large pressure gradients. Perforated tunnels are for these reasons unsuited for testing large models at subsonic speeds.
3. Slotted tunnels with many slots partake strongly of the nature of porous-wall tunnels.
4. At Mach numbers well below one, theoretical corrections are approximately applicable for the interference in coarsely slotted but not in finely slotted or perforated tunnels.
5. Both perforated and slotted boundaries eliminate the tunnel choking near Mach number 1.
6. In transonic tunnels designed for small boundary interference, the interference does not increase with approach to Mach number one as predicted by the linearized subsonic theory, but remains small. With properly small models, therefore, both slotted and perforated tunnels are suitable for Mach numbers near one.
7. The perforated tunnel is believed to have some advantage over the slotted tunnel for the prevention of shock-wave reflection, but its performance

is strongly affected by the wall boundary layer.

8. The practical removal of the supersonic interference on a two-dimensional model over a small range of Mach numbers appears possible by use of perforated walls.

9. For three-dimensional models, the removal of the supersonic interference does not appear practical, but it can be greatly reduced. The models must therefore be small relative to the tunnel size.

10. The supersonic interference is irregular, and care must therefore be exercised in supersonic testing to locate any Mach numbers for which excessive interference may be present. The moments are particularly sensitive to such interference.

11. For reducing and spreading out the effects of the supersonic interference, the rectangular test section is preferable to that of circular shape.

REFERENCES

1. Katzoff, S., and Barger, Raymond L.: Boundary-Induced Downwash Due to Lift in a Two-Dimensional Slotted Wind Tunnel. NACA TN 4289, 1958.
2. Glauert, H.: Wind Tunnel Interference on Wings, Bodies and Airscrews. R & M No. 1566, British A.R.C., 1933.
3. Allen, H. Julian, and Vincenti, Walter G.: Wall-Interference in a Two-Dimensional-Flow Wind Tunnel with Consideration of the Effect of Compressibility. NACA TR No. 782, 1944.
4. Goethert, P.: Wind-Tunnel Corrections at High Subsonic Speeds Particularly for an Enclosed Circular Tunnel. NACA TM 1300, 1952.
5. Baranoff, A. v.: Tunnel Correction for Compressible Subsonic Flow. NACA TM No. 1162, 1947.
6. Baldwin, Barrett S., Jr., Turner, John P., and Knechtel, Earl D.: Wall Interference in Wind Tunnels with Slotted and Porous Boundaries at Subsonic Speeds. NACA TM 3176, 1954.
7. Herriot, John G.: Blockage Corrections for Three-Dimensional-Flow Closed-Throat Wind Tunnels, with Consideration of the Effect of Compressibility. NACA TR 995, 1950.
8. Ludwig, H.: Widerstandskorrektur in Hochgeschwindigkeitskanälen. Deutsche Luftfahrtforschung Forschungsbericht Nr. 1955, 1944.
9. Katz, Ellis: Flight Investigation From High Subsonic to Supersonic Speeds to Determine the Zero-Lift Drag of a Transonic Research Vehicle Having Wings of 45° Sweepback, Aspect Ratio 4, Taper Ratio 0.6, and NACA 65A006 Airfoil Sections. NACA RM L9H30, 1949.
10. Thompson, Jim Rogers: Measurements of the Drag and Pressure Distribution on a Body of Revolution Throughout Transition from Subsonic to Supersonic Speeds. NACA RM L9J27, 1950. *checked*
11. Kurbjun, Max C., and Thompson, Jim Rogers: Transonic Drag Characteristics and Pressure Distribution on the Body of a Wing-Body Combination Consisting of a Body of Revolution of Fineness Ratio 12 and a Wing Having Sweepback of 45° , Aspect Ratio 4, Taper Ratio 0.6, and NACA 65A006 Airfoil Sections. NACA RM L52E12, 1952. *checked*
12. Donlan, Charles J., Meyers, Boyd C., II, and Mattson, Axel T.: A Comparison of the Aerodynamic Characteristics at Transonic Speeds of Four Wing-Fuselage Configurations as Determined from Different Test Techniques. NACA RM L50H02, 1950. *checked*
13. Preston, J. H., and Sweeting, N. E.: The Experimental Interference on a Large Chord Symmetrical Joukowski Aerofoil Spanning a Closed Tunnel. R & M No. 1997. British ARC, 1942.

14. Theodorsen, Theodore: The Theory of Wind-Tunnel Wall Interference. NACA Rep. 410, 1931.
15. Wieselsberger, Carl: Über den Einfluss der Windkanalbegrenzung auf den Widerstand insbesondere im Bereiche der kompressiblen Strömung. Luftfahrtforschung, Bd. 19, Lfg. 4, May 6, 1942, pp. 124-128.
16. Wright, Ray H., and Ward, Vernon G.: NACA Transonic Wind-Tunnel Test Sections. NACA Rep. 1231, 1955.
17. Davis, Don D., Jr., and Moore, Dewey: Analytical Study of Blockage and Lift-Interference Corrections for Slotted Tunnels Obtained by the Substitution of an Equivalent Homogeneous Boundary for the Discrete Slots. NACA RM L53E07b, 1953. *Unclassified*
18. Katzoff, S., Gardner, Clifford S., Diesendruck, Leo, and Eisenstadt, Bertram J.: Linear Theory of Boundary Effects in Open Wind Tunnels with Finite Jet Lengths. NACA Rep. 976, 1950.
19. Guderley, Gottfried: Wall Corrections for a Wind Tunnel with Longitudinal Slots at Subsonic Velocities. WADC Tech. Rep. 54-22, 1954. *Unclassified*
20. Berndt, Sune B.: Theoretical Aspects of the Calibration of Transonic Test Sections. Report 74. Swedish FFA, 1957.
21. Pistolesi, E.: On the Interference of a Wind Tunnel With a Mixed Boundary. Cornell Aero. Lab., Inc., Dec. 1949. (From Commentationes, Pont. Acad. Sci., Anno IV, vol. IV, No. 9, 1940). *Unclassified*
22. Maeder, P. F.: Theoretical Investigation of Subsonic Wall Interference in Rectangular Slotted Test Sections, Tech. Rept. WT-11, Brown University, 1953. *Unclassified*
23. Maeder, P. F., Anderson, G. F., and Carroll, J. B.: Experimental Investigation of Subsonic Wall Interference in Rectangular Slotted Test Sections. Tech. Note WT-16, Brown University, 1955. *Unclassified*
24. Goethert, B. H.: Flow Establishment and Wall Interference in Transonic Wind Tunnels. AEDC-TR-54-44, 1954. *Unclassified*
25. Spiegel, Joseph M., Tunnell, Phillips J., and Wilson, Warren S.: Measurements of the Effects of Wall Outflow and Porosity on Wave Attenuation in a Transonic Wind Tunnel with Perforated Walls. NACA TN 4360, 1958. *Unclassified*
26. Goodman, Theodore R.: The Porous Wall Wind Tunnel. Part II: Interference Effect on a Cylindrical Body in a Two-Dimensional Tunnel at Subsonic Speed. Report No. AD-594-A-3. Cornell Aero. Lab., Inc., 1950. *Unclassified*
27. Stokes, George M., Davis, Don D., Jr., and Sellers, Thomas E.: An Experimental Study of Porosity Characteristics of Perforated Materials in Normal and Parallel Flow. NACA TN 3085, 1954.
28. Maeder, P. F.: Some Aspects of the Behavior of Perforated Transonic Wind Tunnel Walls. Tech. Rept. W7-15. Brown University, 1954. *Unclassified*

29. Goodman, Theodore R.: The Porous Wall Wind Tunnel. Part IV: Subsonic Interference Problems in a Circular Tunnel. Report No. AD-706-A-2, Cornell Aeronautical Laboratory, Inc., 1951. *Uncl Conf.*
30. Kassner, Rudolf R.: Subsonic Flow Over a Body between Porous Walls. WADC Tech. Rep. 52-9, 1952. *Uncl.*
31. Spiegel, Joseph M., and Tunnell, Phillips J.: An Analysis of Shock-Wave Cancellation and Reflection for Porous Walls Which Obey an Exponential Mass-Flow Pressure-Difference Relation. NACA TN 3223, 1954.
32. Mikami, Kinya: Wall Corrections for Transonic Wind Tunnels. Part II: Some Aspects of Wall Interference Effects of a Supersonic Slotted-Throat Wind Tunnel. TACP Report 9, 1954. *Uncl.*
33. Wright, Ray H., Ritchie, Virgil S., and Pearson, Albin O.: Characteristics of the Langley 8-Foot Transonic Tunnel with Slotted Test Section. NACA Rep. 1389, 1958.
34. Daniels, Lloyd E.: Effects of the Upstream Influence of a Shock Wave at Supersonic Speeds in the Presence of a Separated Boundary Layer. WADC TR 54-31, 1954. *Uncl.*
35. Love, Eugene S.: A Summary of Information on Support Interference at Transonic and Supersonic Speeds. NACA RM L53K12, 1954. *Uncl.*
36. Ritchie, Virgil S.: Effects of Certain Flow Nonuniformities on Lift, Drag, and Pitching Moment for a Transonic-Airplane Model Investigated at a Mach Number of 1.2 in a Nozzle of Circular Cross Section. NACA RM L9E20a, 1949. *Uncl.*
37. Allen, H. J., and Spiegel, J. M.: Transonic Wind Tunnel Development at the NACA. Institute of the Aeronautical Sciences publication. SMF Fund Paper No. FF-12, 1954. *Uncl.*
38. Goodman, Theodore R.: The Porous Wall Wind Tunnel. Part III: The Reflection and Absorption of Shock Waves at Supersonic Speeds. Rept. No. AD-706-A-1, Cornell Aero. Lab., Inc., 1950. *Uncl. Conf.*
39. Spiegel, Joseph M., and Lawrence, Leslie F.: A Description of the Ames 2- by 2-Foot Transonic Wind Tunnel and Preliminary Evaluation of Wall Interference. NACA RM A55I21, 1956. *Uncl.*
40. Young, A. D.: The Calculation of the Total and Skin Friction Drags of Bodies of Revolution at Zero Incidence. R & M No. 1874, British ARC, 1939.
41. Sleeman, William C., Jr., Klevatt, Paul L., and Linsley, Edward L.: Comparison of Transonic Characteristics of Lifting Wings from Experiments in a Small Slotted Tunnel and the Langley High-Speed 7- by 10-Foot Tunnel. NACA RM L51F14, 1951. *Uncl.*
42. Whitcomb, Charles F., and Osborne, Robert S.: An Experimental Investigation of Boundary Interference on Force and Moment Characteristics of Lifting Models in the Langley 16- and 8-Foot Transonic Tunnels. NACA RM L52L29, 1953. *Uncl.*

43. Osborne, Robert S., and Mugler, John P., Jr.: Aerodynamic Characteristics of a 45° Sweptback Wing-Fuselage Combination and the Fuselage Alone Obtained in the Langley 8-Foot Transonic Tunnel. NACA RM L52E14, 1952. *Unclass.* ✓

44. Hallissy, Joseph M., and Bowman, Donald R.: Transonic Characteristics of a 45° Sweptback Wing-Fuselage Combination. Effect of Longitudinal Wing Position and Division of Wing and Fuselage Forces and Moments. NACA RM L52K04, 1952. *Unclass.* ✓

TABLE I.- FIRST-ORDER BOUNDARY INTERFERENCE IN TWO-DIMENSIONAL AND IN CIRCULAR WIND TUNNELS WITH OPEN AND WITH CLOSED BOUNDARIES

Kind of interference	Value for incompressible flow				Compressibility factor	References
	Two-dimensional closed	Two-dimensional open	Circular closed	Circular open		
Downwash at model in presence of bound lift vortex	0	$-v^* = \frac{\Gamma}{4h}$			1	2 and appendix
Streamline curvature at model in presence of bound lift vortex	$\frac{1}{V} \frac{\partial v^*}{\partial x} = \frac{\pi \Gamma}{48h^2 V}$	$\frac{1}{V} \frac{\partial v^*}{\partial x} = \frac{-\pi \Gamma}{24h^2 V}$			$\frac{1}{\beta}$	2, 3, 4, and appendix
Downwash at model in presence of trailing vortices			$-v^* = \frac{-\Gamma s}{2\pi r_0^2}$	$-v^* = \frac{\Gamma s}{2\pi r_0^2}$	1	2, 4, 5, and 6
Induced velocity at model in x-direction in presence of doublet	$u^* = \frac{\pi m}{24h^2}$	$u^* = \frac{-\pi m}{48h^2}$	$u^* = \frac{2.4m}{2\pi^2 r_0^3}$	$u^* = \frac{-0.63m}{2\pi^2 r_0^3}$	$\frac{1}{\beta^3}$	2, 3, 4, 5, 6, and 7
Induced velocity at model in x-direction in presence of source	$u^* = \frac{b}{4h}$	0	$u^* = \frac{b}{2\pi r_0^2}$	0	$\frac{1 + (\gamma - 1)M^2}{\beta^2}$	3, 4, 7, and appendix
Velocity gradient at model in x-direction in presence of source	$\frac{\partial u^*}{\partial x} = \frac{\pi b}{24h^2}$	$\frac{\partial u^*}{\partial x} = \frac{-\pi b}{48h^2}$	$\frac{\partial u^*}{\partial x} = \frac{2.4b}{2\pi^2 r_0^3}$	$\frac{\partial u^*}{\partial x} = \frac{-0.63b}{2\pi^2 r_0^3}$	$\frac{1 + (\gamma - 1)M^2}{\beta^3}$	3, 7, 8, and appendix

h is half height of tunnel
r₀ radius of circular tunnel
s half distance between trailing vortices
m_l doublet strength for incompressible flow
b source strength for incompressible flow

Note that h and s represent half the value of corresponding quantities used in some of the references.

¹In the two-dimensional case part of the compressibility factor is sometimes applied to the doublet strength, which then becomes m/β .


TABLE II.- THEORETICAL FIRST-ORDER BOUNDARY INTERFERENCE

WITH A SMALL MODEL IN A CIRCULAR WIND TUNNEL

WITH UNIFORMLY SPACED STREAMWISE SLOTS.

DESIGNED FOR ZERO SOLID

BLOCKAGE INTERFERENCE

Kind of interference	Quality factor k 	References
Downwash at model in presence of lift	-0.27	6 and 17
Streamline curvature at model in presence of lift	-0.01	19
Induced velocity at model in x-direction in presence of doublet	0	6, 17, and 19
Induced velocity at model in x-direction in presence of source	0	19 and appendix
Velocity gradient at model in x-direction in presence of source	0	19 and appendix

k is factor by which closed tunnel interference must be multiplied to obtain slotted tunnel interference.



TABLE III.- THEORETICAL FIRST-ORDER BOUNDARY INTERFERENCE WITH A SMALL MODEL IN

SQUARE WIND TUNNEL HAVING SLOTTED TOP AND BOTTOM WALLS

AND SOLID SIDE WALLS. THE EQUALLY SPACED

SLOTS ARE DESIGNED FOR ZERO

SOLID BLOCKAGE

Kind of interference	Quality factor k or k'		References
	Two-dimensional 	Three-dimensional 	
Downwash at model in presence of lift	$k' = 0.46$	$k = -0.63$	1, 17, 22, 23, and appendix
Streamline curvature at model in presence of lift	$k = -0.20$	-0.28	23 and appendix
Induced velocity at model in x-direction in presence of doublet	0	0	6, 17, and 22
Induced velocity at model in x-direction in presence of source	0	0	17, 22, and appendix
Velocity gradient at model in x-direction in presence of source	0	0	17, 22, and appendix

k and k' are factors by which interference in closed and open tunnels, respectively, must be multiplied to obtain slotted tunnel interference.

TABLE IV.- THEORETICAL FIRST-ORDER BOUNDARY INTERFERENCE WITH SMALL MODELS

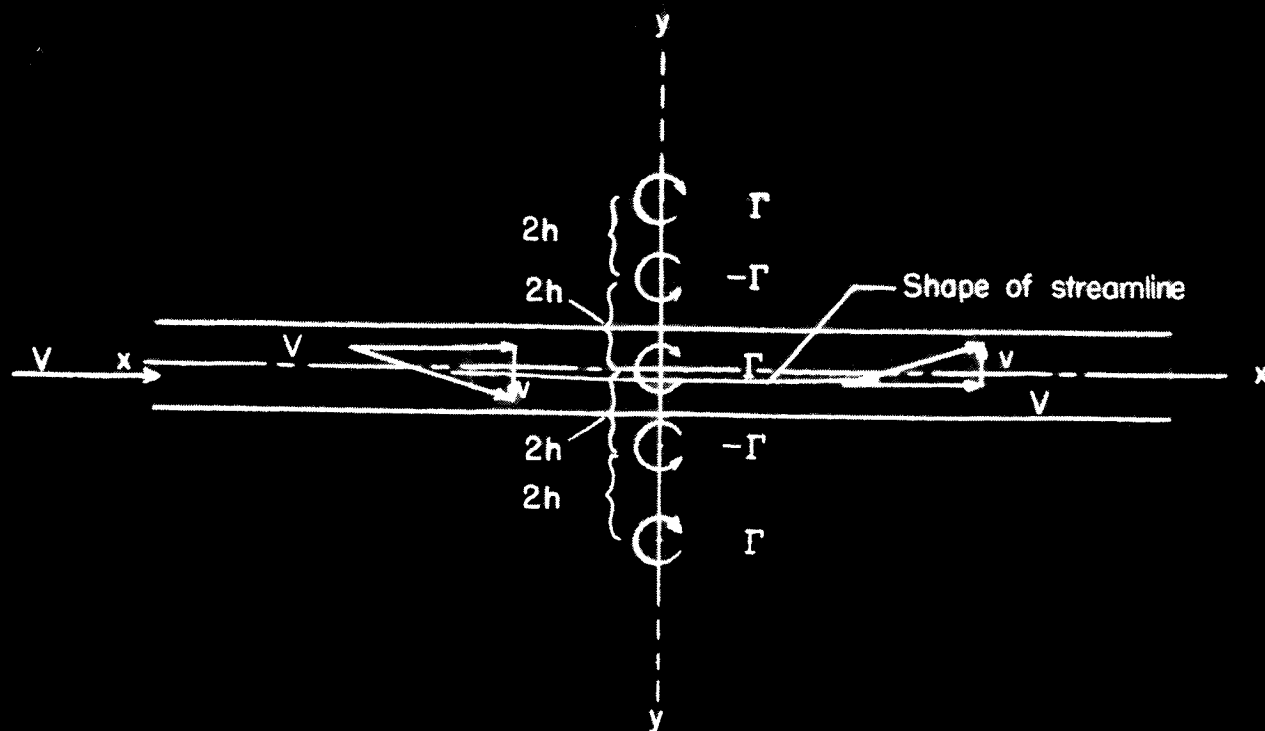
IN TWO-DIMENSIONAL AND IN CIRCULAR WIND TUNNELS WITH UNIFORMLY POROUS

BOUNDARIES. POROSITY DESIGNED FOR ZERO VELOCITY INCREMENT AT

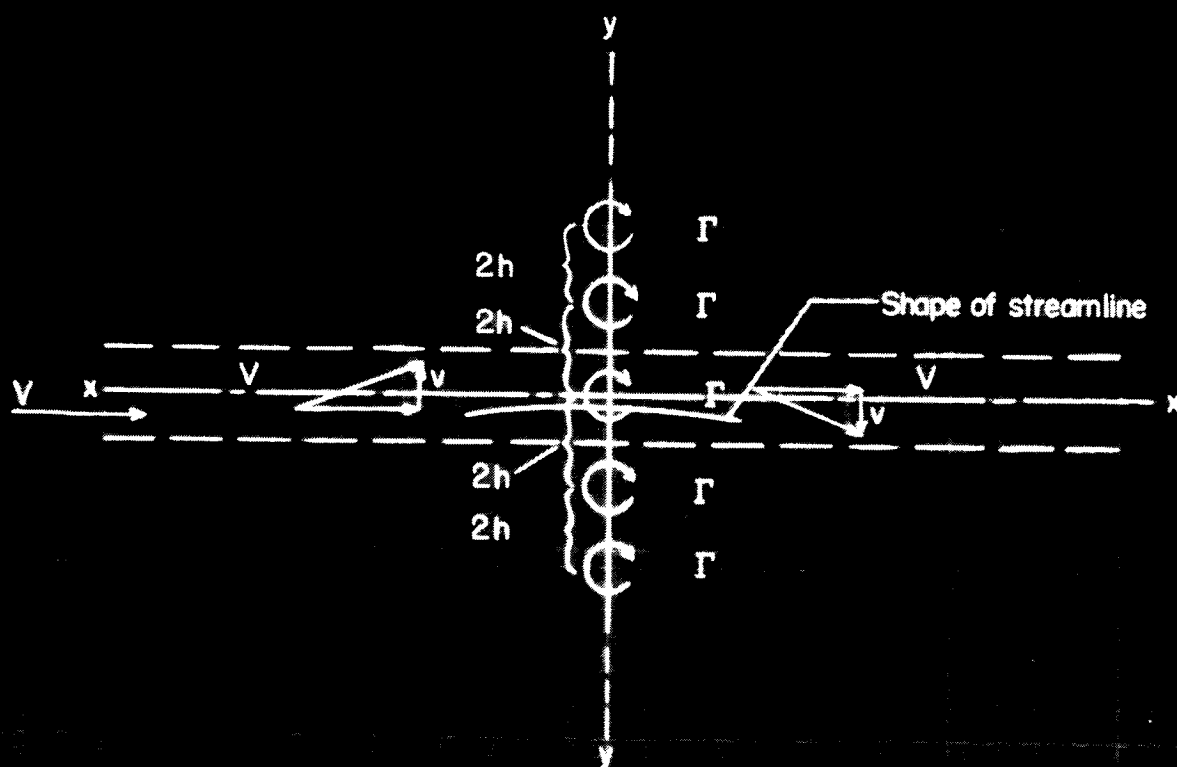
MODEL DUE TO SOLID BLOCKAGE

Kind of interference	Values		References
	Two-dimensional	Circular	
Downwash at model due to lift interference	$k' = 0.42$	$k = 0.037$	6, 29, and appendix
Streamline curvature at model due to lift interference	$k = 0.45$	$k = 0.60$	6 and appendix
Induced velocity in x-direction at model due to solid blockage interference	0	0	6, 26, 29, and 30
Velocity gradient in x-direction at model due to solid blockage interference	$\frac{\partial u^*}{\partial x} = \frac{0.50b}{2\pi\beta^4 h^3}$	$\frac{\partial u^*}{\partial x} = \frac{1.47m}{2\pi^2\beta^4 r_0^4}$	6 and 30
Induced velocity in x-direction at model due to interference in presence of source	$k = -0.56$	$k = -0.43$	Appendix
Velocity gradient in x-direction at model due to interference in presence of source	0	0	Appendix

k and k' are factors by which interference in closed and open tunnels, respectively, must be multiplied to obtain porous tunnel interference.

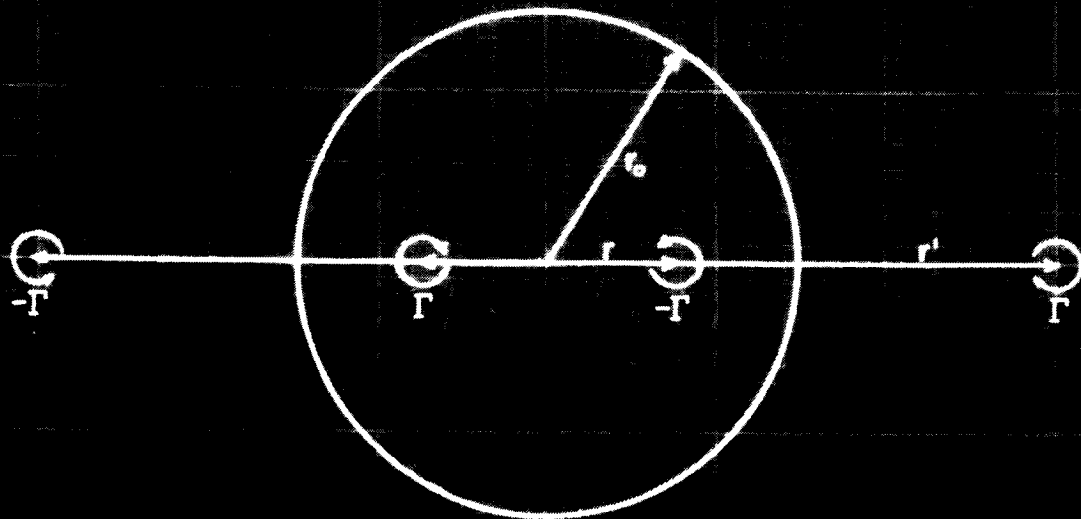


(a) Closed tunnel.

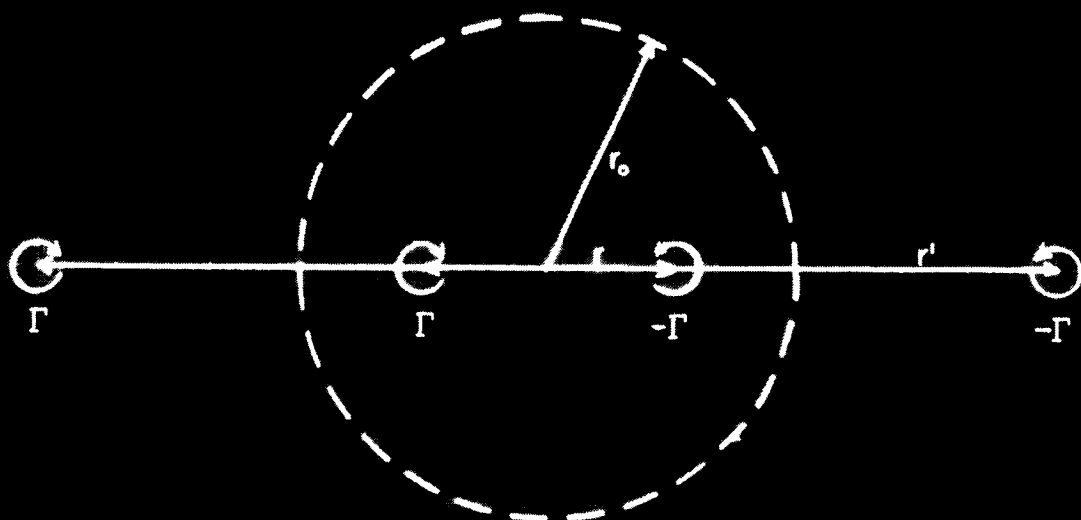


(b) Open tunnel.

Figure 1.- Lift vortex in two-dimensional tunnel.

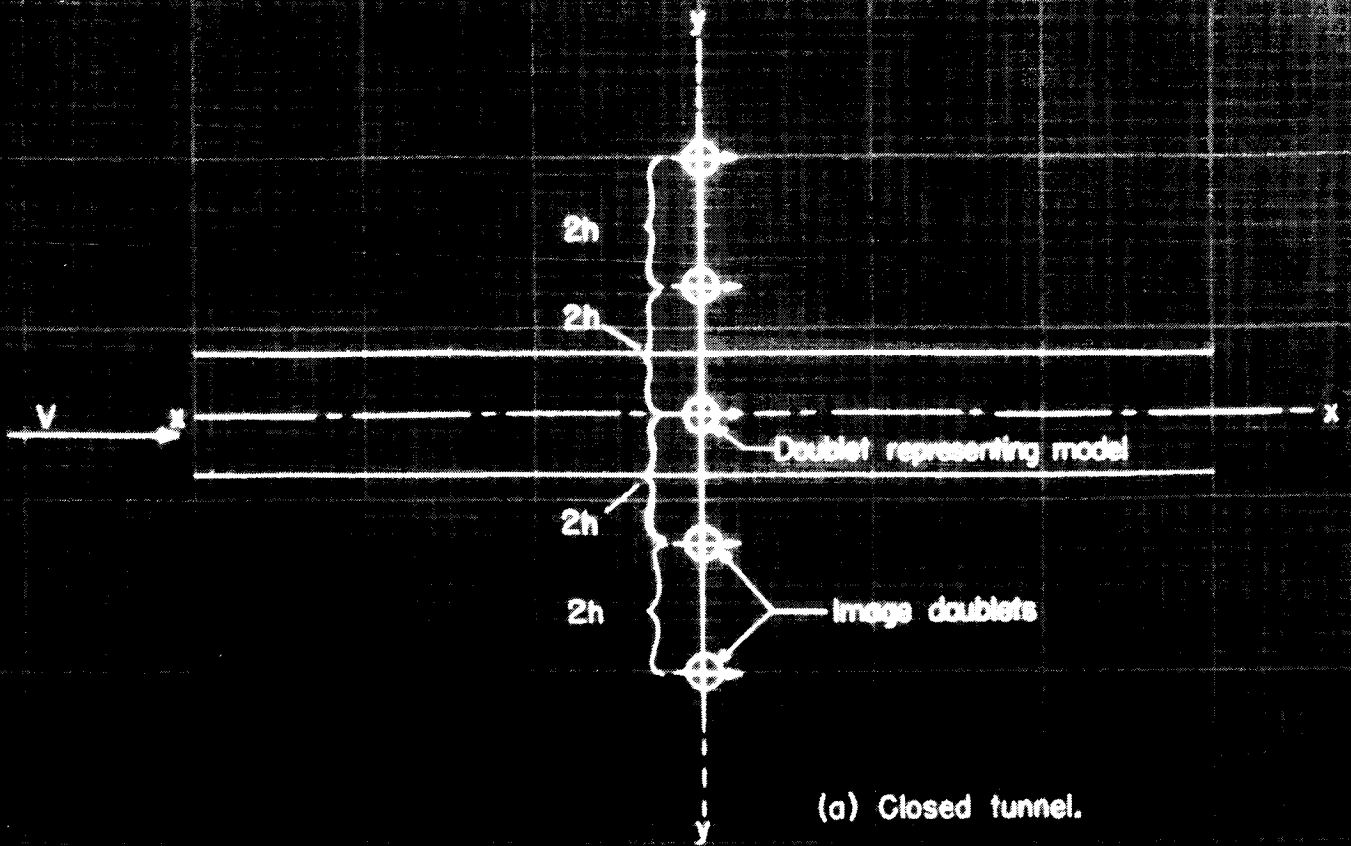


(a) Closed tunnel.

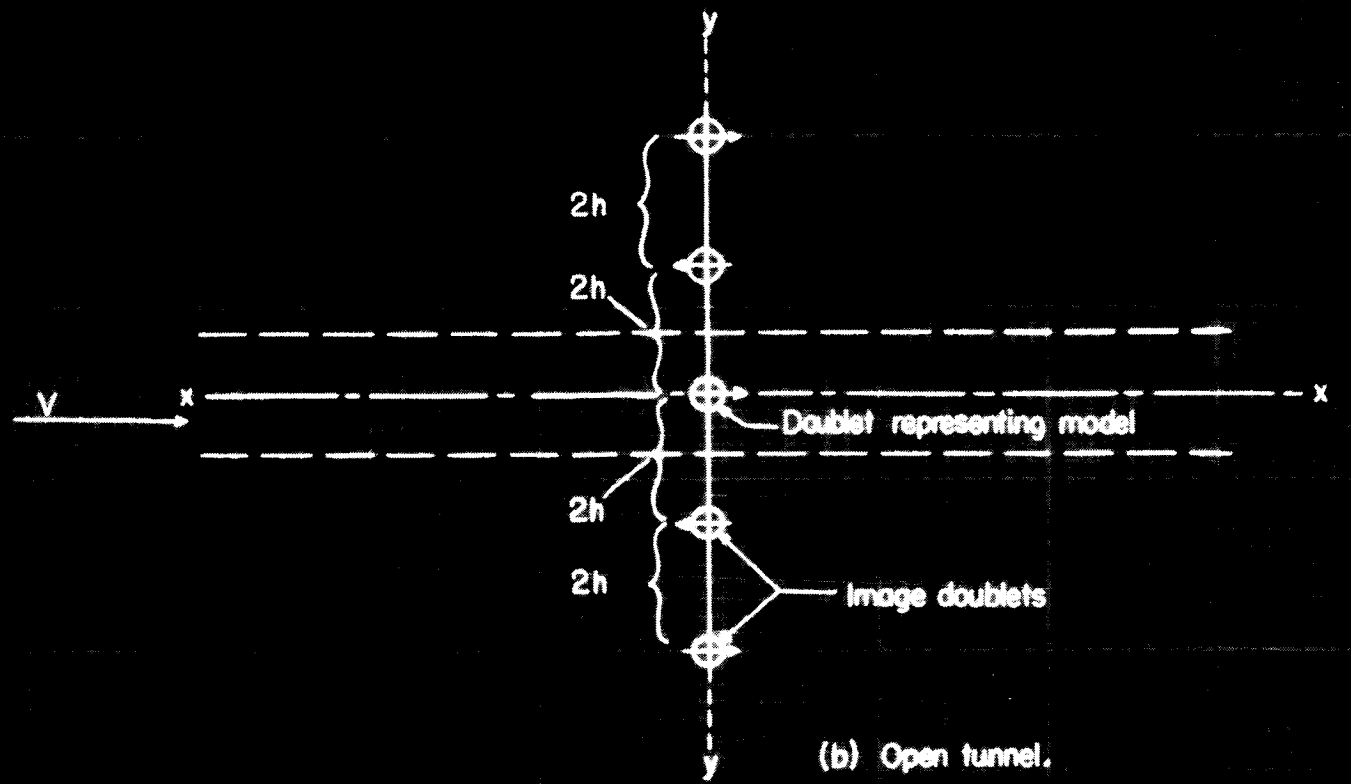


(b) Open tunnel.

Figure 2.- Trailing vortices in circular tunnels.



(a) Closed tunnel.



(b) Open tunnel.

Figure 3.- Source-sink doublet in two-dimensional tunnel.

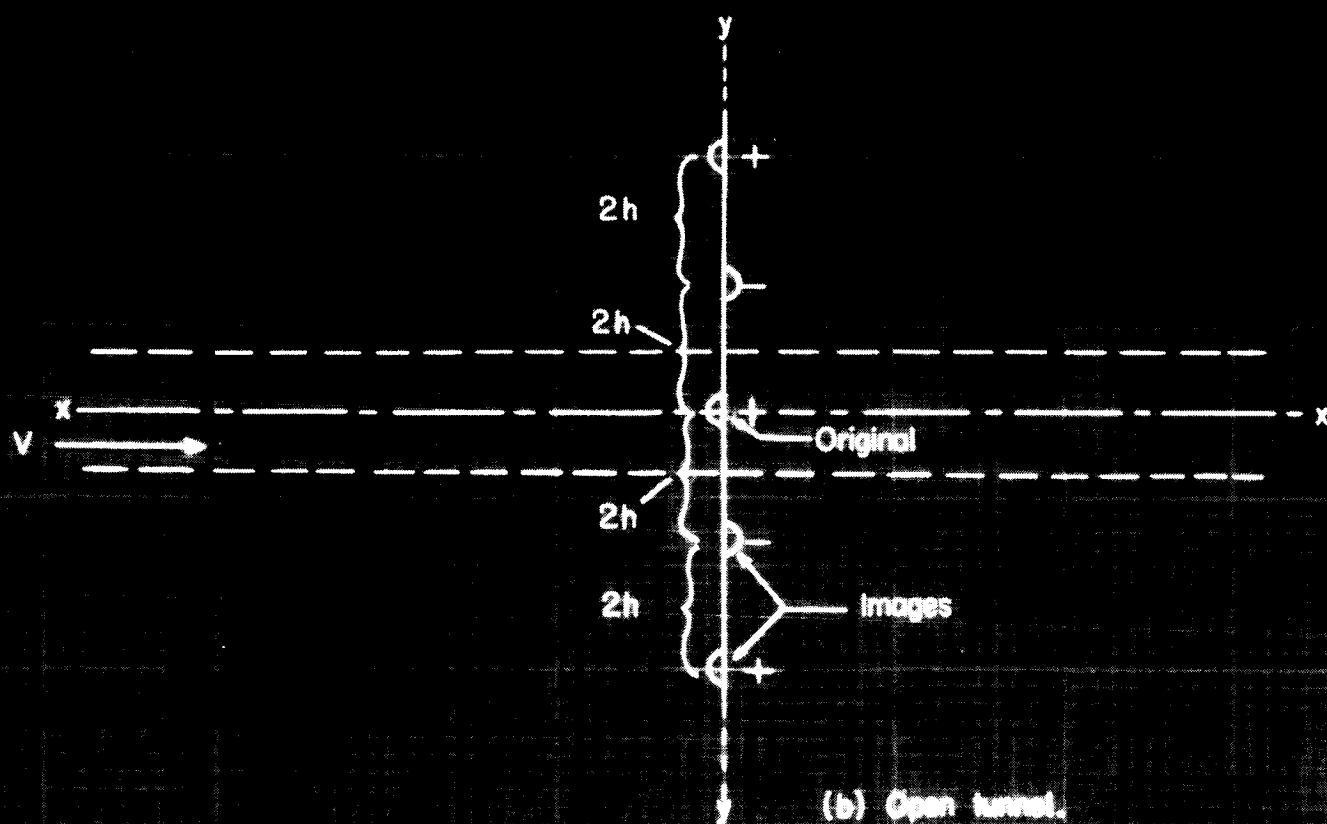
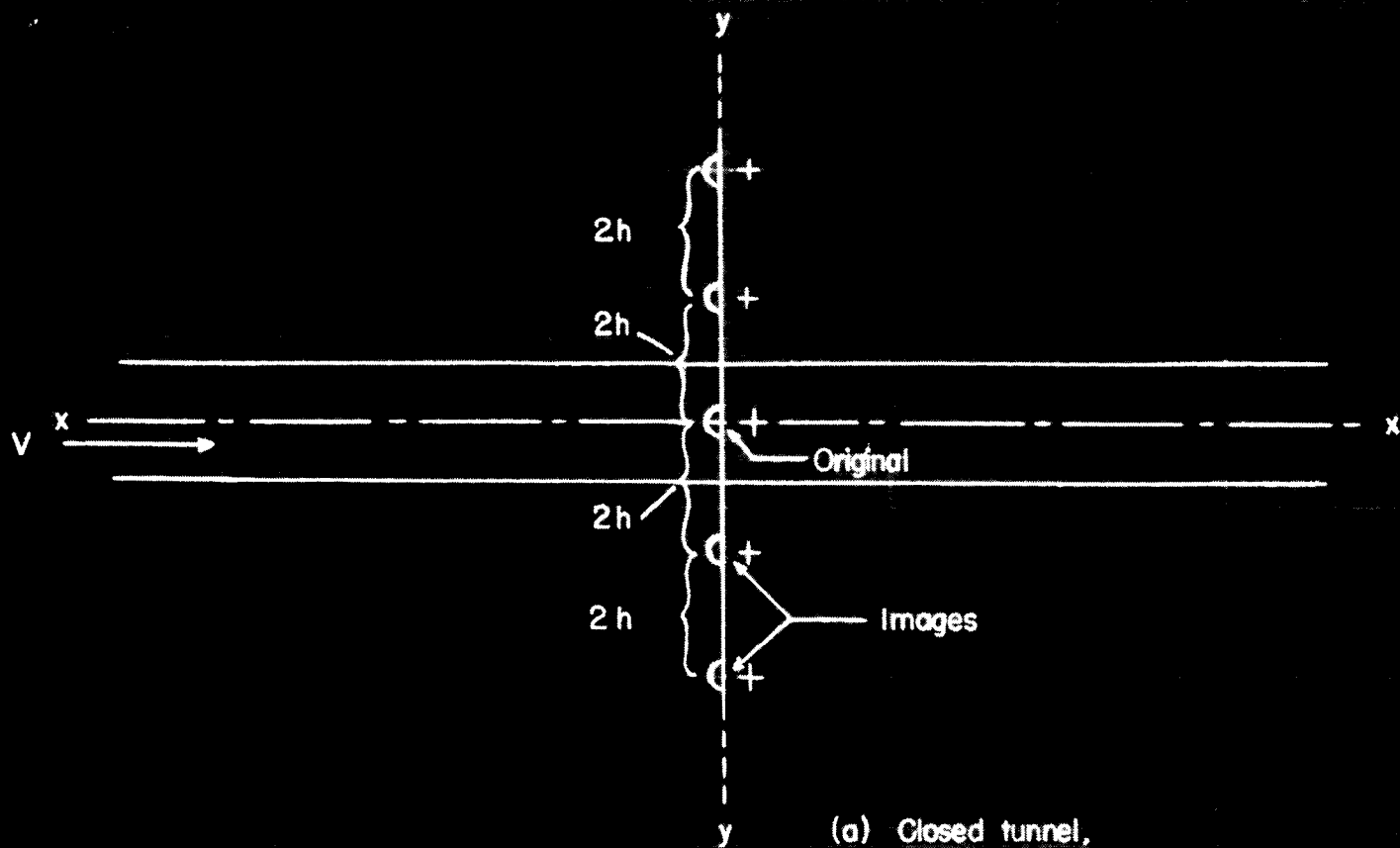


Figure 4.- Sources or sinks in two-dimensional tunnel.

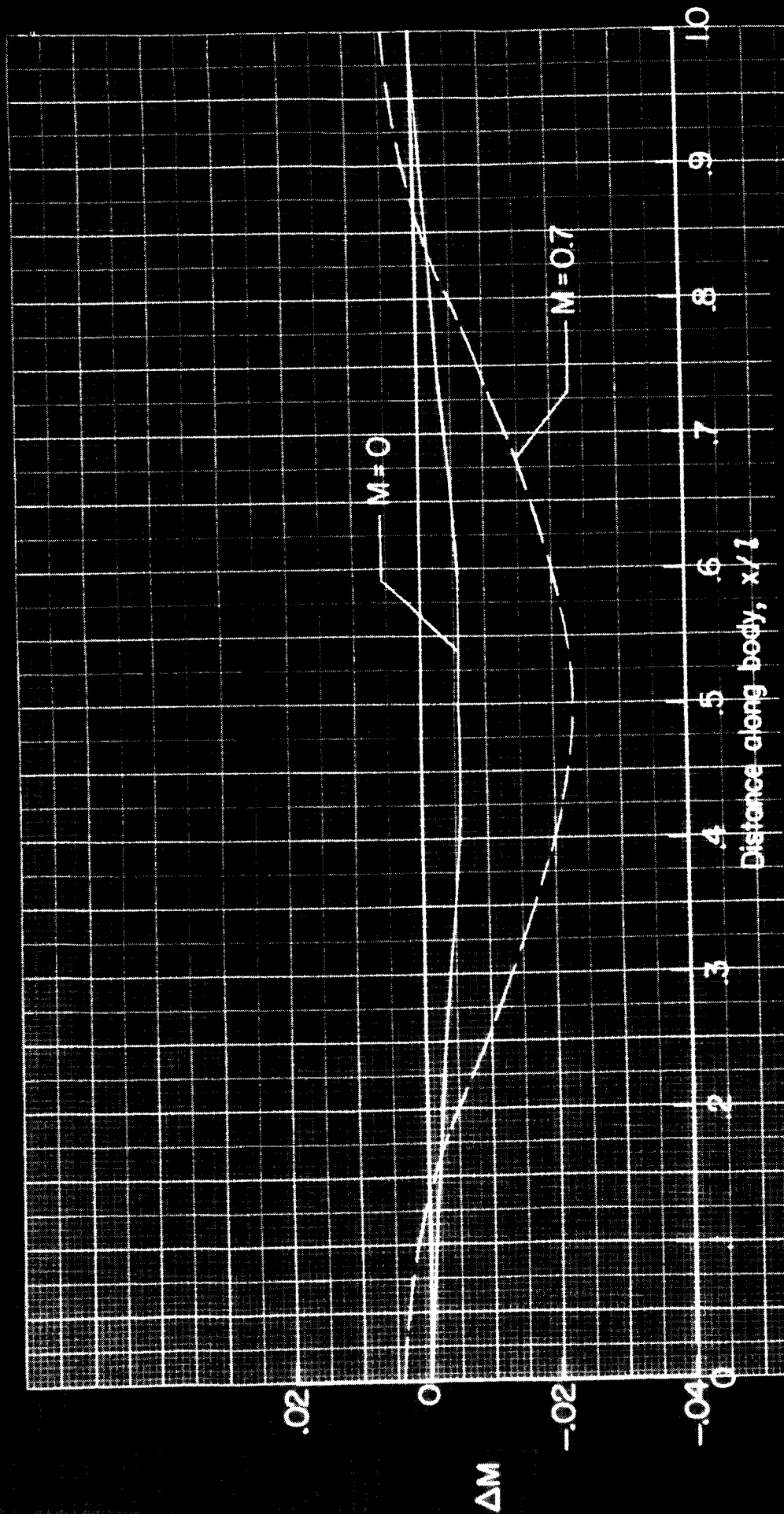


Figure 5.- Variation of increment of Mach number due to solid blockage interference on fineness-ratio-6 body of revolution in open circular wind tunnel. Body length 2 1.75 times tunnel diameter.

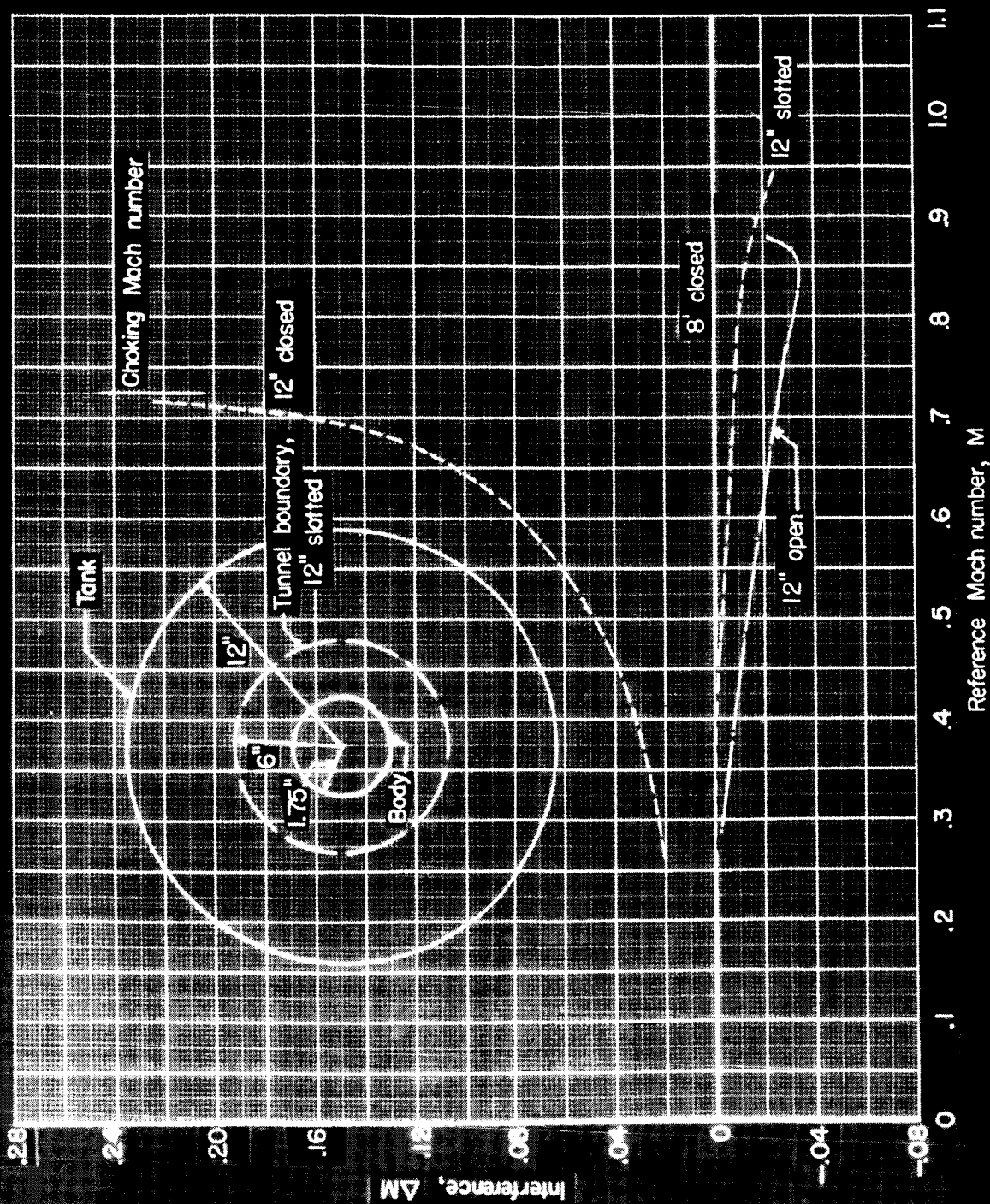


Figure 6.- Blockage interference at center of 3.5-inch-diameter prolate spheroid of fineness ratio 6 in 12-inch-diameter circular tunnels.

SPALLING-WOOD COMPANY
BOSTON, MASS.
LITHOGRAPHED IN U. S. A.

NO. 2-111 SEMCO GRAPH PAPER
250 X 175 DIVISIONS
GUARANTEED - ALL MAG. PAPER

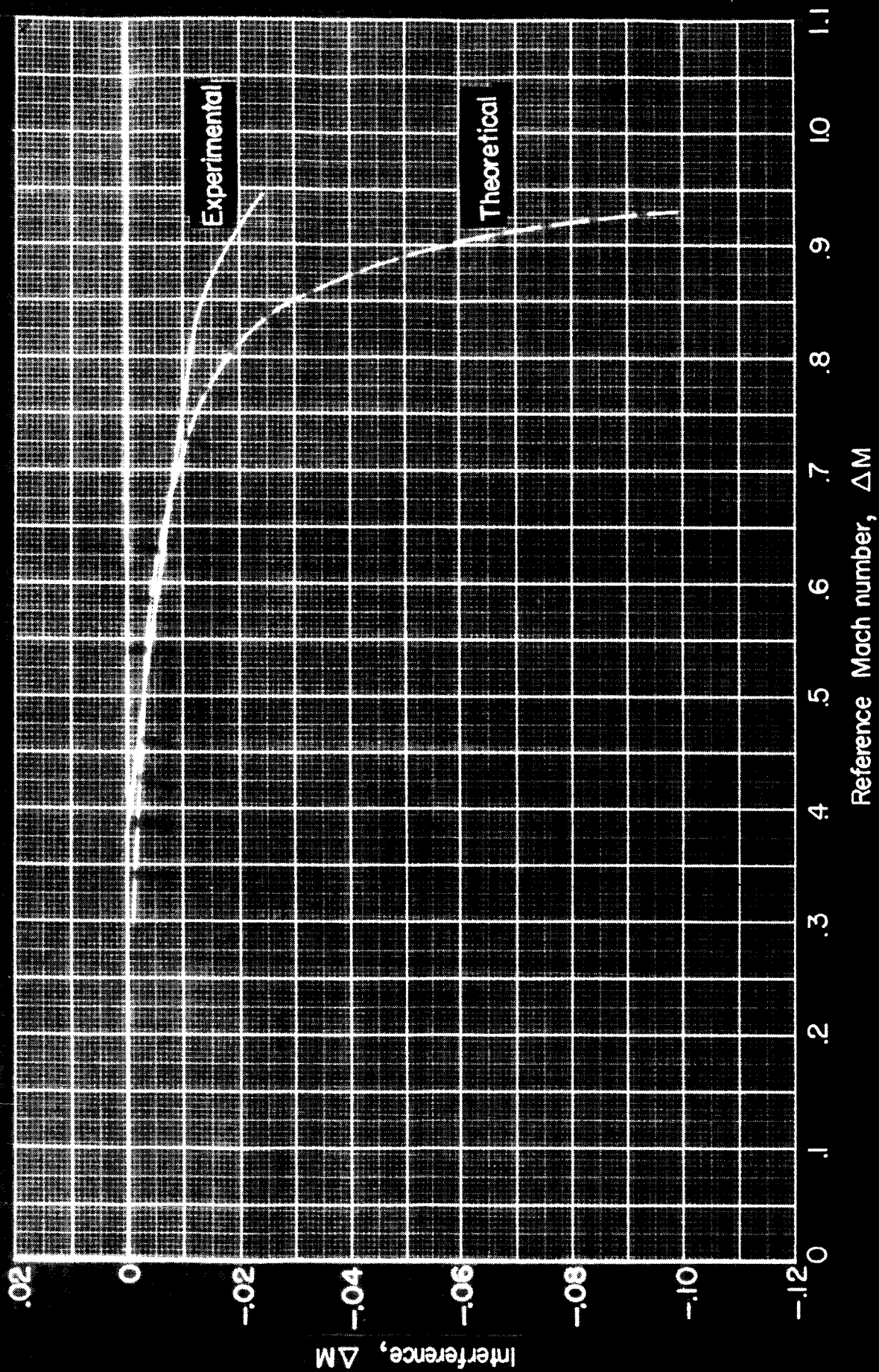


Figure 7.- Comparison of theoretical with experimental blockage interference at center of 3.5-inch-diameter prolate spheroid of fineness ratio 6 in 12-inch-diameter slotted circular tunnel.

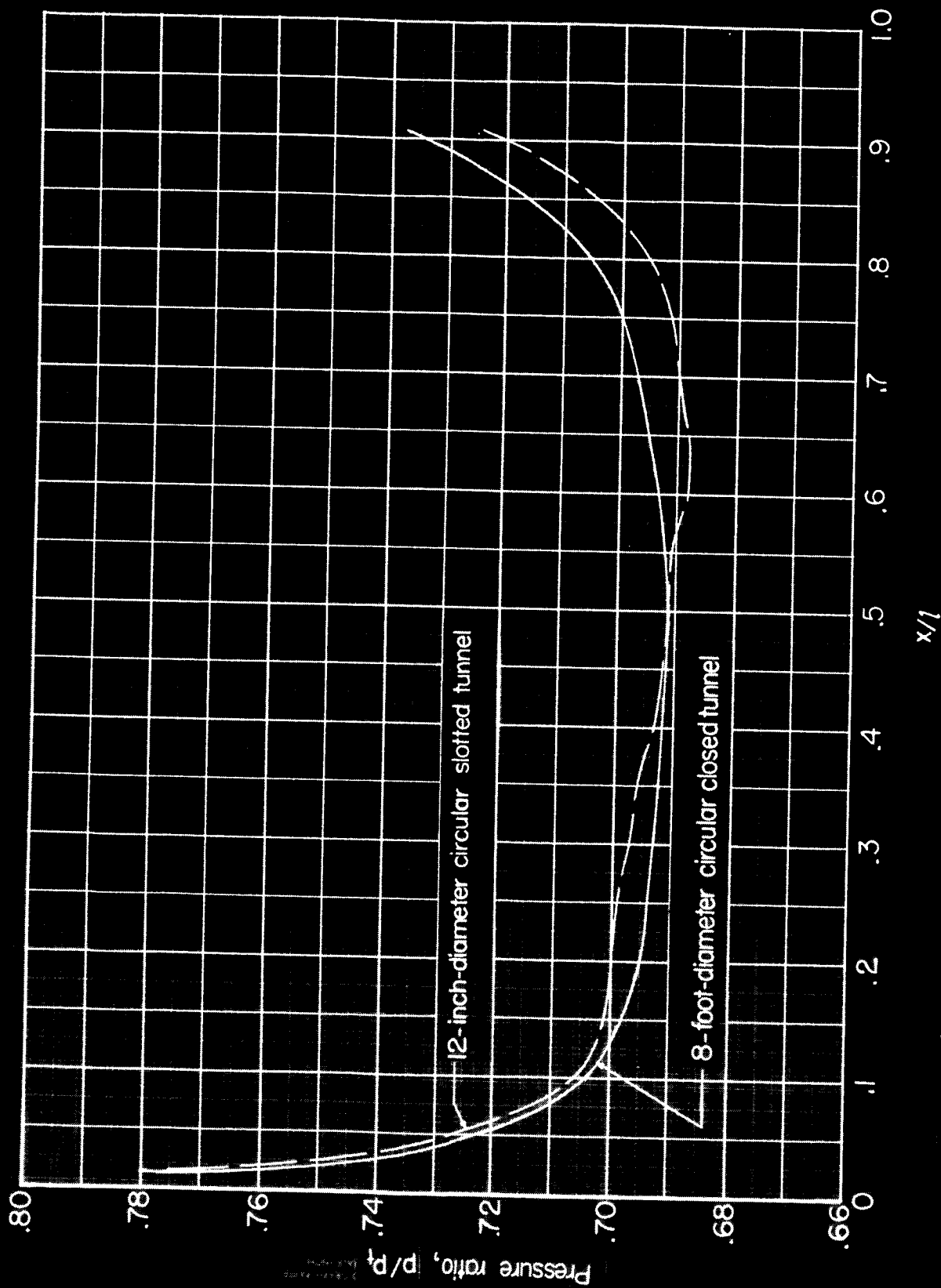


Figure 8.- Comparison of pressure distribution corrected for interference at center of body on 3.5-inch-diameter prolate spheroid of fineness ratio 6 in 12-inch-diameter circular slotted tunnel with pressure distribution on same body in 8-foot circular closed tunnel. Effective Mach number 0.7. Length of body l measured from nose.

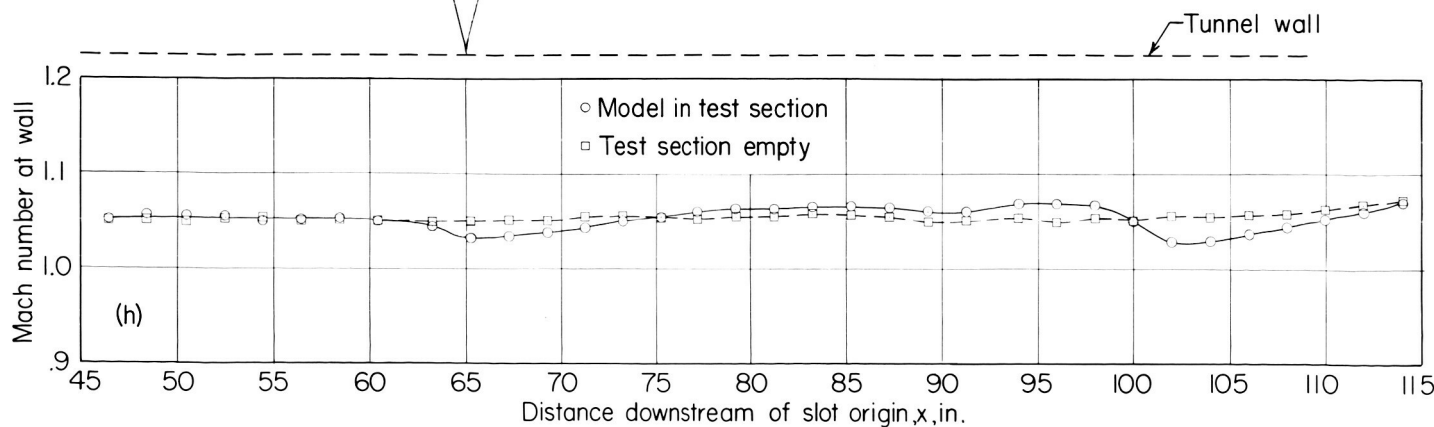
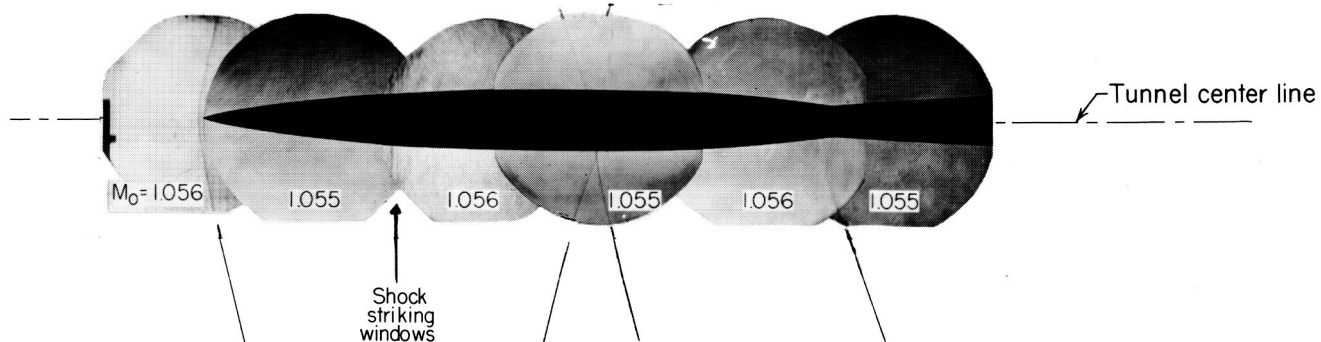
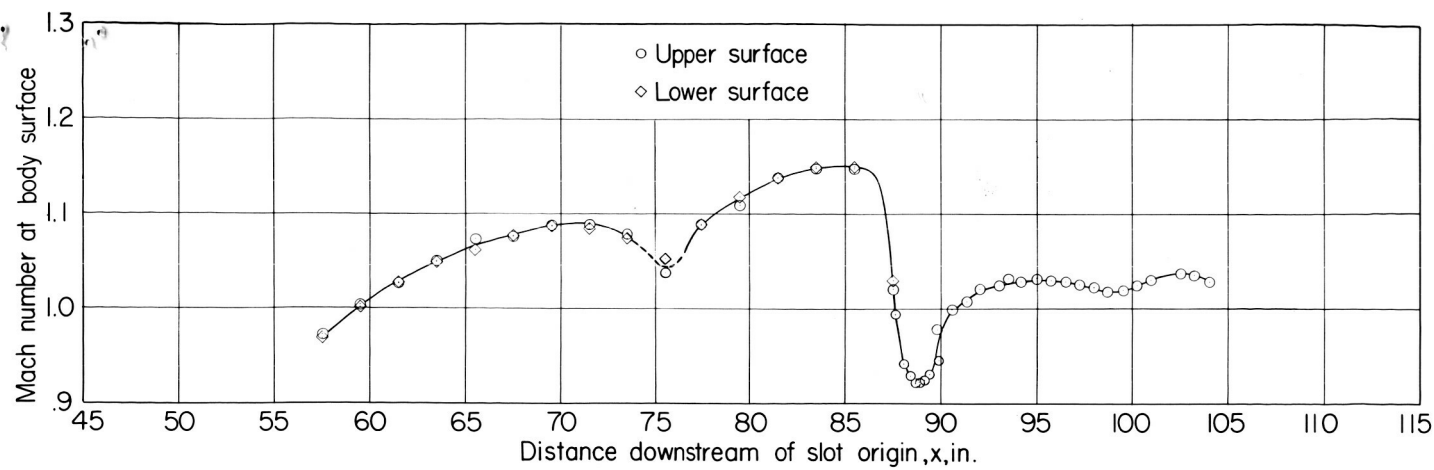


Figure 9.- Shock reflection from slotted boundary of 8-foot transonic tunnel. Stream Mach number = 1.056.

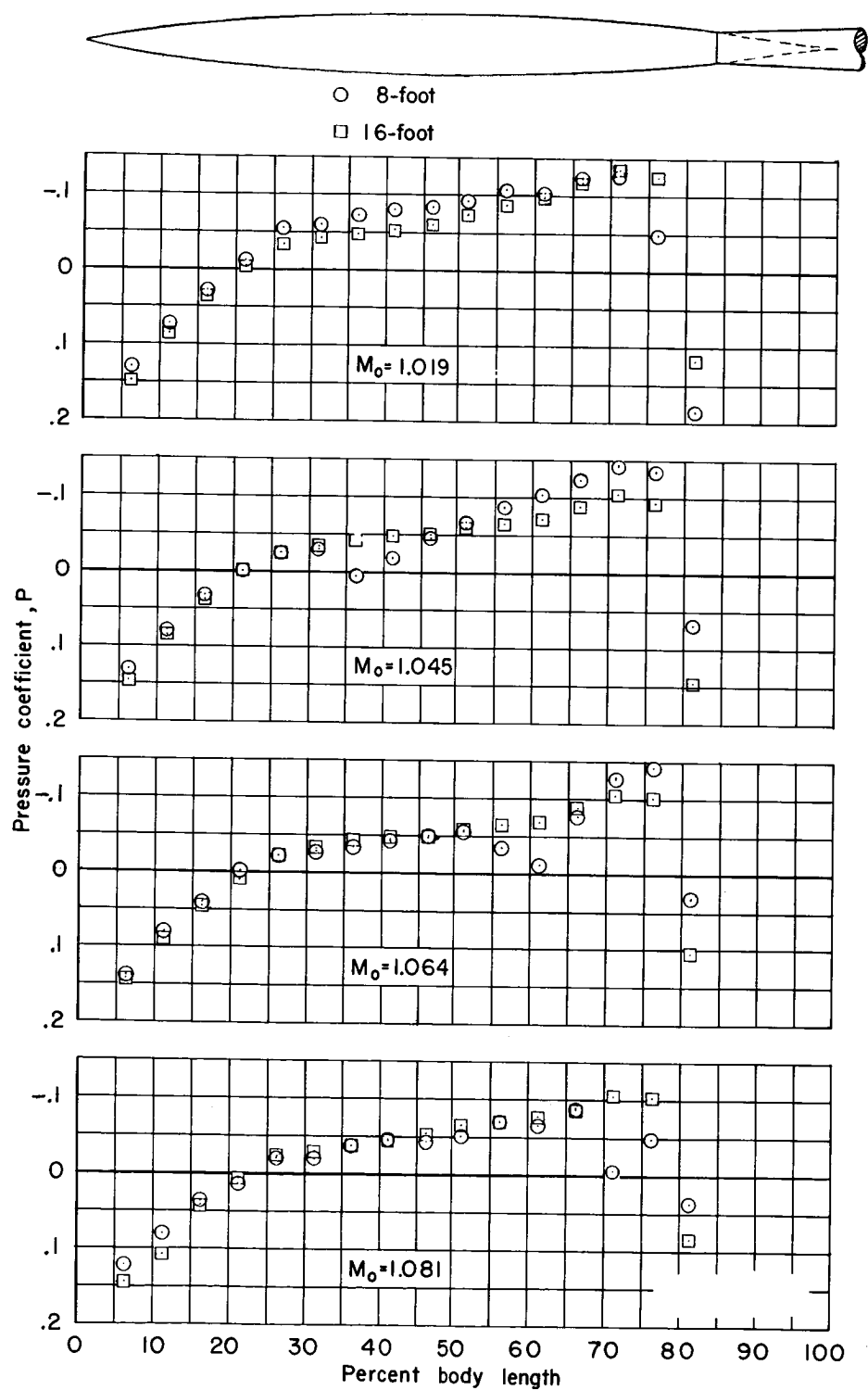


Figure 10.- Comparison of body-surface pressure distributions on a body of revolution tested at supersonic speeds in the slotted test sections of the Langley 8-foot and 16-foot transonic tunnels.

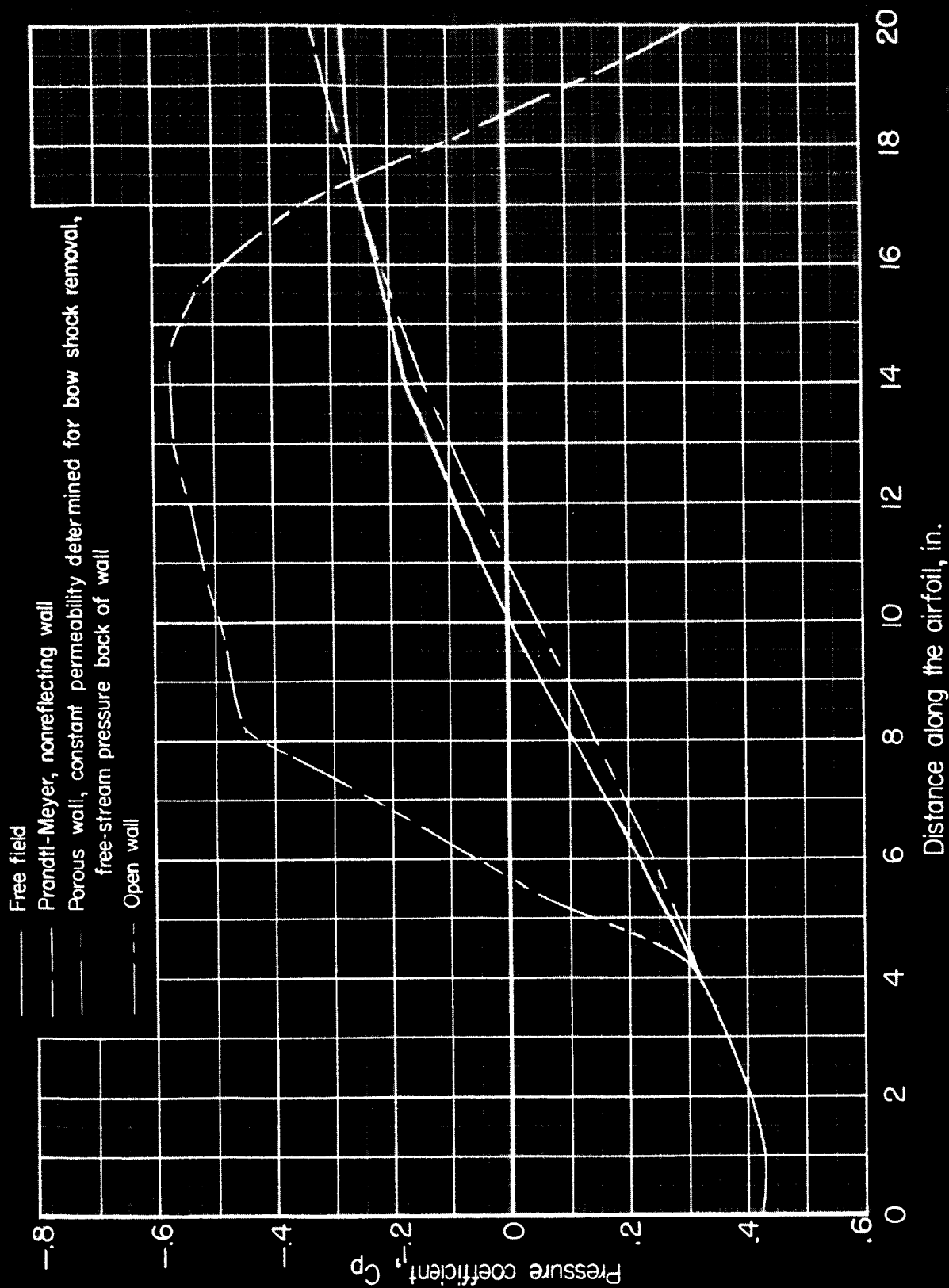


Figure 11.- Pressure coefficients at surface of two-dimensional model with several different boundary conditions. $M = 1.400$; blockage 24 percent.

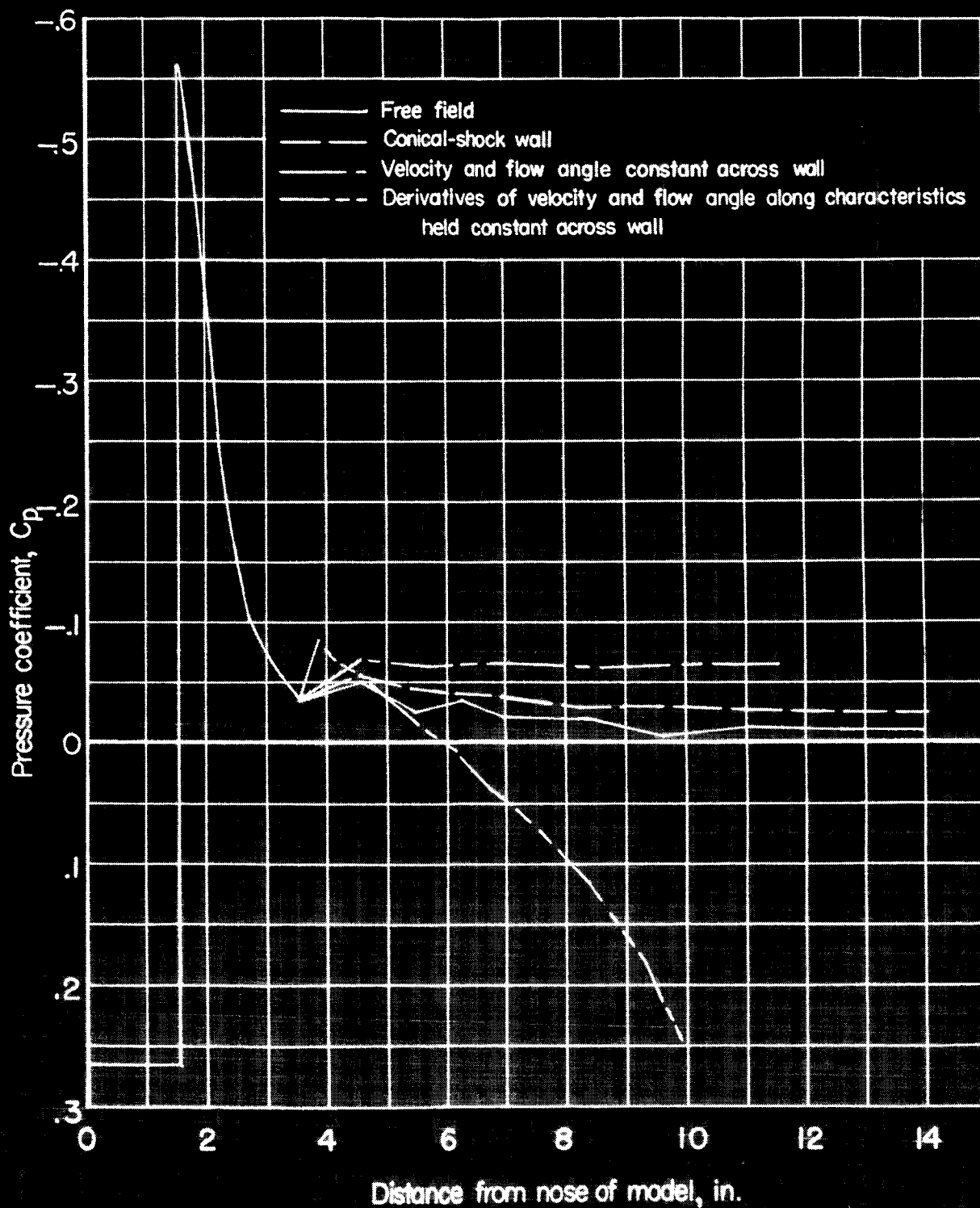


Figure 12.- Pressure coefficients at surface of cone-cylinder model with various non-reflecting tunnel boundaries. $M = 1.194$; blockage 1.80 percent.

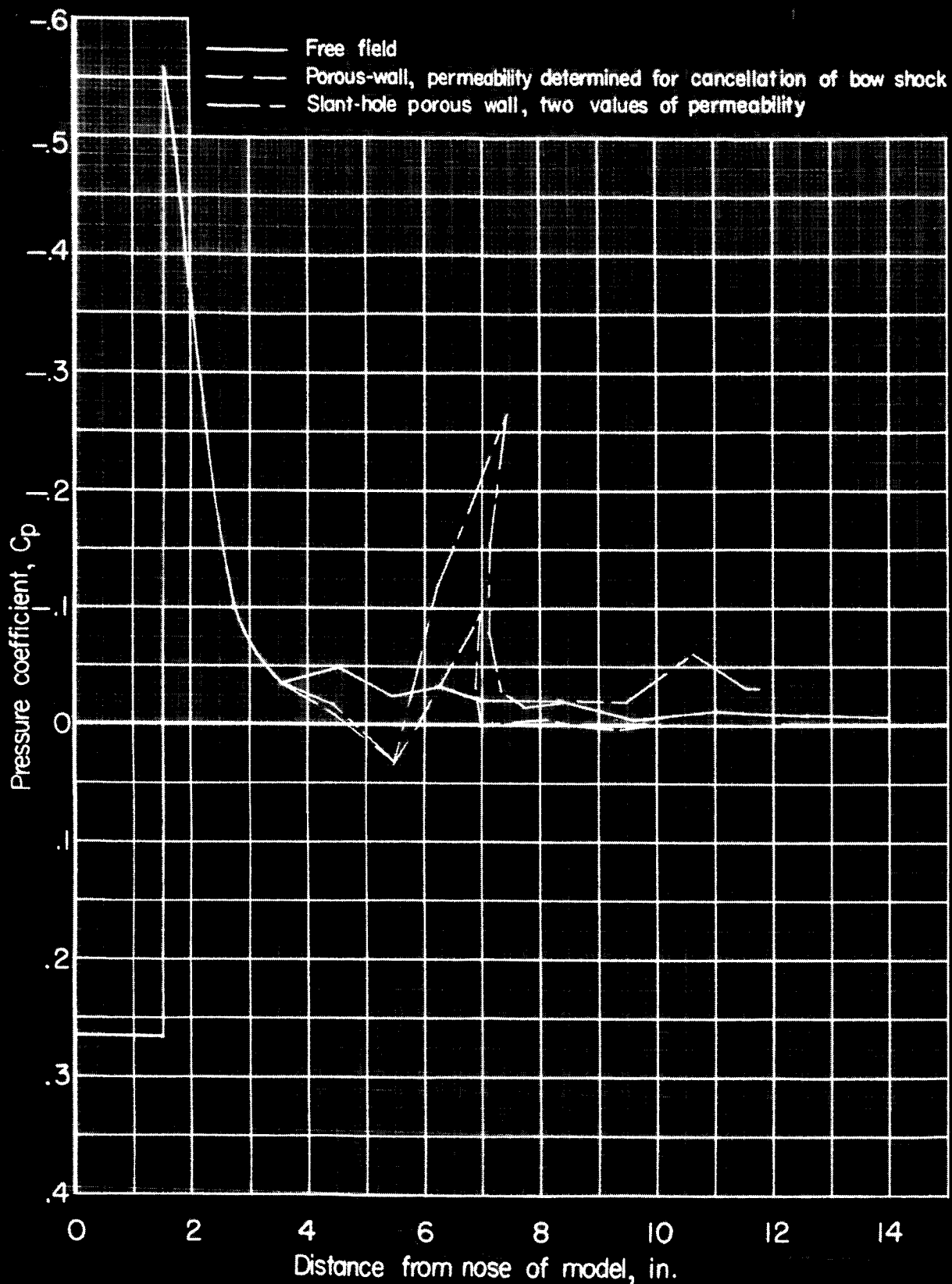


Figure 13.- Pressure coefficients at surface of cone-cylinder model with porous tunnel boundaries. $M = 1.194$; blockage 1.80 percent; constant stream pressure behind walls.

Langley 8-foot transonic tunnel (boundary interference present)

○ Body at center line; free-fall data (corrected for tare)

○ Body at center line

○ Body 10.3 inches off center line

} Pressure-distribution data (includes skin friction estimated from reference 40)

Langley 16-foot transonic tunnel (no boundary interference)

△ Pressure-distribution data (includes skin friction estimated from reference 40)

--- Free-fall data (reference 10)

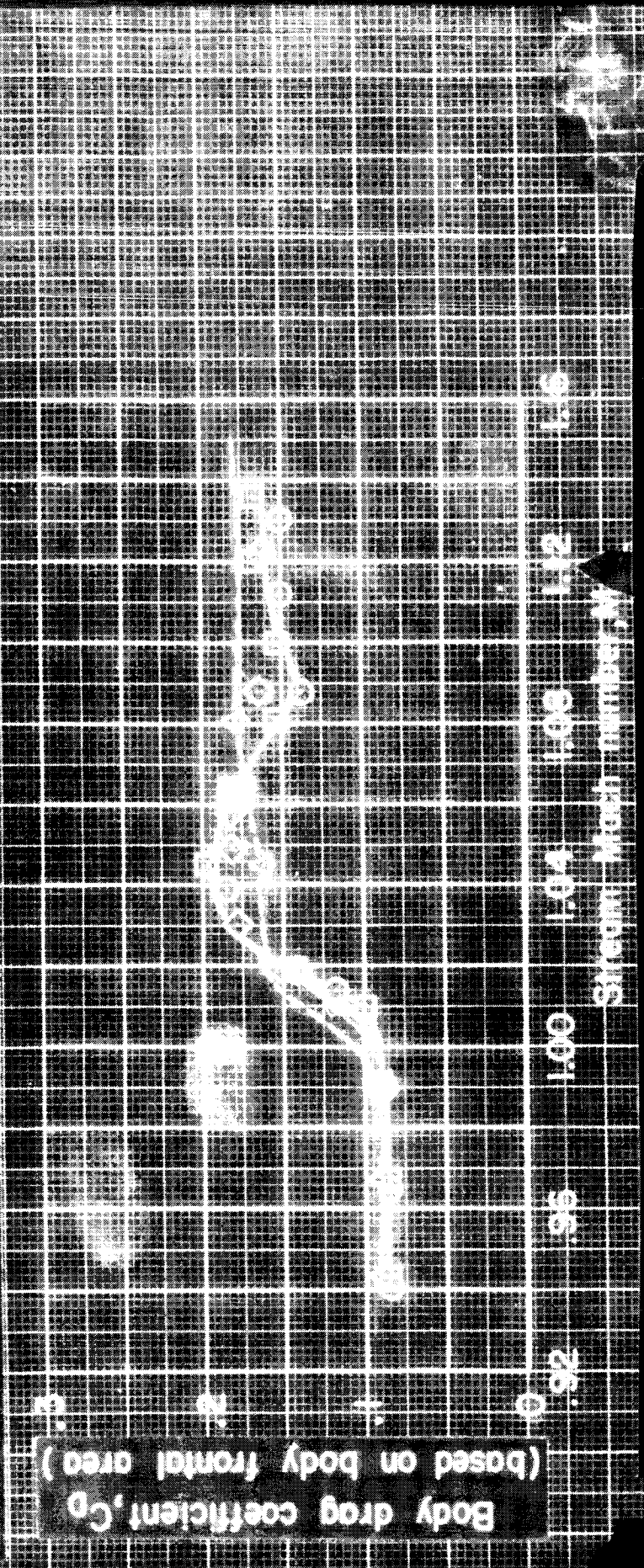


Figure 14.- Comparison of drag coefficients on 33.5-inch-long nonlifting body of revolution in the Langley 8-foot transonic tunnel with those obtained from free-fall data and from tests in the Langley 16-foot transonic tunnel.

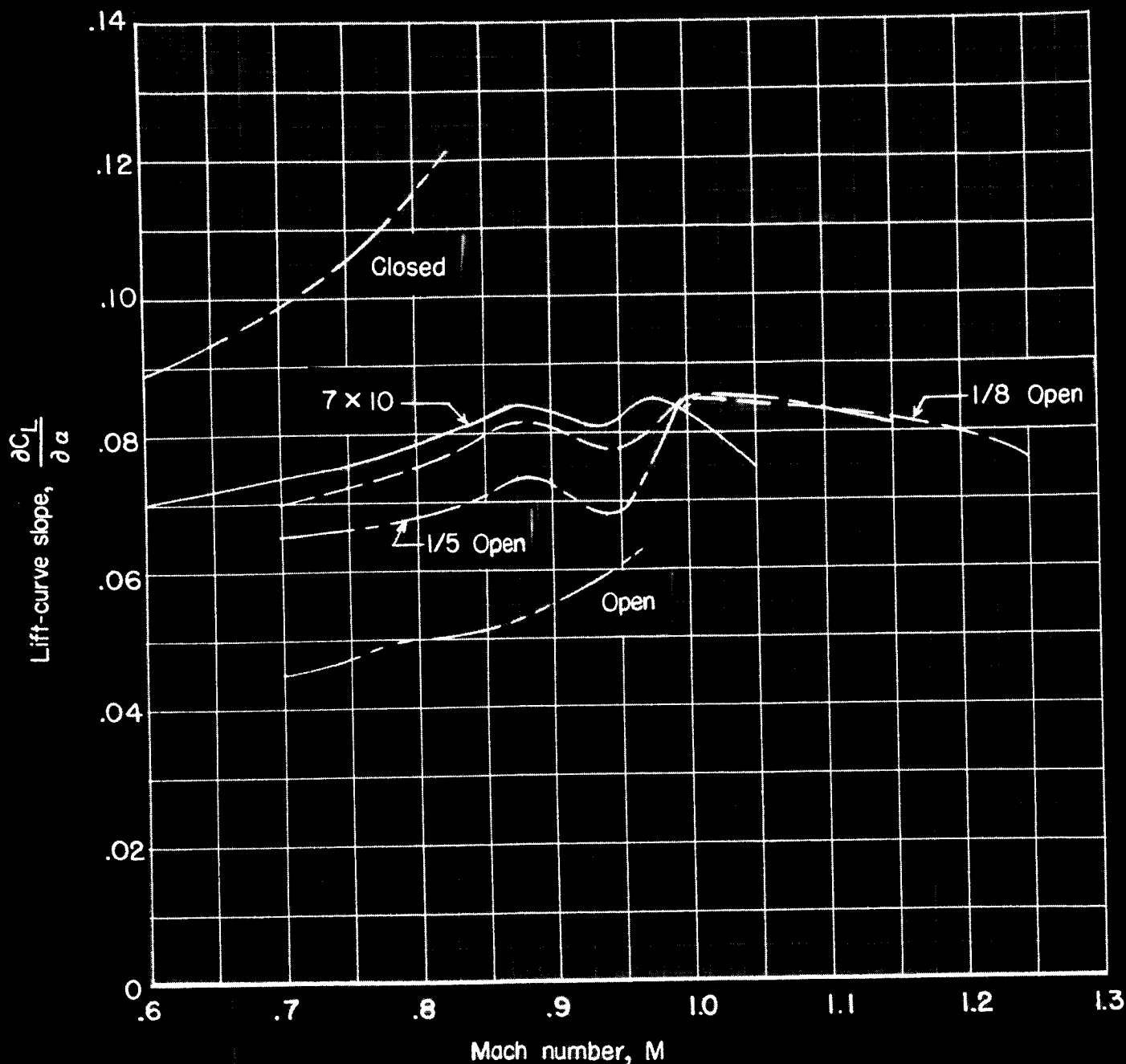


Figure 15.- Comparison of lift-curve slopes for a large wall-mounted wing in small slotted, open, and closed tunnels with lift on same wing in the closed Langley 7 x 10-foot tunnel.

SHAW-WALKER ENGINEERING CO.
BOSTON, MASS.

NO. 2 1010 SEMCO - GRAPH PAPER
10 X 10 PER HALF INCH

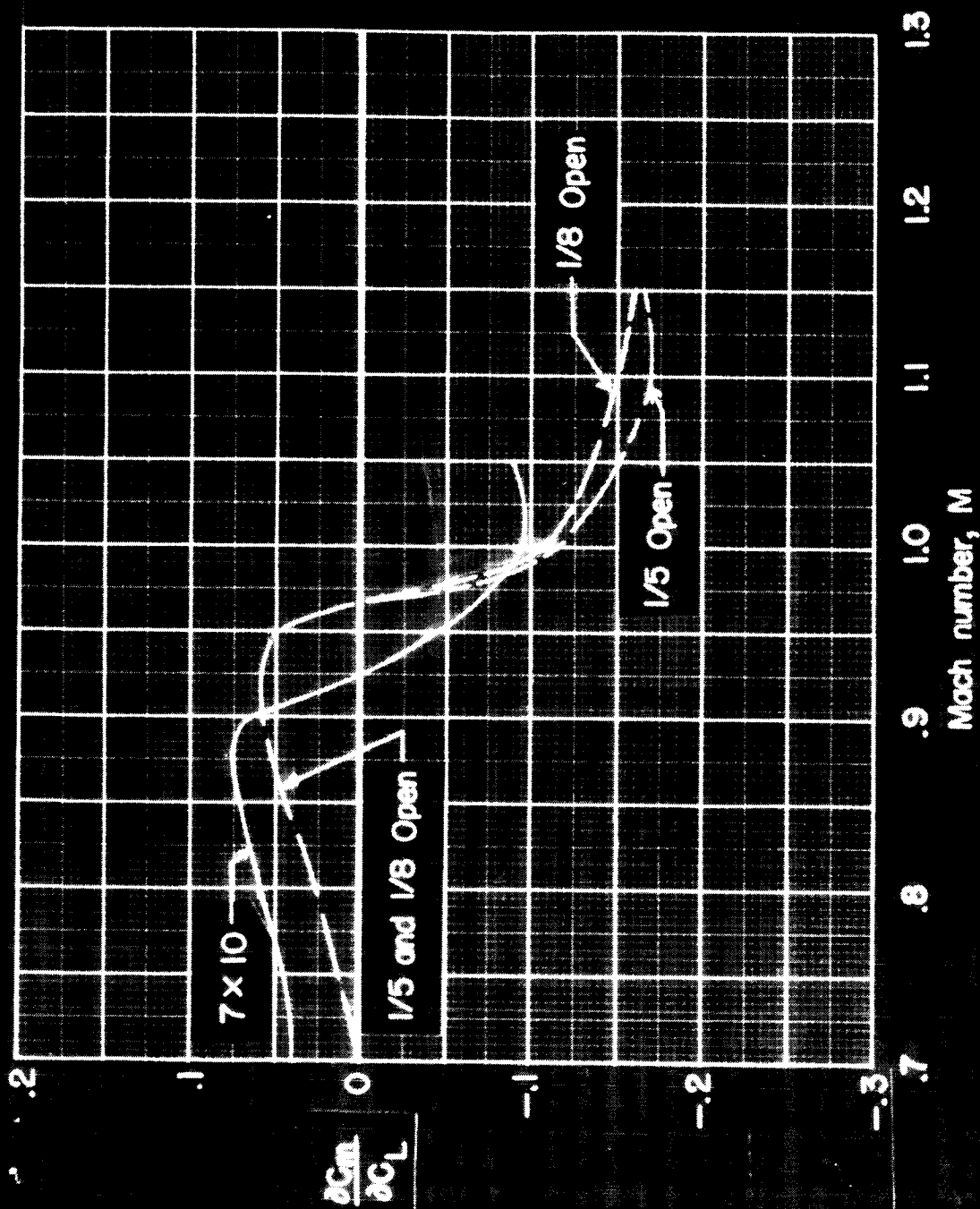


Figure 16.- Comparison of pitching-moment characteristics of wall-mounted wing in small slotted tunnels with those of same wing in the Langley 7 x 10-foot tunnel.

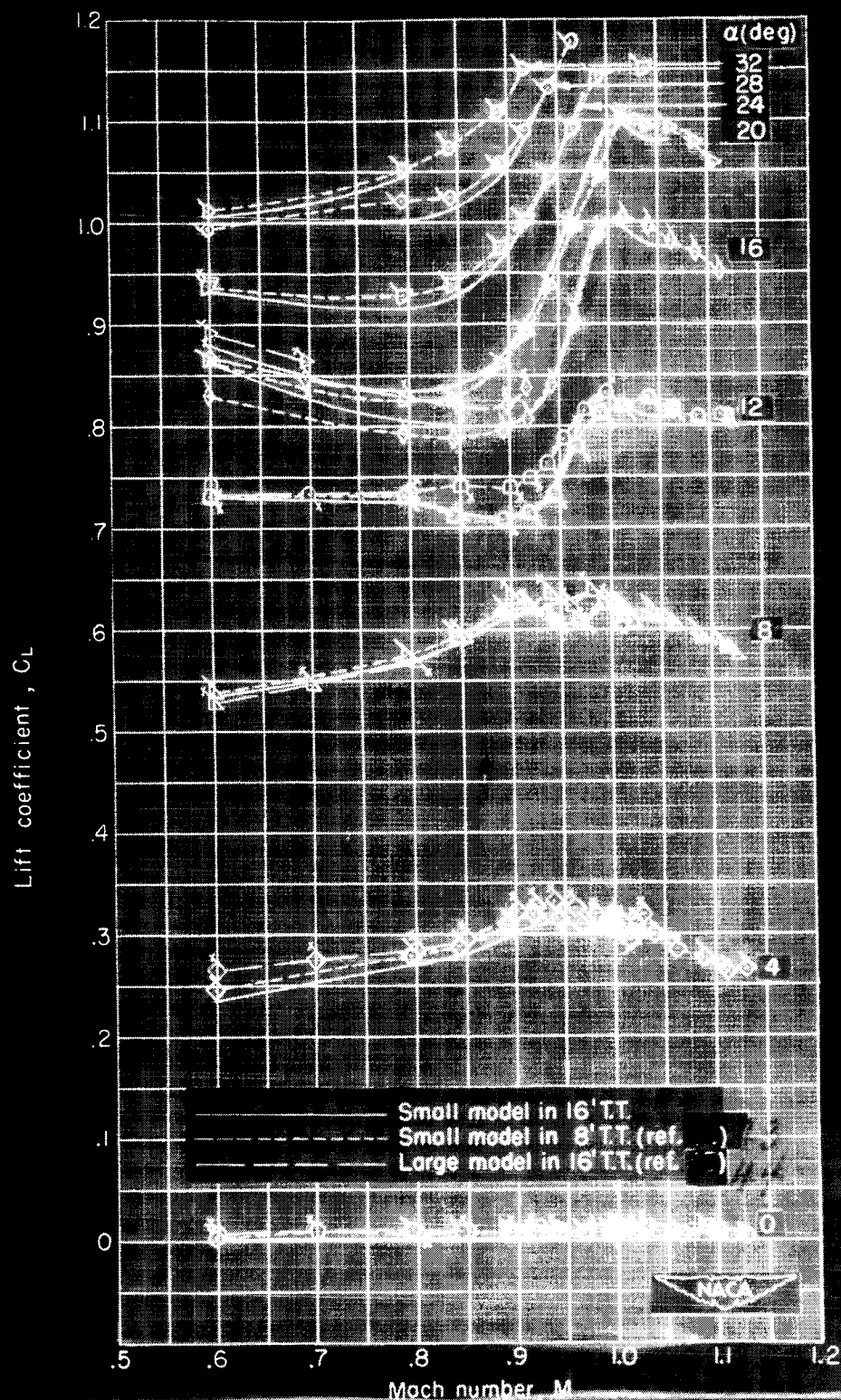


Figure 17.- Comparison of lift coefficients for winged models in Langley 8-foot and 16-foot transonic tunnels. (Single flagged symbols indicate data from small model in the 8-foot tunnel, cross-flagged symbols indicate data from large model in 16-foot tunnel.)

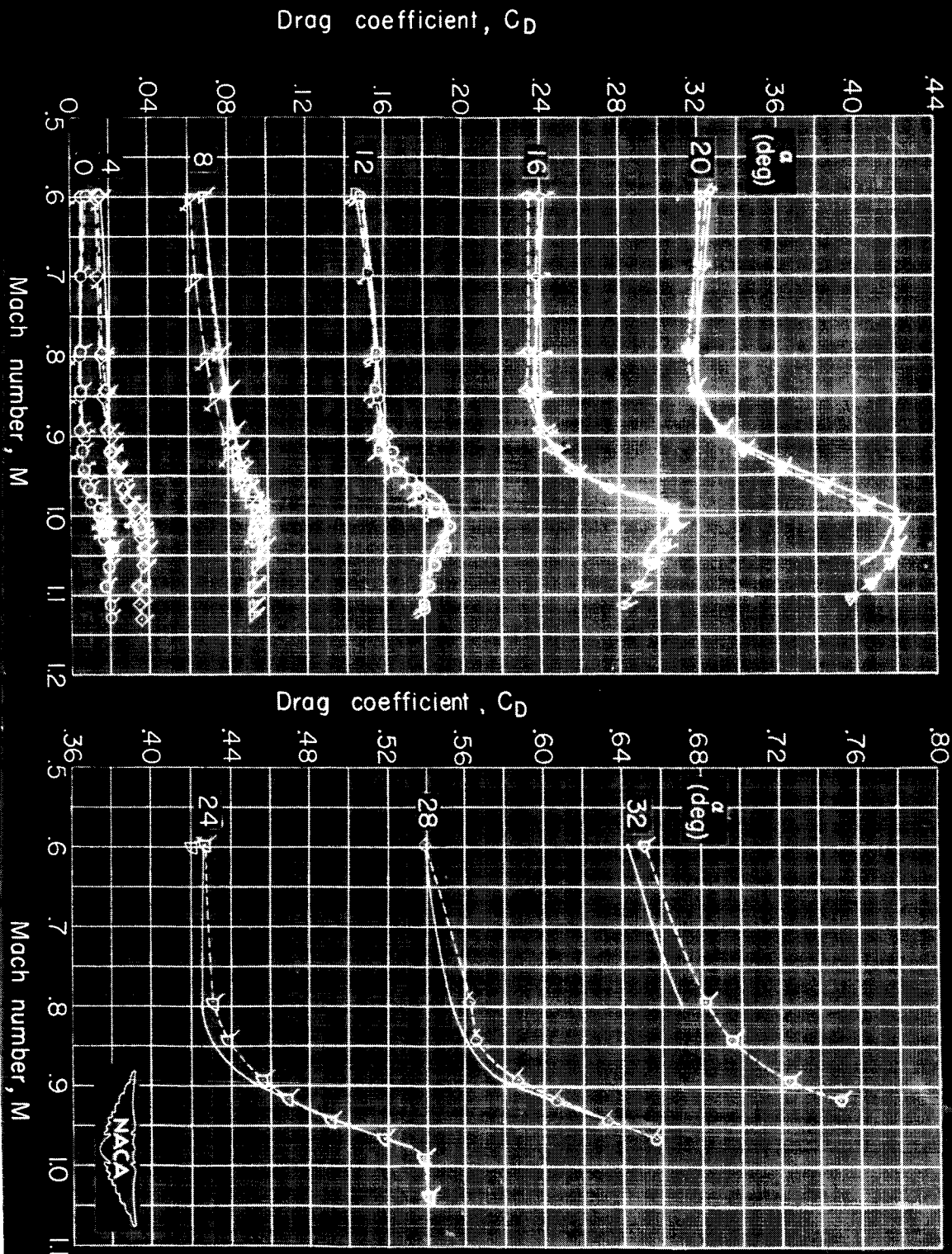


Figure 18.- Comparison of drag coefficients for winged models in Langley 8-foot and 16-foot transonic tunnels. (Single flagged symbols indicate data from small model in the 8-foot tunnel, cross-flagged symbols indicate data from large model in 16-foot tunnel.)

Small model in 16' TT (ref. 1)
 Small model in 8' TT (ref. 2)
 Large model in 16' TT (ref. 3)



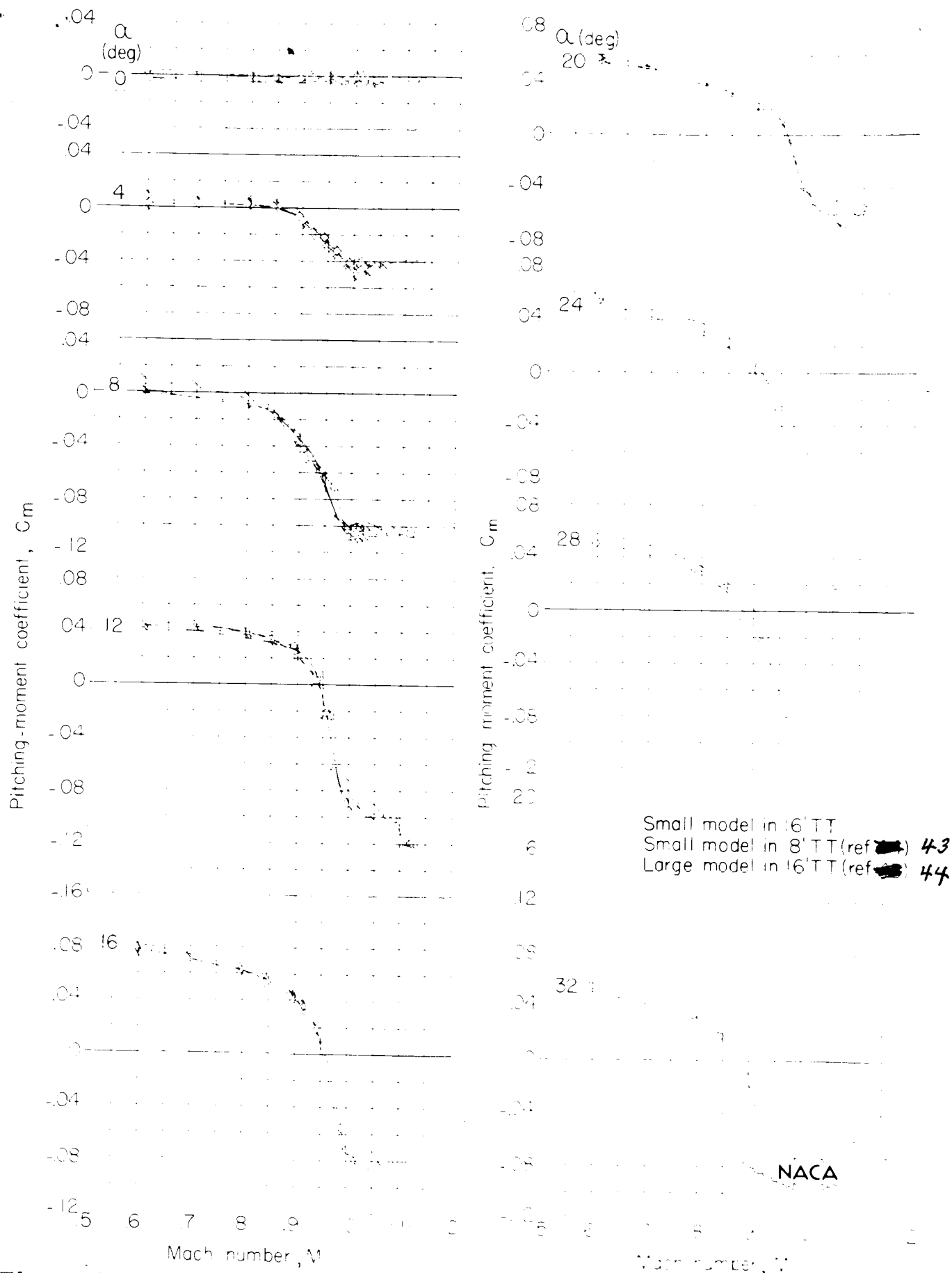


Figure 19.- Comparison of pitching-moment coefficients for winged models in Langley 8-foot and 16-foot transonic tunnels. (Single flagged symbols indicate data from small model in the 8-foot tunnel, cross-flagged symbols indicate data from large model in 16-foot tunnel.)

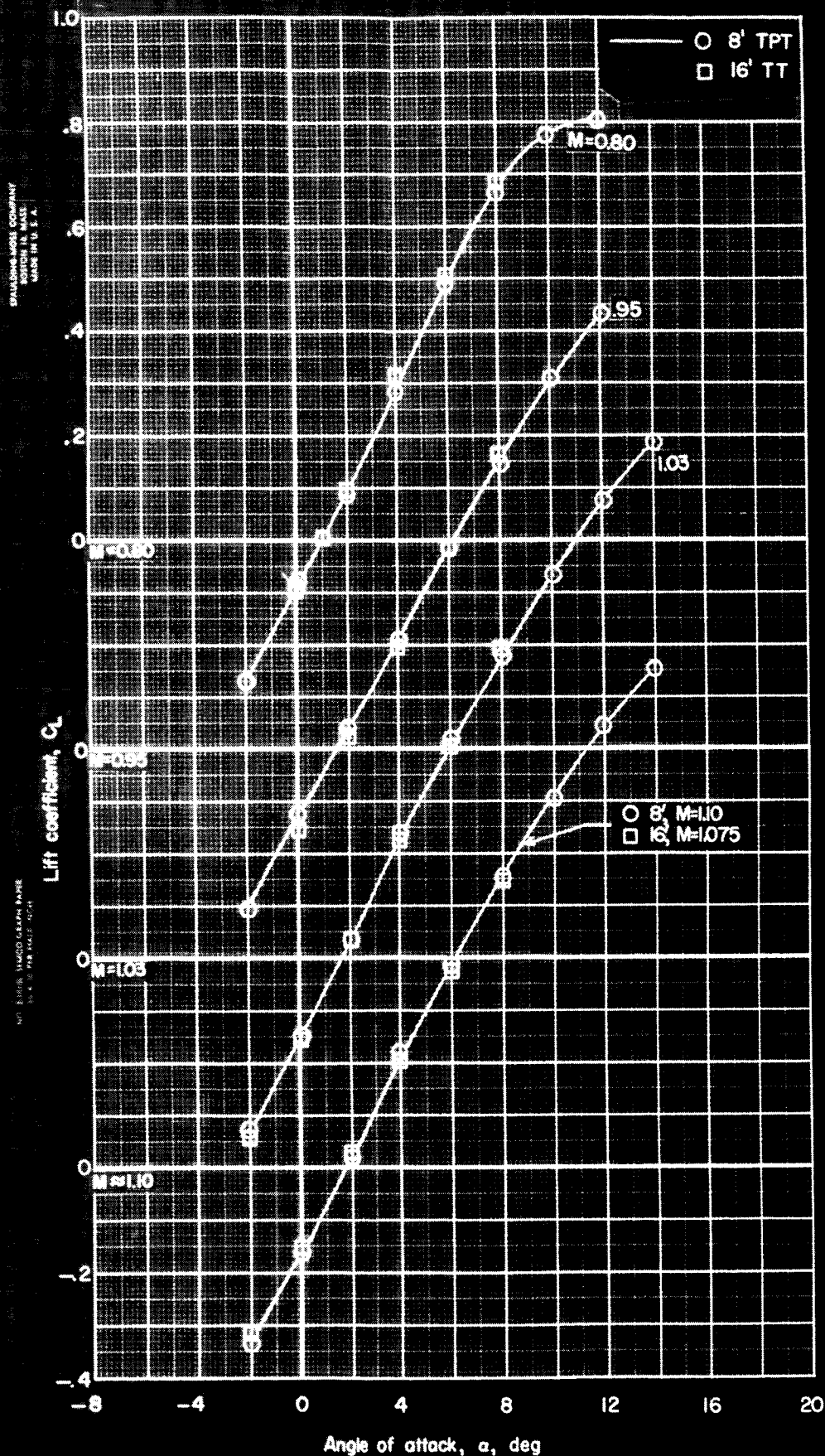


Figure 20.- Comparison of lift coefficients for a large complete model tested in the Langley 8-foot transonic pressure tunnel and in the Langley 16-foot transonic tunnel.

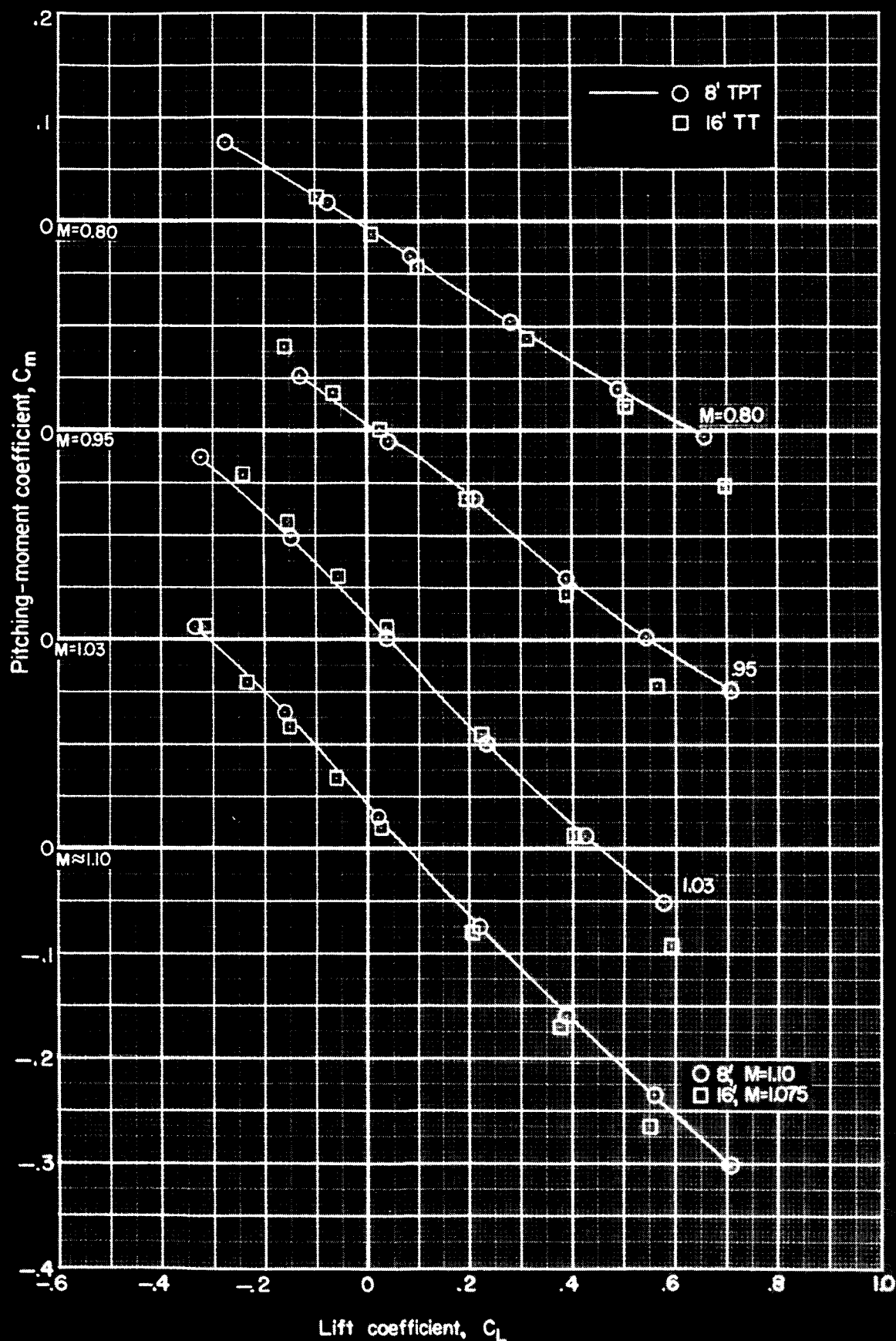


Figure 21.- Comparison of moment coefficients for a large complete model tested in the Langley 8-foot transonic pressure tunnel and in the Langley 16-foot transonic tunnel.

APPENDIX

SUBSONIC BOUNDARY INTERFERENCE IN
PRESENCE OF SOME SIMPLE SINGULARITIES

TABLE OF CONTENTS

	Page
Two-Dimensional Vortex	i
Two-Dimensional Source	vii
Three-Dimensional Point Source in Circular Tunnel	xi

APPENDIX

SUBSONIC BOUNDARY INTERFERENCE IN PRESENCE OF SOME SIMPLE SINGULARITIES

For use in reference the subsonic wind-tunnel interferences in the presence of three simple singularities are briefly derived. These singularities are the two-dimensional vortex, used to represent the lift of a two-dimensional wing, the two-dimensional source, used to represent the wake of the two-dimensional wing, and the three-dimensional point source, used to represent the wake of a three-dimensional model. The derivations are heavily dependent on the theory of reference 6, and, except as otherwise noted, the symbols are the same as used in that reference. In all cases the singularity is placed at the center of the tunnel and the x-axis is taken positive downstream along the tunnel axis or center line.

Two-Dimensional Vortex

The potential of the two-dimensional vortex in unrestricted subsonic flow is

$$\phi_1 = \frac{-\Gamma}{2\pi} \tan^{-1} \frac{\beta y}{x} \quad (1)$$

As in reference 6, page 8, ϕ_1 and the interference potential ϕ^* have been substituted into equation 9(b) of that reference to give, for the upper wall

$$\begin{aligned} \left[-igG^* - igK \frac{\partial G^*}{\partial y} + \frac{1}{R} \frac{\partial G^*}{\partial y} \right]_{y=h} = & \frac{\Gamma}{4\pi^2} \left[- \int_{-\infty}^{\infty} \frac{\beta y}{x^2 + \beta^2 y^2} e^{igx} dx + \right. \\ & K \int_{-\infty}^{\infty} \frac{\beta^3 y^2 - \beta x^2}{(x^2 + \beta^2 y^2)^2} e^{igx} dx + \\ & \left. \frac{1}{R} \int_{-\infty}^{\infty} \frac{\beta x}{x^2 + \beta^2 y^2} e^{igx} dx \right]_{y=h} \quad (2) \end{aligned}$$

where the indicated derivations of ϕ_1 have been taken before taking the transforms.

From reference 6, page 9, a solution for G^* having the required odd dependence on y is

$$G^* = B(g)\sinh(\beta gy) \quad (3)$$

Evaluation of the integrals in (2), use of (3), and substitution of the boundary value h for y yields for $B(g)$, on separation of real and imaginary parts

$$B(g) = \frac{-\Gamma}{4\pi g} e^{-\beta|g|h} \left\{ \frac{\frac{\beta}{R} \frac{g}{|g|} [\sinh(\beta gh) + K\beta g \cosh(\beta gh)] + \frac{\beta}{R} \left[1 - \frac{K}{h} \beta|g|h\right] \cosh(\beta gh)}{[\sinh(\beta gh) + K\beta g \cosh(\beta gh)]^2 + \left[\frac{\beta}{R} \cosh(\beta gh)\right]^2} \right\} -$$

$$\frac{i\Gamma}{4\pi g} e^{-\beta|g|h} \left\{ \frac{\left[1 - \frac{K}{h} \beta|g|h\right] [\sinh(\beta gh) + K\beta g \cosh(\beta gh)] - \left(\frac{\beta}{R}\right)^2 \frac{g}{|g|} \cosh(\beta gh)}{[\sinh(\beta gh) + K\beta g \cosh(\beta gh)]^2 + \left[\frac{\beta}{R} \cosh(\beta gh)\right]^2} \right\} \quad (4)$$

Use of equation (4) with equation (3) and of equation (3) with equation (13b) of reference 6 gives, with $q = \beta gh$

$$\phi^*(x,y) = \frac{-\Gamma\beta}{2\pi R} \int_0^\infty \frac{\left[\sinh(q) + \frac{Kq}{h} \cosh(q) + \left(1 - \frac{Kq}{h}\right) \cosh(q) \right] e^{-q} \sinh\left(\frac{qy}{h}\right) \cos\left(\frac{qx}{\beta h} \frac{dq}{q}\right)}{\left[\sinh(q) + \frac{Kq}{h} \cosh(q) \right]^2 + \left[\frac{\beta}{R} \cosh(q) \right]^2} -$$

$$\frac{\Gamma}{2\pi} \int_0^\infty \frac{\left[\left(1 - \frac{Kq}{h}\right) \left(\sinh(q) + \frac{Kq}{h} \cosh(q) \right) - \left(\frac{\beta}{R}\right)^2 \cosh(q) \right] e^{-q} \sinh\left(\frac{qy}{h}\right) \sin\left(\frac{qx}{\beta h} \frac{dq}{q}\right)}{\left[\sinh(q) + \frac{Kq}{h} \cosh(q) \right]^2 + \left[\frac{\beta}{R} \cosh(q) \right]^2} \quad (5)$$

Since on the center line, $y = 0$, the potential ϕ^* is zero, a constant, the interference velocity in the free-stream direction x is zero there.

The upwash velocity is

$$w^* = \frac{\partial \phi^*}{\partial y} = \frac{-\Gamma}{2\pi h} \frac{\beta}{R} \int_0^\infty \frac{\left[\sinh(q) + \frac{Kq}{h} \cosh(q) + \left(1 - \frac{Kq}{h}\right) \cosh(q) \right] e^{-q} \cosh\left(\frac{qy}{h}\right) \cos\left(\frac{qx}{\beta h}\right) dq}{\left[\sinh(q) + \frac{Kq}{h} \cosh(q) \right]^2 + \left[\frac{\beta}{R} \cosh(q) \right]^2} -$$

$$\frac{\Gamma}{2\pi h} \int_0^\infty \frac{\left[\left(1 - \frac{Kq}{h}\right) \left(\sinh(q) + \frac{Kq}{h} \cosh(q) \right) - \left(\frac{\beta}{R}\right)^2 \cosh(q) \right] e^{-q} \cosh\left(\frac{qy}{h}\right) \sin\left(\frac{qx}{\beta h}\right) dq}{\left[\sinh(q) + \frac{Kq}{h} \cosh(q) \right]^2 + \left[\frac{\beta}{R} \cosh(q) \right]^2} \quad (6)$$

With V the free-stream velocity the streamline curvature is given by

$$\frac{1}{V} \frac{\partial w^*}{\partial x} = \frac{\Gamma}{2\pi V \beta h^2} \frac{\beta}{R} \int_0^\infty \frac{\left[\sinh(q) + \frac{Kq}{h} \cosh(q) + \left(1 - \frac{Kq}{h}\right) \cosh(q) \right] e^{-q} \cosh\left(\frac{qy}{h}\right) \sin\left(\frac{qx}{\beta h}\right) q dq}{\left[\sinh(q) + \frac{Kq}{h} \cosh(q) \right]^2 + \left[\frac{\beta}{R} \cosh(q) \right]^2} -$$

$$\frac{\Gamma}{2\pi V \beta h^2} \int_0^\infty \frac{\left[\left(1 - \frac{Kq}{h}\right) \left(\sinh(q) + \frac{Kq}{h} \cosh(q) \right) - \left(\frac{\beta}{R}\right)^2 \cosh(q) \right] e^{-q} \cosh\left(\frac{qy}{h}\right) \cos\left(\frac{qx}{\beta h}\right) q dq}{\left[\sinh(q) + \frac{Kq}{h} \cosh(q) \right]^2 + \left[\frac{\beta}{R} \cosh(q) \right]^2} \quad (7)$$

In the closed tunnel, $\frac{1}{R} \rightarrow \infty$

$$w^*_{\text{closed}} = \frac{\Gamma}{2\pi h} \int_0^\infty \frac{e^{-q} \cosh\left(\frac{qy}{h}\right) \sin\left(\frac{qx}{\beta h}\right) dq}{\cosh(q)} \quad (8)$$

At $x = 0$ the upwash is zero. Similarly as $x \rightarrow -\infty$ the upwash again approaches zero because $\frac{e^{-q} \cosh\left(\frac{qy}{h}\right)}{\cosh(q)}$ remains continuous and bounded.

The curvature at $x = y = 0$ in the closed tunnel is

$$\left(\frac{1}{V} \frac{\partial w^*}{\partial x} \right)_{\substack{\text{closed} \\ x=0 \\ y=0}} = \frac{\Gamma}{2\pi V \beta h^2} \int_0^\infty \frac{e^{-q} q dq}{\cosh(q)} = \frac{\pi}{48} \frac{\Gamma}{V \beta h^2} \quad (9)$$

These results agree with those quoted in reference 2 for $\beta \rightarrow 1$ when the differences in definition of h and w are taken into account.

For the ideal porous wall $K = 0$, the upwash is

$$w_{\text{porous}}^* = -\frac{\Gamma}{2\pi h} \frac{\beta}{R} \int_0^\infty \frac{[\sinh(q) + \cosh(q)] e^{-q} \cosh\left(\frac{qy}{h}\right) \cos\left(\frac{qx}{\beta h}\right) dq}{[\sinh(q)]^2 + \left[\frac{\beta}{R} \cosh(q)\right]^2} -$$

$$\frac{\Gamma}{2\pi h} \int_0^\infty \frac{[\sinh(q) - \left(\frac{\beta}{R}\right)^2 \cosh(q)] e^{-q} \cosh\left(\frac{qy}{h}\right) \sin\left(\frac{qx}{\beta h}\right) dq}{[\sinh(q)]^2 + \left[\frac{\beta}{R} \cosh(q)\right]^2} \quad (10)$$

At $x = 0$, $y = 0$ a downwash exists.

$$-w_{\text{porous}}^* \Big|_{\substack{x=0 \\ y=0}} = \frac{\Gamma}{2\pi h} \frac{\beta}{R} \int_0^\infty \frac{dq}{[\sinh(q)]^2 + \left[\frac{\beta}{R} \cosh(q)\right]^2}$$

$$= \frac{\Gamma}{4\pi h} \cos^{-1} \left[\frac{\left(\frac{\beta}{R}\right)^2 - 1}{\left(\frac{\beta}{R}\right)^2 + 1} \right] \quad (11)$$

where the inverse cosine function is to be taken positive. The upwash at $x \rightarrow -\infty$ is again zero, so that (11) gives the total downwash in the porous tunnel.

The curvature of the flow at $x = y = 0$ is, from (7)

$$\begin{aligned} \left(\frac{1}{V} \frac{\partial w^*}{\partial x} \right)_{\substack{\text{porous} \\ x=0 \\ y=0}} &= \frac{-\Gamma}{2\pi\beta h^2 V} \int_0^\infty \frac{\left[\sinh(q) - \left(\frac{\beta}{R} \right)^2 \cosh(q) \right] e^{-q} dq}{\left[\sinh(q) \right]^2 + \left[\frac{\beta}{R} \cosh(q) \right]^2} \\ &= \frac{-\Gamma}{4\pi\beta h^2 V} \left[\frac{\pi^2}{6} - \frac{\pi\lambda}{2} + \frac{\lambda^2}{4} \right] \end{aligned} \quad (12)$$

where $\lambda = \cos^{-1} \left[\frac{1 - \left(\frac{\beta}{R} \right)^2}{1 + \left(\frac{\beta}{R} \right)^2} \right]$ and is to be taken positive.

If λ is replaced with $2r$

$$\left(\frac{1}{V} \frac{\partial w^*}{\partial x} \right)_{\substack{\text{porous} \\ x=0 \\ y=0}} = \frac{-\Gamma\pi}{24\beta h^2 V} \left[1 - \frac{6r}{\pi} + \frac{6r^2}{\pi^2} \right]$$

where $\tan r \left(= \frac{\beta}{R} \right)$ is inverse to the tangent of r defined in reference 26. It follows on reference of equation (19) of reference 26 that the flow curvature is zero for a value of β/R inverse to that for which the solid blockage is zero.

For the ideal slotted wall, $1/R = 0$,

$$w^*_{\text{slotted}} = -\frac{\Gamma}{2\pi h} \int_0^\infty \frac{\left(1 - \frac{Kq}{h} \right) e^{-q} \cosh\left(\frac{qy}{h}\right) \sin\left(\frac{qx}{\beta h}\right) dq}{\sinh(q) + \frac{Kq}{h} \cosh(q)} \quad (13)$$

Equation (13) yields nothing at $x = 0$, $y = 0$, but as $x \rightarrow -\infty$, the ∞ at $q = 0$ produces

$$w^*_{\substack{\text{slotted} \\ y=0 \\ x \rightarrow -\infty}} \rightarrow \frac{\Gamma}{2\pi h} \frac{\pi}{2} \lim_{q \rightarrow 0} \frac{q \left(1 - \frac{Kq}{h}\right) e^{-q}}{\sinh(q) + \frac{Kq}{h} \cosh q} = \frac{\Gamma}{4h \left(1 + \frac{K}{h}\right)} \quad (14)$$

Relative to the flow at $-\infty$ therefore a downwash, $\frac{+\Gamma}{4h \left(1 + \frac{K}{h}\right)}$ exists at the model.

The curvature at $x = 0, y = 0$ is

$$\left(\frac{1}{V} \frac{\partial w^*}{\partial x}\right)_{\substack{\text{slotted} \\ x=0 \\ y=0}} = \frac{-\Gamma}{2\pi \beta h^2 V} \int_0^\infty \frac{\left[\left(1 - \frac{Kq}{h}\right)\right] e^{-q} q \, dq}{\sinh(q) + \frac{Kq}{h} \cosh(q)} \quad (15)$$

The integral has been approximately evaluated for $K/h = 1.18$, which is about the value required to give zero blockage. For this case

$$\left(\frac{1}{V} \frac{\partial w^*}{\partial x}\right)_{\substack{\text{slotted} \\ x=0 \\ y=0}} = \frac{-\Gamma}{2\pi \beta h^2 V} 0.084 = -0.0134 \frac{\Gamma}{\beta h^2 U}$$

which is slightly more than 10 percent of that in open tunnel and of opposite sign and slightly more than 20 percent in absolute value of that in closed tunnel. For the open jet, $K = 1/R = 0$, the upwash is

$$w^*_{\text{open}} = \frac{-\Gamma}{2\pi h} \int_0^\infty \frac{e^{-q} \cosh\left(\frac{qy}{h}\right) \sin\left(\frac{qx}{\beta h}\right) dq}{\sinh(q)} \quad (16)$$

which is evidently zero at the position of the model, $x = y = 0$. On the center line, $y = 0$, far upstream, $x \rightarrow -\infty$, the upwash becomes

$$w^*_{\substack{\text{open} \\ y=0 \\ x \rightarrow -\infty}} \rightarrow \frac{\Gamma}{2\pi h} \frac{\pi}{2} \lim_{q \rightarrow 0} \frac{qe^{-q}}{\sinh(q)} = \frac{\Gamma}{4h} \quad (17)$$

Relative to conditions far upstream, therefore, a downwash $\frac{\Gamma}{4h}$ exists at the model. This result agrees with that given on page 46 of reference 2, when it is remembered that the h used there is twice that used in this development and that $k_L = \Gamma/cV$.

The curvature at $x = 0, y = 0$ is

$$\left(\frac{1}{V} \frac{\partial w^*}{\partial x} \right)_{\substack{\text{open} \\ x=0 \\ y=0}} = \frac{-\Gamma}{2\pi\beta h^2 U} \int_0^\infty \frac{e^{-q}}{\sinh(q)} q \, dq = \frac{-\pi\Gamma}{24\beta h^2 U} \quad (18)$$

which for $\beta = 1$ agrees with the value given on page 44 of reference 2.

Two-Dimensional Source

For a two-dimensional source in unrestricted subsonic flow the potential is

$$\phi_1 = \frac{b}{2\pi\beta} \log_e \sqrt{x^2 + \beta^2 y^2} \quad (19)$$

where b is the source strength. Substitution of this relation for ϕ_1 into equation (9b) of reference 6 for the upper wall condition gives

$$\begin{aligned} & \left[\frac{\partial \phi^*}{\partial x} + K \frac{\partial^2 \phi^*}{\partial x \partial y} + \frac{1}{R} \frac{\partial \phi^*}{\partial y} \right]_{y=h} \\ &= \frac{-b}{2\pi\beta} \left[\frac{x}{x^2 + \beta^2 y^2} - K \frac{2\beta^2 xy}{(x^2 + \beta^2 y^2)^2} + \frac{1}{R} \frac{\beta^2 y}{x^2 + \beta^2 y^2} \right]_{y=h} \end{aligned}$$

Instead of equation (14b) of reference 6 is

$$\left(-igG^* - igK \frac{\partial G^*}{\partial y} + \frac{1}{R} \frac{\partial G^*}{\partial y}\right)_{y=h}$$

$$= -\frac{b}{4\pi^2\beta} \left(i\pi \frac{g}{|g|} e^{-\beta|g|h} - iK\beta\pi g e^{-\beta|g|h} + \frac{\pi\beta e^{-\beta|g|h}}{R} \right)$$

The solution

$$G^* = A(g) \cosh(\beta g y) \quad (20)$$

given in equation (15) of reference 6 is appropriate for the present development, whence

$$A(g) = \frac{b}{2\pi\beta} \frac{e^{-\beta|g|h}}{g} \frac{\left[\left(\frac{g}{|g|} - K\beta g \right) (\cosh(\beta g y) + K\beta g \sinh(\beta g h)) - \left(\frac{\beta}{R} \right)^2 \sinh(\beta g h) \right]}{\left[\cosh(\beta g h) + K\beta g \sinh(\beta g h) \right]^2 + \left[\frac{\beta}{R} \sinh(\beta g h) \right]^2}$$

$$+ \frac{ib}{4\pi\beta} \frac{e^{-\beta|g|h}}{g} \frac{\left[\frac{\beta}{R} \frac{g}{|g|} \sinh(\beta g h) + \frac{\beta}{R} (\cosh(\beta g h) + K\beta g \sinh(\beta g h)) \right]}{\left[\cosh(\beta g h) + K\beta g \sinh(\beta g h) \right]^2 + \left[\frac{\beta}{R} \sinh(\beta g h) \right]^2} \quad (21)$$

Use of equation (21) in equation (20) and of (20) in equation (15b) of reference 6 yields, with $q = \beta g h$

$$\varphi^* = \frac{b}{2\pi\beta} \int_0^\infty \frac{\left[\left(1 - \frac{K}{h} q \right) (\cosh(q) + \frac{K}{h} q \sinh(q)) - \left(\frac{\beta}{R} \right)^2 \sinh(q) \right] e^{-q} \cosh\left(\frac{qy}{h}\right) \cos\left(\frac{qx}{\beta h}\right) \frac{dq}{q}}{\left[\cosh(q) + \frac{K}{h} q \sinh(q) \right]^2 + \left[\frac{\beta}{R} \sinh(q) \right]^2}$$

$$+ \frac{b}{4\pi\beta} \frac{\beta}{R} \int_0^\infty \frac{\left[\sinh(q) + \cosh(q) + \frac{K}{h} q \sinh(q) \right] e^{-q} \cosh\left(\frac{qy}{h}\right) \sin\left(\frac{qx}{\beta h}\right) \frac{dq}{q}}{\left[\cosh(q) + \frac{K}{h} q \sinh(q) \right]^2 + \left[\frac{\beta}{R} \sinh(q) \right]^2} \quad (22)$$

The interference velocity is

$$u^* = \frac{\partial \phi^*}{\partial x} = \frac{-b}{2\pi\beta^2 h} \int_0^\infty \frac{\left[\left(1 - \frac{Kq}{h}\right) \left(\cosh(q) + \frac{Kq}{h} \sinh(q)\right) - \left(\frac{\beta}{R}\right)^2 \sinh(q) \right] e^{-q} \cosh\left(\frac{qy}{h}\right) \sin\left(\frac{qx}{\beta h}\right) dq}{\left[\cosh(q) + \frac{Kq}{h} \sinh(q) \right]^2 + \left[\frac{\beta}{R} \sinh q \right]^2} - \frac{b}{2\pi\beta^2 h} \frac{\beta}{R} \int_0^\infty \frac{\left[\sinh(q) + \cosh(q) + \frac{Kq}{h} \sinh(q) \right] e^{-q} \cosh\left(\frac{qy}{h}\right) \cos\left(\frac{qx}{\beta h}\right) dq}{\left[\cosh(q) + \frac{Kq}{h} \sinh(q) \right]^2 + \left[\frac{\beta}{R} \sinh q \right]^2} \quad (23)$$

The velocity gradient in the x-direction at the position of the model, $x = 0$, $y = 0$ is

$$\left(\frac{\partial u^*}{\partial x}\right) = \frac{-b}{2\pi\beta^3 h^2} \int_0^\infty \frac{\left[\left(1 - \frac{Kq}{h}\right) \left(\cosh(q) + \frac{Kq}{h} \sinh(q)\right) - \left(\frac{\beta}{R}\right)^2 \sinh(q) \right] e^{-q} dq}{\left[\cosh(q) + \frac{Kq}{h} \sinh(q) \right]^2 + \left[\frac{\beta}{R} \sinh(q) \right]^2} \quad (24)$$

For the closed tunnel, $1/R \rightarrow \infty$ the velocity interference at the position of the model, $x = 0$, $y = 0$, is given by equation (23) as zero. Far upstream, however, $x \rightarrow -\infty$ the velocity interference

$$u^*_{\text{closed}} \xrightarrow[y=0]{x \rightarrow -\infty} \frac{-b}{2\pi\beta^2 h} \lim_{q \rightarrow 0} \frac{\pi q e^{-q}}{2 \sinh q} = \frac{-b}{4\beta^2 h} \quad (25)$$

which for $\beta \rightarrow 1$ agrees with the usual result. That is, the flow at the model has a velocity interference $b/4\beta^2 h$ relative to the flow far upstream. The velocity gradient at the model is, from (24)

$$\left(\frac{\partial u^*}{\partial x}\right) = \frac{b}{2\pi\beta^3 h^2} \int_0^\infty \frac{e^{-q}}{\sinh(q)} q dq = \frac{b}{2\pi\beta^3 h^2} \frac{\pi^2}{12} = \frac{\pi b}{24\beta^3 h^2} \quad (26)$$

For the ideal porous wall, $K = 0$

$$u^*_{\text{porous}} = \frac{-b}{2\pi\beta^2 h} \int_0^\infty \frac{\left[\cosh(q) - \left(\frac{\beta}{R}\right)^2 \sinh(q) \right] e^{-q} \cosh\left(\frac{qy}{h}\right) \sin\left(\frac{qx}{\beta h}\right) dq}{\left[\cosh(q) \right]^2 + \left[\frac{\beta}{R} \sinh(q) \right]^2} -$$

$$\frac{b}{2\pi\beta^2 h} \frac{\beta}{R} \int_0^\infty \frac{\cosh\left(\frac{qy}{h}\right) \cos\left(\frac{qx}{\beta h}\right) dq}{\left[\cosh(q) \right]^2 + \left[\frac{\beta}{R} \sinh(q) \right]^2} \quad (27)$$

At the model position equation (27) becomes

$$u^*_{\text{porous}} \Big|_{\substack{x=0 \\ y=0}} = -\frac{b}{2\pi\beta^2 h} \frac{\beta}{R} \int_0^\infty \frac{dq}{\left[\cosh(q) \right]^2 + \left[\frac{\beta}{R} \sinh(q) \right]^2}$$

$$= -\frac{b\lambda}{4\pi\beta^2 h} \quad (28)$$

where $\lambda = \cos^{-1} \left[\frac{1 - \left(\frac{\beta}{R}\right)^2}{1 + \left(\frac{\beta}{R}\right)^2} \right]$ is to be taken positive. The interference

velocity far upstream is zero, so that (28) gives the total contribution. The gradient in the porous tunnel at the position of the model is from (24)

$$\left(\frac{\partial u^*}{\partial x} \right)_{\text{porous}} \Big|_{\substack{x=0 \\ y=0}} = \frac{-b}{2\pi\beta^3 h^2} \int_0^\infty \frac{\left[\cosh(q) - \left(\frac{\beta}{R}\right)^2 \sinh(q) \right] e^{-q} q dq}{\left[\cosh(q) \right]^2 + \left[\frac{\beta}{R} \sinh(q) \right]^2} \quad (29)$$

The integral in equation (29) is the same as that in equation (22) of reference 6 and the gradient due to wake blockage will therefore be zero for the same value of β/R as will the solid blockage be zero.

For the ideal slotted tunnel, $1/R = 0$, the interference velocity is zero both at the model and far upstream. The gradient becomes

$$\left(\frac{\partial u^*}{\partial x}\right)_{\substack{\text{slotted} \\ x=0 \\ y=0}} = \frac{-b}{2\pi\beta^3 h^2} \int_0^\infty \frac{\left(1 - \frac{K}{h}q\right)e^{-q} dq}{\cosh(q) + \frac{Kq}{h} \sinh(q)} \quad (30)$$

The integral in equation (30) is the same as that in equation (23) of reference 6, so that the gradient is zero for the same value of K/h as is the solid blockage zero.

For the open tunnel $K = 1/R = 0$ the interference velocity u^* is again zero both at the model and far upstream. The velocity gradient at the model, $x = 0$, $y = 0$ is from (24)

$$\left(\frac{\partial u^*}{\partial x}\right)_{\substack{\text{open} \\ x=0 \\ y=0}} = \frac{-b}{2\pi\beta^3 h^2} \int_0^\infty \frac{e^{-q} dq}{\cosh(q)} = \frac{-\pi b}{48\beta^3 h^2} \quad (31)$$

Three-Dimensional Point Source in Circular Tunnel

The potential of the point source in unrestricted flow is

$$\phi_1 = \frac{-b}{4\pi \sqrt{x^2 + \beta^2 r^2}} \quad (32)$$

where b is the source strength and r is the cylindrical radial coordinate perpendicular to the x axis. Instead of equation (33) of reference 6 is

$$G_1 = \frac{-b}{8\pi^2} \int_{-\infty}^{\infty} \frac{e^{igx}}{\sqrt{x^2 + \beta^2 r^2}} dx = \frac{-b}{4\pi^2} K_0(\beta r |g|) \quad (33)$$

The next equation of reference 6 becomes

$$\begin{aligned} A(g) & \left[-igI_0(\beta gr_0) - igK\beta gI_1(\beta gr_0) + \frac{1}{R}\beta gI_1(\beta gr_0) \right] \\ & = \frac{b}{4\pi^2} \left[-igK_0(\beta r_0 |g|) - igK(-\beta |g|)K_1(\beta r_0 |g|) + \frac{1}{R}(-\beta |g|)K_1(\beta r_0 |g|) \right] \end{aligned}$$

where I_0 , I_1 , K_0 and K_1 are modified Bessel functions of the first and second kind, respectively. Solution for $A(g)$ gives, with $q = \beta r_0 g$

$$\begin{aligned} A(g) & = \frac{b}{4\pi^2} \left\{ \frac{\left[-|q|\frac{K}{r_0}K_1(|q|)I_0(q) + K_0(|q|)I_0(q) + q\frac{K}{r_0}K_0(|q|)I_1(q) - \left(q|q|\frac{K^2}{r_0^2} + \frac{|q|}{q}\frac{\beta^2}{R^2} \right)K_1(|q|)I_1(q) \right]}{\left[I_0(q) + q\frac{K}{r_0}I_1(q) \right]^2 + \left[\frac{\beta}{R}I_1(q) \right]^2} \right\} + \\ & \frac{1}{4\pi^2} \frac{b}{R} \left\{ \frac{\left[-\frac{|q|}{q}K_1(|q|)I_0(q) - K_0(q)I_1(q) \right]}{\left[I_0(q) + q\frac{K}{r_0}I_1(q) \right]^2 + \left[\frac{\beta}{R}I_1(q) \right]^2} \right\} \end{aligned}$$

On taking the inverse transform of G^* the equation corresponding to equation (34) of reference 6 is

$$\varphi^* = \frac{2b}{4\pi^2 \beta r_0} \left\{ \int_0^\infty \frac{A}{C} I_0\left(\frac{qr}{r_0}\right) \cos\left(\frac{qx}{\beta r_0}\right) dq - \frac{\beta}{R} \int_0^\infty \frac{B}{C} I_0\left(\frac{qr}{r_0}\right) \sin\left(\frac{qx}{\beta r_0}\right) dq \right\} \quad (34)$$

where

$$\begin{aligned} A\left(q, \frac{K}{r_0}, \frac{\beta}{R}\right) & = \left[-q\frac{K}{r_0}K_1(q)I_0(q) + K_0(q)I_0(q) + \right. \\ & \left. q\frac{K}{r_0}K_0(q)I_1(q) - \left(q^2\frac{K^2}{r_0^2} + \frac{\beta^2}{R^2} \right)K_1(q)I_1(q) \right] \end{aligned}$$

$$G_1 = \frac{-b}{8\pi^2} \int_{-\infty}^{\infty} \frac{e^{igx}}{\sqrt{x^2 + \beta^2 r^2}} dx = \frac{-b}{4\pi^2} K_0(\beta r |g|) \quad (33)$$

The next equation of reference 6 becomes

$$\begin{aligned} A(g) & \left[-igI_0(\beta gr_0) - igK\beta gI_1(\beta gr_0) + \frac{1}{R}\beta gI_1(\beta gr_0) \right] \\ & = \frac{b}{4\pi^2} \left[-igK_0(\beta r_0 |g|) - igK(-\beta |g|)K_1(\beta r_0 |g|) + \frac{1}{R}(-\beta |g|)K_1(\beta r_0 |g|) \right] \end{aligned}$$

where I_0 , I_1 , K_0 and K_1 are modified Bessel functions of the first and second kind, respectively. Solution for $A(g)$ gives, with $q = \beta r_0 g$

$$\begin{aligned} A(g) = \frac{b}{4\pi^2} & \left\{ \frac{\left[-|q|\frac{K}{r_0}K_1(|q|)I_0(q) + K_0(|q|)I_0(q) + q\frac{K}{r_0}K_0(|q|)I_1(q) - \left(q|q|\frac{K^2}{r_0^2} + \frac{|q|}{q}\frac{\beta^2}{R^2} \right)K_1(|q|)I_1(q) \right]}{\left[I_0(q) + q\frac{K}{r_0}I_1(q) \right]^2 + \left[\frac{\beta}{R}I_1(q) \right]^2} \right\} + \\ & \frac{1}{4\pi^2} \frac{b}{R} \left\{ \frac{\left[-\frac{|q|}{q}K_1(|q|)I_0(q) - K_0(q)I_1(q) \right]}{\left[I_0(q) + q\frac{K}{r_0}I_1(q) \right]^2 + \left[\frac{\beta}{R}I_1(q) \right]^2} \right\} \end{aligned}$$

On taking the inverse transform of G^* the equation corresponding to equation (34) of reference 6 is

$$\varphi^* = \frac{2b}{4\pi^2 \beta r_0} \left\{ \int_0^\infty \frac{A}{C} I_0\left(\frac{qr}{r_0}\right) \cos\left(\frac{qx}{\beta r_0}\right) dq - \frac{\beta}{R} \int_0^\infty \frac{B}{C} I_0\left(\frac{qr}{r_0}\right) \sin\left(\frac{qx}{\beta r_0}\right) dq \right\} \quad (34)$$

where

$$\begin{aligned} A\left(q, \frac{K}{r_0}, \frac{\beta}{R}\right) & = \left[-q\frac{K}{r_0}K_1(q)I_0(q) + K_0(q)I_0(q) + \right. \\ & \quad \left. q\frac{K}{r_0}K_0(q)I_1(q) - \left(q^2\frac{K^2}{r_0^2} + \frac{\beta^2}{R^2} \right)K_1(q)I_1(q) \right] \end{aligned}$$

$$B(q) = [K_1(q)I_0(q) + K_0(q)I_1(q)] = \frac{1}{q}$$

$$C\left(q, \frac{K}{r_0}, \frac{\beta}{R}\right) = \left[\left(I_0(q) + q \frac{K}{r_0} I_1(q) \right)^2 + \left(\frac{\beta}{R} I_1(q) \right)^2 \right]$$

The axial interference velocity is

$$u^* = \frac{\partial \varphi^*}{\partial x} = \frac{-b}{2\pi^2 \beta^2 r_0^2} \left\{ \int_0^\infty \frac{A}{C} I_0\left(\frac{qr}{r_0}\right) \sin\left(\frac{qx}{\beta r_0}\right) q \, dq + \frac{\beta}{R} \int_0^\infty \frac{I_0\left(\frac{qr}{r_0}\right) \cos\left(\frac{qx}{\beta r_0}\right) dq}{C} \right\} \quad (35)$$

and the gradient in the axial direction

$$\frac{\partial u^*}{\partial x} = \frac{-b}{2\pi^2 \beta^3 r_0^3} \left\{ \int_0^\infty \frac{A}{C} I_0\left(\frac{qr}{r_0}\right) \cos\left(\frac{qx}{\beta r_0}\right) q^2 dq - \frac{\beta}{R} \int_0^\infty \frac{I_0\left(\frac{qr}{r_0}\right) \sin\left(\frac{qx}{\beta r_0}\right) q \, dq}{C} \right\} \quad (36)$$

At the position of the source, $x = r = 0$ the velocity and velocity gradient become, respectively

$$u^*_{\substack{x=0 \\ r=0}} = \frac{-b}{2\pi^2 \beta^2 r_0^2} \frac{\beta}{R} \int_0^\infty \frac{dq}{C} \quad (37)$$

and

$$\left(\frac{\partial u^*}{\partial x} \right)_{\substack{x=0 \\ r=0}} = \frac{-b}{2\pi^2 \beta^3 r_0^3} \int_0^\infty \frac{A}{C} q^2 dq \quad (38)$$

The integral in equation (38) is the same as that in equation (35) of reference 6, which applies for the velocity interference in the presence of a doublet. It follows that if the velocity interference at the model due to solid blockage is zero the velocity gradient at the model due to wake blockage is also zero.

In the closed tunnel, $1/R \rightarrow \infty$, equation (37) gives zero velocity interference at the position of the source. However equation (35) shows that far upstream, $x \rightarrow -\infty$, the interference velocity becomes

$$u_{\substack{\text{closed} \\ x \rightarrow -\infty \\ r=0}}^* = \lim_{x \rightarrow -\infty} \frac{b}{2\pi\beta^2 r_o^2} \int_0^\infty \frac{K_1(q)I_1(q)}{[I_1(q)]^2} q \sin\left(\frac{qx}{\beta r_o}\right) dq$$

$$= \frac{-b}{2\pi\beta^2 r_o^2}$$

At the position of the source therefore an interference velocity $\frac{+b}{2\pi\beta^2 r_o^2}$ occurs, as is easily derived from continuity considerations.

For the ideal porous wall, $K = 0$, the interference far upstream is zero, but at the position of the source equation (37) yields

$$u_{\substack{\text{porous} \\ r=0 \\ x=0}}^* = \frac{-b}{2\pi\beta^2 r_o^2} \frac{\beta}{R} \int_0^\infty \frac{dq}{[I_0(q)]^2 + \left[\frac{\beta}{R} I_1(q)\right]^2} \quad (39)$$

This equation can be evaluated for appropriate values of β/R .

In the ideal slotted tunnel, $1/R = 0$, and in the open tunnel, $1/R = K = 0$, the velocity interference is easily shown to be zero both at the source and far upstream.